AD_____

AWARD NUMBER: W81XWH-10-1-0596

TITLE: Targeting Class I PI3Ks in the Treatment of T-cell Acute Lymphoblastic Leukemia

PRINCIPAL INVESTIGATOR: Adolfo Ferrando, Ph.D.

CONTRACTING ORGANIZATION: Columbia University
New York NY, 10032

REPORT DATE: August 2013

TYPE OF REPORT: Final

PREPARED FOR: U.S. Army Medical Research and Materiel Command
Fort Detrick, Maryland 21702-5012

REPORT DOCUMENTATION PAGE

Form Approved
OMB No. 0704-0188

1. REPORT DATE	2. REPORT TYPE	3. DATES COVERED
August 2013	Final	1 August 2010 – 31 July 2013

4. TITLE AND SUBTITLE

Targeting Class I PI3Ks in the Treatment of T-cell Acute Lymphoblastic Leukemia

5a. CONTRACT NUMBER

5b. GRANT NUMBER
W81XWH-10-1-0596

5c. PROGRAM ELEMENT NUMBER

6. AUTHOR(S)

Adolfo A. Ferrando

Email: af2196@columbia.edu

5d. PROJECT NUMBER

5e. TASK NUMBER

5f. WORK UNIT NUMBER

7. PERFORMING ORGANIZATION NAME(S) AND ADDRESS(ES)

Columbia University
New York, NY 10032

8. PERFORMING ORGANIZATION REPORT NUMBER

9. SPONSORING / MONITORING AGENCY NAME(S) AND ADDRESS(ES)
U.S. Army Medical Research and Materiel Command
Fort Detrick, Maryland 21702-5012

10. SPONSOR/MONITOR'S ACRONYM(S)

11. SPONSOR/MONITOR'S REPORT NUMBER(S)

12. DISTRIBUTION / AVAILABILITY STATEMENT
Approved for Public Release; Distribution Unlimited

13. SUPPLEMENTARY NOTES

14. ABSTRACT

This research project aims to evaluate the antileukemic activity of inhibiting the PI3K pathway in T-cell acute lymphoblastic leukemia (T-ALL) using genetic models and pharmacologic approaches. In this project we have established a broad panel of primary T-ALL cultures and primary xenograft models of human T-ALL as experimental therapeutic platform (Aim 3 Task1). In in vitro evaluation of the activity of the CAL130 inhibitor in primary T-ALL cells demonstrated significant antileukemic effects of this drug (Aim 3, Task 2). We have performed an initial evaluation of the efficacy of CAL130 treatment in T-ALL cells xenografted in immunodeficient mice (Aim 3, task 3) and analysis of the impact of PTEN and NOTCH mutations in CAL130 response (Aim 3 Task 6). Finally we have established a synergistic effect between the inhibition of the PI3K-AKT pathway and glucocorticoid therapy in vitro (Aim 3 Task 4)and in vivo (Aim 3 Task 5). Overall these results highlight the role of the PI3K pathway as therapeutic target for the treatment of T-ALL and warrant the clinical testing of PI3K inhibitors alone and in combination with glucocorticoids in the clinic.

15. SUBJECT TERMS
Leukemia, chemotherapy, PI3K inhibitor

16. SECURITY CLASSIFICATION OF:			17. LIMITATION OF ABSTRACT	18. NUMBER OF PAGES	19a. NAME OF RESPONSIBLE PERSON
a. REPORT	b. ABSTRACT	c. THIS PAGE			USAMRMC
U	U	U	UU	79	19b. TELEPHONE NUMBER *(include area code)*

Table of Contents

Introduction

This research project aims to evaluate the antileukemic activity of inhibiting the PI3K pathway in T-cell acute lymphoblastic leukemia (T-ALL). The experimental plan includes the analysis of genetic inactivation of PI3K gamma and PI3K delta in experimental mouse models of T-ALL and the analysis of pharmacologic inactivation of the PI3K pathway in human T-ALL cell lines and in primary patient samples in vitro and in vivo.
Aims 2 and 3 of this project are developed in Dr Tom Diacovo's laboratory (CoPI in this grant). Specific experimental developments generated in my lab are reported here. A separate report covering additional experimental results is submitted by the Diacovo lab.

Body

Genetic interaction between PI3K gamma and PI3K delta and NOTCH1 in T-ALL.

PI3K gamma and PI3K delta are critical mediators of PI3K signaling in the lymphoid system. To test the pontential antileuklemic effects of PI3K gamma and PI3K delta ablation in T-cell transformation we used a NOTCH1 induced leukemia model and PI3K gamma and PI3K delta knockout mice. As reported in pur interim progress report these experiments showed that genetic ablation of PI3K gamma and PI3K delta completely abrogated the capacity of a strongly oncogenic form of NOTCH1 to induce TALL (**Figure 1)**.

In vivo evaluation of the activity of the CAL130 inhibitor in T-ALL (Aim 2, Task 1).

Our preliminary results had demonstrated a strong antileukemic effect of the CAL130 PI3K gamma and PI3K delta small molecule inhibitor against T-ALL cell lines in vitro. Next we aimed to evaluate the therapeutic efficacy of this drug in vivo. Towards this goal we generated CCRF-CEM labeled with luciferase via lentiviral infection with a LUC-neo vector followed by neomycin selection. We first analyzed the response of CCRF-CEM cells to CAL130 in a subcutaneous model in which we followed tumor growth via luciferase bioimaging (**Figure 2**). This analysis allowed a detailed quantization of the tumor response and demonstrated a rapid effect of CAL130 with significant responses after only 4 days of treatment. In addition these cells were xenografted in nod-scid mice and analyzed for disease progression via luciferase bioimaging and survival analysis (**Figures 3 and 4**). A detailed analysis of cell dose and survival was used to establish a cell dose that allowed for robust xenograft close to 100% efficiency while providing a tumor latency of over 3 weeks for experimental therapeutic experiments (**Figure 3**). As reported in our interim progress reports treatment of animals xenografted with CCRF-CEM cells with CAL130 showed effective antileukemic responses that confirmed the high cytotoxic effect of this drug against this T-ALL cell line in vivo (**Figures 2 and 4**).

Development of primary T-ALL cultures and primary xenograft models of human T-ALL and testing of CAL130 antileukemic effects in vitro (Aim 3 Task 1, Task 2, Task 3 and Task 6).

Preliminary results included in our grant proposal demonstrated an antileukemic effect of dual PI3Kgamma and PI3Kdelta with CAL130 in T-ALL cell lines. To establish if primary human T-ALL cells can respond to pharmacologic inhibition of class I PI3Ks by CAL-130 we have generated a panel of T-ALL primary cultures using a novel method which involves the co-culture of T-cell lymphoblasts with MS5 mouse stroma cells engineered to express high levels of the *NOTCH1* ligand Delta-like1 (MS5-DL1) and media supplemented with human serum and cytokines (IL7, SCF, FLT3L and insulin). Twelve primary T-ALL samples have been expanded using this protocol which allows the growth and expansion of T-ALL cells while retaining their genetic profile and stroma- and cytokine-dependence. Following the experimental plan

described in Aim 2 of our research proposal we have tested the antileukemic effects of CAL130 in a broad panel of primary T-ALL samples cultures in MS5-DL1 stroma.

Primary T-ALL tumors have been evaluated via flow cytometry analysis of cell viability using calibrating beads and differential count of tumor and supporting stroma cells in the presence of CAL130 or vehicle only. The results of these experiments confirmed the antileukemic effects of CAL130 observed in T-ALL cell lines. Notably different tumors showed variable responses to the drug which partially correlated with the expression of PTEN (**Figure 5**).
In addition, we expanded 30 primary T-ALL patient samples via injection into immunodeficient Rag2/gamma(c) double knockout animals. This extended xenograft panel has been molecularly characterized via targeted resequencing of the NOTCH1 oncogene, analysis of PTEN expression, resequencing of an extended panel of T-ALL oncogenes and tumor supressors (NOTCH1, FBXW7, PTEN, TAL1d, WT1, PHF6, FBXW7, RUNX1 and IL7R) and gene expression profiling using oligonucleotide microarrays (**Fig. 6**). Finally and with goal of analyzing the effects of CAL130 against human primary T-ALL cells in vivo we generated an extended experimental group of mice xenografted with a human primary T-ALL sample which demonstrated strong response to CAL130. This sample was characteristically negative for PTEN expression. Treatment of Rag gammaC mice xenografted with human primary T-ALL cells showed antileukemic effects of CAL130 in vivo as assesses by analysis of cell cycle progression in peripheral blood lymphoblasts and by partial reconstitution of normal hematopoiesis compared to vehicle only treated controls.

Effects of PI3K-AKT inhibition in combination with chemotherapy (Aim 3, Task 4 and Task 5)
Analysis of the antileukemic effects of CAL130 in combination with chemotherapy showed a marked interaction between inhibition of the PI3K pathway and glucocorticoid therapy in T-ALL. Over the last year we have analyzed the mechanisms mediating this interaction and tested the effects of PI3K activation in glucocorticoid resistance in vitro and in vivo. To test the effects of PI3K-AKT activation in glucocorticoid resistance we performed *PTEN* inactivation in DND41 cells by shRNA knockdown, which resulted in drastic reduction of PTEN protein levels and increased phosphorylation of AKT1 compared to control cells infected with shRNAs targeting the Luciferase gene (**Fig. 7a**). Treatment of *PTEN* knockdown and control DND41 cells with dexamethasone showed that loss of PTEN and consequent AKT1 activation results in blunted induction of glucocorticoid induced apoptosis in T-ALL (**Fig. 7b,c**). The glucocorticoid receptor (NR3C1) functions as a ligand activated transcription factor. Gene expression analysis showed a marked reduction in the regulation of glucocorticoid upregulated and glucocorticoid downregulated transcripts in DND41 PTEN knockdown cells treated with dexamethasone compared with dexamethasone treated knockdown control cells (**Fig. 7d-f**). Consistently, expression of an activated myristoylated form of AKT1 (MYR-AKT1) diminished the capacity of the glucocorticoid receptor to activate a luciferase reporter construct under the control of a synthetic glucocorticoid response element (**Fig. 7g**). Overall these results suggest that AKT1 can promote glucocorticoid resistance via inhibition of the glucocorticoid receptor.
To test if AKT1 can interact and inhibit the glucocorticoid receptor protein, we transfected 293T cells with plasmid constructs driving the expression of Flag-tagged AKT1 and HA-tagged NR3C1 and isolated glucocorticoid receptor-containing protein complexes via immunoprecipitation using an anti-HA antibody. Western blot analysis demonstrated the presence of Flag-AKT1 in HA-NR3C1 immunoprecipitates, suggesting that AKT1 can interact with NR3C1 *in vivo* (**Fig. 8a**). Reciprocal immunoprecipitation experiments confirmed the association between Flag-AKT1 and HA-NR3C1 (**Fig. 8b**). Moreover, immunoprecipitation of NR3C1 protein complexes from the T-ALL cell lines DND41 demonstrated that endogenous NR3C1 and AKT1 can interact in T-ALL lymphoblast cells (**Fig. 8c**). In addition, immunofluorescence analysis showed colocalization of NR3C1 and AKT1 in DND41 cells (**Fig.8d**). Finally, glutathione-S-transferase (GST)-pulldown assays showed that recombinant GST-NR3C1 fusion protein can directly interact with His-tagged AKT1 *in vitro* (**Fig. 8e**).

AKT1 kinase substrates are typically phosphorylated by AKT at RXRXXS/T motifs. Phospho-AKT motif scanning analysis of NR3C1 revealed a potential AKT phosphorylation motif ^{131}RSTS^{134} (**Fig. 3f**), suggesting that the glucocorticoid receptor could be an AKT1 substrate phosphorylated at serine 134. Notably, mass spectrometry analysis of HA-NR3C1 protein isolated from MYR-AKT1 expressing cells demonstrated the presence of serine phosphorylation at position 134 of the glucocorticoid receptor (**Fig. 8g,h**). Mass spectrometry of the digested peptides by nanoLC-ESI-MS/MS verified the presence of NRC31 phosphorylation at S134 [ratio non-phosphorylated peptide: phosphorylated peptide (non-P:P)= 1.5:1] in addition to other previously characterized NR3C1 phospho-sites including T8 (non-P:P= 10:1), S45 (non-P:P= 20:1), S203 (non-P:P= 1:1) and S267 (non-P:P= 25:1). To further test this possibility, we expressed HA-tagged wild type NR3C1 (HA-NR3C1) or an HA-tagged form of the glucocorticoid receptor with a serine to alanine substitution at position 134 (HA-NR3C1 S134A) in cells infected with retroviruses expressing MYR-AKT1. Protein immunoprecipitation of NR3C1 with an antibody against HA and subsequent Western blot analysis with an antibody recognizing the phospho-RXXS/T AKT phosphorylation motif showed the presence of a HA-NR3C1 phospho-AKT band in cells expressing the wild type glucocorticoid receptor, but not in cells expressing the HA-NR3C1 S134A mutant (**Fig. 8i**). Next, we performed *in vitro* kinase assays in which we analyzed the capacity of the AKT1 kinase to phosphorylate the wild type or S134A glucocorticoid receptor proteins. This assay demonstrated that AKT1 can effectively phosphorylate recombinant wild type NR3C1 protein *in vitro*, but not the serine 134 to alanine NR3C1 mutant protein (**Fig. 8j**). Finally, and most notably, western blot analysis with the AKT phosphorylation motif antibody showed decreased AKT phosphorylated NR3C1 in NR3C1 immunoprecipitates from CCRF-CEM T-ALL cells treated with MK2206, a highly potent and selective AKT inhibitor (**Fig. 8k**).

After establishing the interaction and phosphorylation of the glucocorticoid receptor by AKT1 we sought to elucidate the relevance of the NR3C1 S134 phosphorylation for glucocorticoid receptor function. Glucocorticoid induced cytoplasmic-nuclear shuttling is strictly required for glucocorticoid receptor activity. U2OS cells, which express undetectable levels of endogenous NR3C1, showed cytoplasmic localization of retrovirally expressed HA-tagged glucocorticoid receptor protein, which was completely relocalized to the nucleus upon dexamethasone treatment (**Fig. 9a**). Notably, expression of MYR-AKT1 in these cells resulted in impaired nuclear relocalization of NR3C1 after dexamethasone treatment (**Fig. 9b**). In addition, and in contrast with wild type glucocorticoid receptor, the NR3C1 S134A mutant protein showed increased nuclear localization in basal conditions and effective nuclear relocalization upon dexamethasone treatment (**Fig. 9c**), even upon expression of MYR-AKT1 (**Fig. 9d**). Next we analyzed the capacity of MK2206 to modulate glucocorticoid induced translocation of NR3C1 to the nucleus in T-ALL cells. CCRF-CEM, a PTEN null, glucocorticoid resistant, T-ALL cell line expressing high levels of AKT activation (**Fig. 9e**) showed cytoplasmic localization NR3C1 in basal conditions, which was only partially relocalized to the nucleus upon dexamethasone treatment (**Fig. 9e**). Inhibition of AKT with MK2206 effectively enhanced glucocorticoid-induced translocation of the NR3C1 protein to the nucleus in these cells (**Fig. 9e**). Notably, similar results were obtained in primary T-ALL lymphoblasts in which inhibition of AKT with MK2206 increased the nuclear translocation of the NR3C1 protein following glucocorticoid treatment (**Fig. 9f**).

Next we analyzed if AKT inhibition with MK2006 could broadly enhance the antileukemic effects of glucocorticoids and reverse glucocorticoid resistance in T-ALL. Treatment of CCRF-CEM cells with increasing doses of dexamethasone in the presence or absence of MK2206 showed effective reversal of glucocorticoid resistance upon AKT inhibition (**Fig. 10a**). Next we analyzed the effects of MK2206 and glucocorticoid *in vivo* in a xenograft model of glucocorticoid-resistant T-ALL. CCRF-CEM cells expressing the luciferase gene were injected intravenously in immunodeficient NOG mice and tumor engraftment was assessed by *in vivo* bioimaging at day 18. Animals harboring homogeneous tumor burdens were treated with vehicle only (DMSO), MK2206, dexamethasone or MK2206 plus dexamethasone for 3 days. In this experiment, animals treated with dexamethasone or MK2206 showed progressive tumor growth similar to

that observed in vehicle-treated controls, while mice treated with MK2206 plus dexamethasone had significant antitumor responses (**Fig. 10b**; $P < 0.05$).

Next, we evaluated the response to the combination treatment MK2206 plus dexamethasone in primary T-ALL lymphoblasts. Towards this goal we established viable *in vitro* cultures of T-ALL leukemia samples supported by bone marrow MS5 stroma cells expressing the Delta like 1 NOTCH1 ligand. Treatment of T-ALL primary leukemia cultures with MK2206 plus dexamethasone in combination showed significantly increased antileukemic effects compared with treatment with dexamethasone or MK2206 alone in primary T-ALLs (**Fig. 10c,d**).

To further test the efficacy of this treatment combination *in vivo* we established leukemia xenografts in NOD rag gamma immunodeficient mice using two independent primary T-ALL samples infected with lentiviruses expressing the luciferase gene. Animals harboring homogeneous tumor burdens by *in vivo* bioimaging were treated with vehicle only (DMSO), MK2206, dexamethasone or MK2206 plus dexamethasone. In this experiment, mice treated with dexamethasone or MK2206 showed progressive tumor growth similar to that observed in vehicle-treated controls, while mice treated with MK2206 plus dexamethasone showed significant antitumor responses (**Fig. 10e-h**).

Finally, we generated a mouse leukemia model in which glucocorticoid resistance is specifically driven by genetic loss of *Pten*. In this model, transplantation of tamoxifen-inducible conditional *Pten* knockout (Rosa26TMCre *Pten*$^{flox/flox}$) hematopoietic progenitors infected with retroviruses expressing a mutant constitutively active form of the NOTCH1 receptor (*NOTCH1* L1601P ΔPEST) resulted in the development of NOTCH1 driven T-ALL tumors as previously described. Next we infected *NOTCH1* Rosa26TMCre *Pten*$^{flox/flox}$ T-ALL lymphoblasts with a luciferase expressing retrovirus and transplanted them into secondary recipients which were treated with vehicle only or tamoxifen in order to generate *Pten*-non-deleted and *Pten*-deleted isogenic tumors, respectively. Treatment of *Pten*-non-deleted tumor bearing mice with dexamethasone showed a significant improvement in survival compared with vehicle only treated controls ($P < 0.01$) (**Figure 11A**). In contrast, and consistent with a role of *Pten* loss and AKT1 activation in promoting glucocorticoid resistance, all mice harboring *Pten*-deleted tumors failed to respond to dexamethasone treatment and showed no survival differences compared to vehicle treated controls (**Figure 11B**).

To test the efficacy of MK2206 and glucocorticoids in combination we treated mice transplanted with *NOTCH1*-induced *Pten*-deleted murine tumors expressing luciferase in secondary recipients, with vehicle only (DMSO), MK2206, dexamethasone or MK2206 plus dexamethasone and monitored their response to therapy by *in vivo* bioimaging. Animals treated with dexamethasone or MK2206 in this experiment showed progressive tumor growth similar to that observed in vehicle-treated controls, while mice treated with MK2206 plus dexamethasone showed significant antitumor responses (**Figure 11C,D**; $P < 0.001$) which translated in significantly improved survival in this group (**Figure 11E**; $P < 0.001$). Finally, we analyzed the role of NR3C1 S134 phosphorylation in the therapeutic response to glucocorticoids and the effects of *Pten* loss in glucocorticoid therapy in this model. Retroviral expression of the glucocorticoid receptor in *Pten* non-deleted lymphoblasts enhanced the response of NOTCH1-induced leukemias to glucocorticoid treatment; an effect that was effectively abrogated upon *Pten* loss (**Figure 11F**). In contrast, expression of the AKT-resistant NR3C1 S134A mutant protein was equally effective at increasing the antileukemic effects of glucocorticoids in *Pten* non-deleted and *Pten* null lymphoblasts (**Figure 11G**). Overall, these results support that pharmacologic inhibition of the PI3K pathway can effectively enhance glucocorticoid response and reverse glucocorticoid resistance in T-ALL.

Key research accomplishments

- Development of an extended panel of primary T-ALL cultures and primary xenograft models of human T-ALL (Aim 3 Task1).
- Demonstration of antileukemic effects of CAL130 against primary human T-ALL samples in vitro (Aim 3, Task 2).

- Demonstration of antileukemic effects of CAL130 against primary human T-ALL samples in vivo (Aim 3, Task 3) and analysis of PTEN and NOTCH status in these samples (Aim 3, Task 6)
- Identification of a therapeutically relevant interaction between the PI3K-AKT signaling pathway and glucocorticoid resistance in T-ALL (Aim 3 Task 4 and task 5)

Reportable outcomes

Manuscripts:

1. Erich Piovan, Jiyang Yu, Valeria Tosello, Daniel Herranz, Alberto Ambesi-Impiombato, Ana Carolina Da Silva, Arianne Perez-Garcia, Isaura Rigo, Mireia Castillo, Stefano Indraccolo, Elisabeth Paietta, Janis Racevskis, Jacob M Rowe, Martin S Tallman, Giuseppe Basso, Jules P Meijerink, Carlos Cordon-Cardo, Andrea Califano and **Adolfo A. Ferrando** Direct reversal of glucocorticoid resistance by AKT inhibition in T-ALL. **Cancer Cell** *in press*

2. Subramaniam PS, Whye DW, Efimenko E, Chen J, Tosello V, De Keersmaecker K, Kashishian A, Thompson MA, Castillo M, Cordon-Cardo C, Davé UP, **Ferrando A**, Lannutti BJ, Diacovo TG. Targeting Nonclassical Oncogenes for Therapy in T-ALL. **Cancer Cell**. 2012; 21:459-72.

Meeting abstracts:

American Society of Hematology 52nd Meeting and Exposition, Orlando, December 2010

*Oncogenic AKT Signaling Negatively Regulates Glucocorticoid Receptor Function to Promote Glucocorticoid Resistance In T Cell Acute Lymphoblastic Leukemia Blood (ASH Annual Meeting Abstracts), Abstract 11
Authors: Erich Piovan, Jiyang Yu, Pedro Real, Gawinowicz Mary Ann, Andrea Califano, and Adolfo Ferrando

Tissue repositories: a human T-ALL primary xenograft bank has been generated with 30 specimens linked to detailed genetic and molecular information

Animal models: a new mouse model for experimental therapeutics of NOTCH1 induced leukemia and analysis of the effects of Pten deletion in therapy response has been generated (luciferaced, NOTCH1HD-DeltaPEST, Rosa26-TM-Cre Pten f/f).

Conclusion

This project has achieved all its proposed goals and objectives and has firmly established the role of the PI3K-AKT pathway as a therapeutic target in T-ALL. The demonstration of a strong antileukemic effect of CAL130 against primary human leukemia samples in vitro and in vivo warrants the clinical testing of this inhibitor in the clinic. Moreover the identification of a strong, specific and mechanistically well defined interaction between inhibition of the PI3K pathway and glucocorticoids resulting in effective reversal of glucocorticoid resistance provides further rationale to implement this combination in the clinic.

References

N/A

Appendices

Appendix 1: Published Manuscript

Subramaniam PS, Whye DW, Efimenko E, Chen J, Tosello V, De Keersmaecker K, Kashishian A, Thompson MA, Castillo M, Cordon-Cardo C, Davé UP, Ferrando A, Lannutti BJ, Diacovo TG. Targeting Nonclassical Oncogenes for Therapy in T-ALL. **Cancer Cell**. 2012; 21:459-72.

Cancer Cell
Article

Targeting Nonclassical Oncogenes for Therapy in T-ALL

Prem S. Subramaniam,[1] Dosh W. Whye,[1] Evgeni Efimenko,[1] Jianchung Chen,[1] Valeria Tosello,[3] Kim De Keersmaecker,[3] Adam Kashishian,[4,5] Mary Ann Thompson,[6] Mireia Castillo,[8] Carlos Cordon-Cardo,[8] Utpal P. Davé,[7] Adolfo Ferrando,[1,2,3] Brian J. Lannutti,[4,5] and Thomas G. Diacovo[1,2,*]
[1]Department of Pediatrics
[2]Department of Pathology and Cell Biology
Columbia University Medical Center, New York, NY 10032, USA
[3]Institute for Cancer Genetics, Columbia University, New York, NY 10032, USA
[4]Calistoga Pharmaceuticals, Seattle, WA 9810, USA
[5]Gilead Sciences, Seattle, WA 9810, USA
[6]Department of Pathology
[7]Department of Medicine and Cancer Biology
Vanderbilt University Medical Center, Nashville, TN 37232, USA
[8]Department of Genetics and Genomic Sciences, The Mount Sinai School of Medicine, New York, NY 10029, USA
*Correspondence: td2142@columbia.edu
DOI 10.1016/j.ccr.2012.02.029

SUMMARY

Constitutive phosphoinositide 3-kinase (PI3K)/Akt activation is common in T cell acute lymphoblastic leukemia (T-ALL). Although four distinct class I PI3K isoforms (α, β, γ, δ) could participate in T-ALL pathogenesis, none has been implicated in this process. We report that in the absence of PTEN phosphatase tumor suppressor function, PI3Kγ or PI3Kδ alone can support leukemogenesis, whereas inactivation of both isoforms suppressed tumor formation. The reliance of PTEN null T-ALL on the combined activities of PI3Kγ/δ was further demonstrated by the ability of a dual inhibitor to reduce disease burden and prolong survival in mice as well as prevent proliferation and promote activation of proapoptotic pathways in human tumors. These results support combined inhibition of PI3Kγ/δ as therapy for T-ALL.

INTRODUCTION

Constitutive activation of the phosphoinositide 3-kinase (PI3K)/Akt signal transduction pathway is a common event in cancer, promoting the growth, proliferation, and survival of various types of tumors including T cell acute lymphoblastic leukemia (T-ALL) (Yuan and Cantley, 2008; Zhao and Vogt, 2008; Gutierrez et al., 2009; Palomero et al., 2008; Silva et al., 2008; Larson Gedman et al., 2009). Class I PI3Ks are a family of lipid kinases that generate the potent second messenger phosphatidylinositol-3,4,5 trisphosphate (PIP_3) in response to ligation of a number of distinct cell surface receptors (Katso et al., 2001; Cantley, 2002). This results in the activation of Akt as well as numerous downstream effector molecules, which ultimately promote cell growth and survival. Class I PI3Ks are heterodimeric molecules composed of a regulatory and a catalytic subunit, the latter consisting of four unique isoforms that include p110α, p110β, p110γ, and p110δ. Each is capable of regulating distinct biological functions in normal tissues and cellular compartments. However, some overlap in activity does exist, as is the case for thymocytes where the combined activities of PI3Kγ and PI3Kδ contribute to cellular processes required for the generation and function of mature T cells (Webb et al., 2005; Swat et al., 2006; Ji et al., 2007). Although the importance of these two PI3K isoforms in T cell biology is well established (Okkenhaug and Vanhaesebroeck, 2003), what role, if any, they

Significance

Loss of PTEN function is a frequent occurrence in cancer resulting in unbridled PI3K/Akt signaling that contributes to tumor pathogenesis. Consequently, much emphasis has been placed on developing inhibitors that target this pathway. Here, we report that PI3Kγ and PI3Kδ act as a tumorigenic bottleneck in PTEN null T-ALL. We also demonstrate that it is possible to exploit the "addiction" of a hematological malignancy to specific PI3K isoforms, enabling the rational design of a PI3Kγ/δ dual inhibitor. This work represents a significant advancement in our understanding of the dynamic interplay that exists between PTEN and particular PI3K isoforms in regulating both normal and abnormal T cell development as well as in sustaining tumor cell proliferation and survival.

play in malignant transformation and tumor cell survival remains to be determined.

Previously, it has been reported that p110α is involved in oncogenesis because function-enhancing mutations in this catalytic subunit are found in many cancers of solid organs (Samuels et al., 2004; Zunder et al., 2008). In contrast, cancer-specific mutations have yet to be identified for the other p110 isoforms. That said, overexpression of p110β, p110γ, or p110δ in an in vitro culture system induces cellular transformation (Kang et al., 2006). Moreover, increased or preferential expression of p110γ and p110δ has been described in chronic and acute forms of myeloid leukemia, respectively (Hickey and Cotter, 2006; Sujobert et al., 2005). However, to our knowledge, overexpression of specific PI3K isoforms has not been reported for T-ALL, and mutations in PI3Kα are rare, suggesting that they are not a major contributor to its pathogenesis (Gutierrez et al., 2009; Lo et al., 2009).

PTEN is a nonredundant plasma-membrane phosphatase that is responsible for counteracting the potential cancer-promoting activities of class I PI3K (Sulis and Parsons, 2003; Salmena et al., 2008). It does so by limiting the levels of PIP_3 generated in response to the activation of these lipid kinases. Clinically, mutations in the *PTEN* tumor suppressor gene are common in multiple types of human cancer, resulting in unbridled PI3K/Akt signaling as well as conferring resistance to chemotherapeutic agents (Carnero et al., 2008; Huang and Hung, 2009). It has been well established that deletion of the tumor suppressor gene *PTEN* in T cell progenitors drives the malignant transformation of these cells within the thymus of mice (Suzuki et al., 2001; Hagenbeek and Spits, 2008; Liu et al., 2010). Moreover, the resulting tumors possess similar genetic and biochemical aberrations associated with a subset of patients with T-ALL including hyperactivation of the PI3K/Akt signaling pathway (Maser et al., 2007; Guo et al., 2008). In fact Gutierrez et al. (2009) have reported a loss of PTEN function due to mutations or deletions in approximately 40% of primary T-ALL samples, suggesting that hyperactivation of the PI3K/Akt signaling pathway is a common feature of this hematological malignancy. Based on these clinical observations and known reliance of thymocyte development on PI3Kγ and PI3Kδ, we set out to determine whether these nonclassical oncogenes contribute to leukemogenesis and if it is possible to exploit tumor cell "addiction" to the activity of distinct PI3K isoforms, thus permitting the rational design of a chemotherapeutic agent to treat T-ALL.

RESULTS

PI3Kγ or PI3Kδ Can Support Malignant Transformation of T Cells

We crossed mice containing both *Pten* alleles floxed by the loxP Cre excision sites with *Lck*-cre transgenic animals (*Lck/Pten*$^{fl/fl}$) alone or together with those lacking p110γ, encoded by *Pik3cg*, and/or p110δ, encoded by *Pik3cd*, catalytic subunits. Consistent with previous studies, >85% of *Lck/Pten*$^{fl/fl}$ mice develop T-ALL and eventually succumb to the disease (median survival of 140 days), which was confirmed by flow cytometric analysis (Figures 1A and 1B). In contrast to PTEN null tumors of solid organs that have been reported to rely on PI3Kβ activity (Jia et al., 2008; Wee et al., 2008), tumorigenesis in the context of a deficiency of PTEN in T cell progenitors appears to be critically dependent on PI3Kγ and PI3Kδ. This is evidenced by the marked delay in the onset of disease and increased survival of *Lck/Pten*$^{fl/fl}$*;Pik3cg*$^{-/-}$*;Pik3cd*$^{-/-}$ triple-mutant mice (TKO) because <20% of animals succumb to T-ALL by 220 days. However, the activity of either isoform alone was sufficient to promote tumor formation, yielding similar median survival times for *Lck/Pten*$^{fl/fl}$*;Pik3cg*$^{-/-}$ and *Lck/Pten*$^{fl/fl}$*;Pik3cd*$^{-/-}$ mice (175 versus 178 days, respectively). Comparable percentages of these animals developed and died of T-ALL (65% versus 64%, respectively), and tumors had evidence of activation of the PI3K/Akt signaling pathway, albeit much reduced as compared to those from *Lck/Pten*$^{fl/fl}$ animals (Figure 1C). However, there was no evidence of overexpression of any *Pik3c* isoform in thymic tumors (Figure 1D).

Further evidence demonstrating that it is the unleashed activities of PI3Kγ and PI3Kδ that provide the signals necessary for the development of T-ALL is suggested by the continued reduction in thymus size and cellularity in 6-week-old TKO mice (Figure 2A). Although absence of PTEN should permit unrestricted activity of all four class I PI3K isoforms, it appears that PI3Kα and PI3Kβ cannot adequately compensate for their γ and δ counterparts as evidenced by the persistent diminution in the total number of $CD4^+CD8^+$ double-positive thymocyte population and near-basal levels of phosphorylated Akt (Ser473) as compared to mice deficient in PTEN alone (Figures 2A and 2B). Cellular alterations associated with p110γ/δ double deficiency also persisted in the peripheral blood and in secondary lymphoid organs of TKO mice and included a paucity of $CD3^+$ T cells (Figures 2C and 2D). No active tumor was found in peripheral blood or spleen of the surviving animals at ~7 months of age as determine by absence of staining for the proliferation marker Ki67 on Thy1.2-positive cells (Figure 2E).

Effect of PI3Kγ/PI3Kδ Dual Inhibition on Thymocyte Signaling and Development

In order to ascertain whether PI3Kγ and PI3Kδ are also required for tumor maintenance and can be targeted therapeutically in T-ALL, we generated a small molecule that preferentially inhibits the function of both p110γ and p110δ catalytic domains, designated CAL-130 (Figure 3A). IC_{50} values of this compound were 1.3 and 6.1 nM for p110δ and p110γ, respectively, as compared to 115 and 56 nM for p110α and p110β. Importantly, this small molecule does not inhibit additional intracellular signaling pathways (i.e., p38 mitogen-activated protein kinase or insulin receptor tyrosine kinase) that are critical for general cell function and survival (Table 1; see Table S1 available online). To demonstrate that CAL-130 can block the activities of both PI3Kδ and PI3Kγ in thymocytes, we evaluated its ability to prevent phosphorylation of Akt (Ser473) and calcium flux in response to T cell receptor (TCR) crosslinking. Previously, we have shown that the combined activities of these two class I PI3K isoforms are necessary for phosphorylation of this protein kinase in this cell population (Swat et al., 2006). Consistent with these results, CAL-130 treatment of thymocytes harvested from 6-week-old WT animals prevented TCR-induced Akt phosphorylation and attenuated calcium flux to levels observed for their *Pik3cg*$^{-/-}$*;Pik3cd*$^{-/-}$ counterparts (Figures 3B, 3C, and S1A).

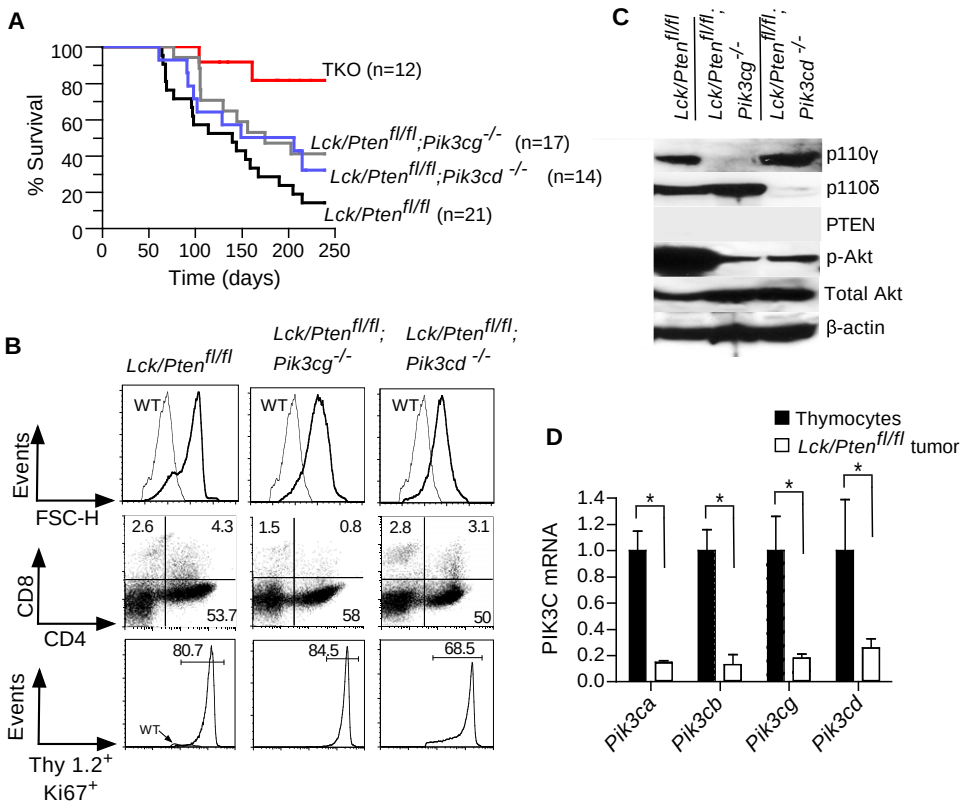

Figure 1. PI3Kγ or PI3Kδ Can Support Leukemogenesis in the Context of PTEN Deficiency

(A) Kaplan-Meyer survival curves demonstrating the requirement for PI3Kγ and PI3Kδ activity in the development of PTEN null T-ALL. All animals were followed for a period of 7 months.

(B) Representative flow cytometric profiles of peripheral blood from diseased mice lacking p110γ or p110δ in the absence of PTEN in T cell progenitors. Forward scatter (FSC) and Ki67 staining are indicators of cell size and proliferation, respectively. Thy 1.2 expression identifies T-lineage cells.

(C) Representative immunoblots depicting p110γ, p110δ, and PTEN expression as well as Akt activation state (phosphorylation of Ser473) in thymic lysates from the same animals.

(D) Quantitative reverse-transcription PCR analysis of *Pik3c (a/b/g/d)* transcript levels in WT thymocytes (n = 5) and tumors (n = 5) harvested from *Lck/Pten*$^{fl/fl}$ mice. Error bars represent ±SD. The difference in *Pik2c* expression levels between the WT thymocytes and tumor cells was statistically significant (*$p < 0.05$) using a Student's t test.

To assess the in vivo efficacy of the inhibitor, we determined its effects on thymi of 6-week-old WT mice, specifically for its ability to recapitulate the phenotype observed when both p110γ and p110δ are deficient. Animals received 10 mg kg^{-1} of the inhibitor orally, which was sufficient to maintain plasma concentrations of 0.33 ± 0.18 μM at the end of 8 hr (Figure 3D). Notably, this dose did not affect either plasma glucose or insulin levels in contrast to the metabolic perturbations associated with tissue-specific deficiencies in p110α and p110β (Figures 3E and 3F) (Jia et al., 2008; Sopasakis et al., 2010). CAL-130 was also found to have a limited ability to impair PDGF-induced activation of PI3Kα as compared to the pan-PI3K/mTOR inhibitor BEZ235 (Figure S1B). Similarly, platelets harvested from *Pik3cg*$^{-/-}$*;Pik3cd*$^{-/-}$ mice 2 hr post-administration of CAL-130 had no obvious defect in ADP-mediated platelet aggregation, a process known to rely predominantly on PI3Kβ (Figure S1C) (Jackson et al., 2005). However, CAL-130 treatment (10 mg kg^{-1} every 8 hr) for a period of 7 days markedly affected the size, cellularity, and overall architecture of the thymus faithfully reproducing the phenotype associated with *Pik3cg*$^{-/-}$*;Pik3cd*$^{-/-}$ mice (Figure 3G). In particular there was a 18-fold reduction in total thymocyte number in comparison to controls, which was primarily due to the loss of DP population (Figure 3H). These observations are consistent with the ability of CAL-130 to preferentially block the function of both PI3Kγ and PI3Kδ.

Antileukemic Effects of Pharmacological Inhibition of PI3Kγ and PI3Kδ in PTEN Null T-ALL Tumors in Mice

The clinical significance of interfering with the combined activities of PI3Kγ and PI3Kδ was determined by administering CAL-130 to *Lck/Pten*$^{fl/fl}$ mice with established T-ALL. Candidate animals for survival studies were ill appearing, had a white blood cell (WBC) count above 45,000 μl^{-1}, evidence of blasts on peripheral smear, and a majority of circulation cells (>75%) staining double positive for Thy1.2 and Ki-67. Mice received an oral dose (10 mg kg^{-1}) of the inhibitor every 8 hr for a period of 7 days and were then followed until moribund. Despite the limited duration of therapy, CAL-130 was highly effective in extending the median survival for treated animals to 45 days as compared 7.5 days for the control group (Figure 4A).

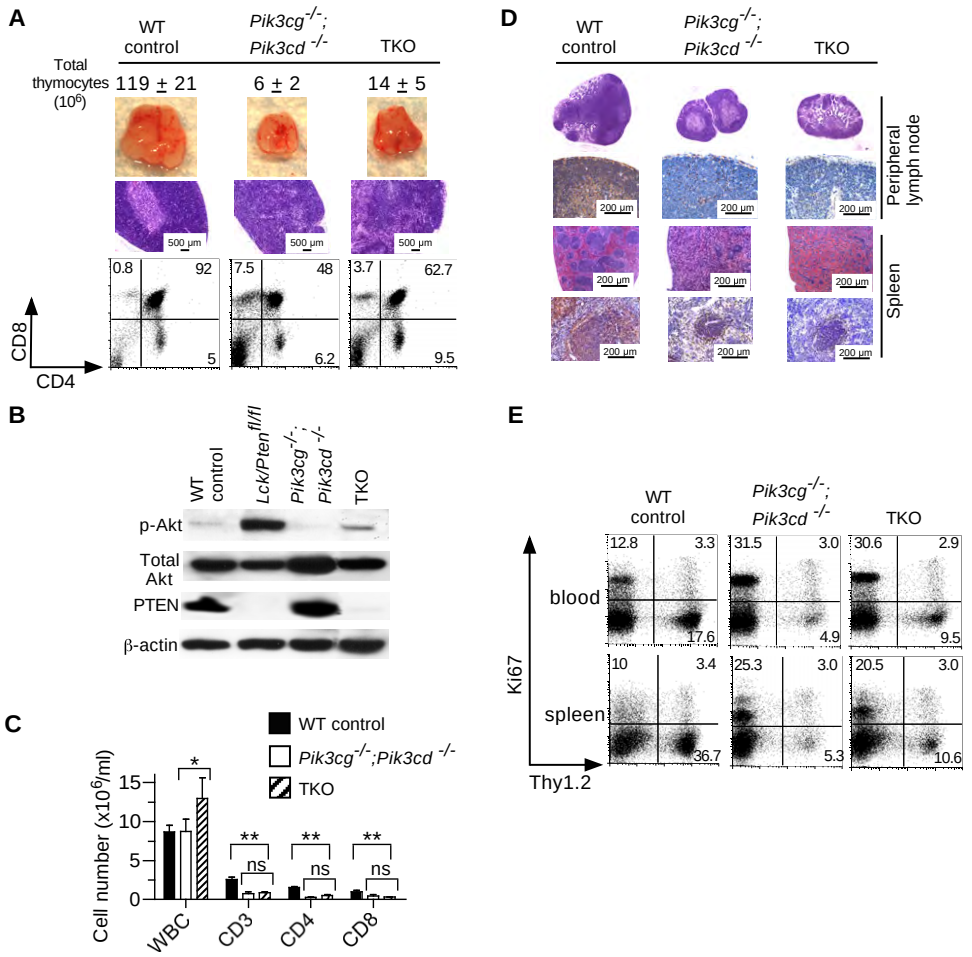

Figure 2. Persistence of Cellular and Structural Defects in Thymi Associated with a Combined Deletion of p110γ/p110δ and PTEN

(A) Hematoxylin and eosin staining (H&E) and flow cytometric analyses of thymi derived from 6-week-old mice lacking both p110γ and p110δ catalytic subunits in the presence or absence of PTEN. The panels are representative of data from five animals in each group.

(B) Immunoblots assessing for Akt phosphorylation (Ser473) and PTEN levels in thymocyte lysates.

(C) Number of WBC and T cell subsets in the peripheral blood of the same animals. *ns (not significant) for *Pik3cg*$^{-/-}$;*Pik3cd*$^{-/-}$ versus TKO; **$p < 0.01$ for WT versus TKO.

(D and E) Representative (D) micrografts of H&E peripheral lymph nodes and spleen and (E) flow cytometry plots of blood and spleen from triple mutant animals (n = 5 mice per genotype). Histological identification of T cells was by immunoperoxidase detection of CD3. Scale bars correspond to 200 μm in secondary lymphoid organs and to 500 μm in thymi. Data represent the mean ± SD.

To determine the effect of CAL-130 on disease burden, we performed sequential blood counts and peripheral smears as well as flow cytometric analyses on *Lck/Pten*$^{fl/fl}$ mice pre- and post-administration of the inhibitor (Figures 4B and S2A–S2C). All animals showed a dramatic reduction in WBC count by day 4 reflected in the loss of the highly proliferative blast population (Thy1.2/Ki-67 double positive, high FSC-H), which remained at low levels for the duration of treatment. Moreover, both CD4 single-positive and CD4/CD8 double-positive T-ALL responded to CAL-130, which corresponded with an increase in apoptosis detected as sub-G0 population after propidium iodide (PI) staining on days 4–7. Treatment of diseased *Lck/Pten*$^{fl/fl}$;*Pik3cg*$^{-/-}$ mice but not their *Lck/Pten*$^{fl/fl}$ counterparts with the PI3Kδ selective inhibitor IC87114 (10 mg kg^{-1} every 8 hr) produced similar results, confirming the critical reliance of PTEN null tumors on the combined activities of PI3Kγ and PI3Kδ (Figures 4C and S2D).

Further evidence to support the ability of CAL-130 to reduce tumor burden was obtained by bioluminescent imaging. *Pten*$^{fl/fl}$ mice were crossed with a strain in which a luciferase cDNA, preceded by a LoxP-stop-LoxP cassette, was introduced into the ubiquitously expressed *ROSA26* locus (Safran et al., 2003). Progenies were then crossed with *Lck*-cre transgenics to delete *Pten* in T cell progenitors and induce expression of luciferase (*Lck/Pten*$^{fl/fl}$;*Gt(ROSA)26Sor*$^{tm1(Luc)Kael}$/J). Imaging of T-ALL tumor-bearing animals was performed just prior to and after 4 days of treatment with CAL-130. Signals at day 4 were dramatically lower in treated animals, consistent with the reduction in the WBC count and the CD4 single-positive population of tumor cells (Figure 4D). Moreover, weights of thymi, liver, spleen, and kidneys from treated *Pten*$^{fl/fl}$ mice were significantly less than that for animals that received vehicle control for 7 days (Figure 4E).

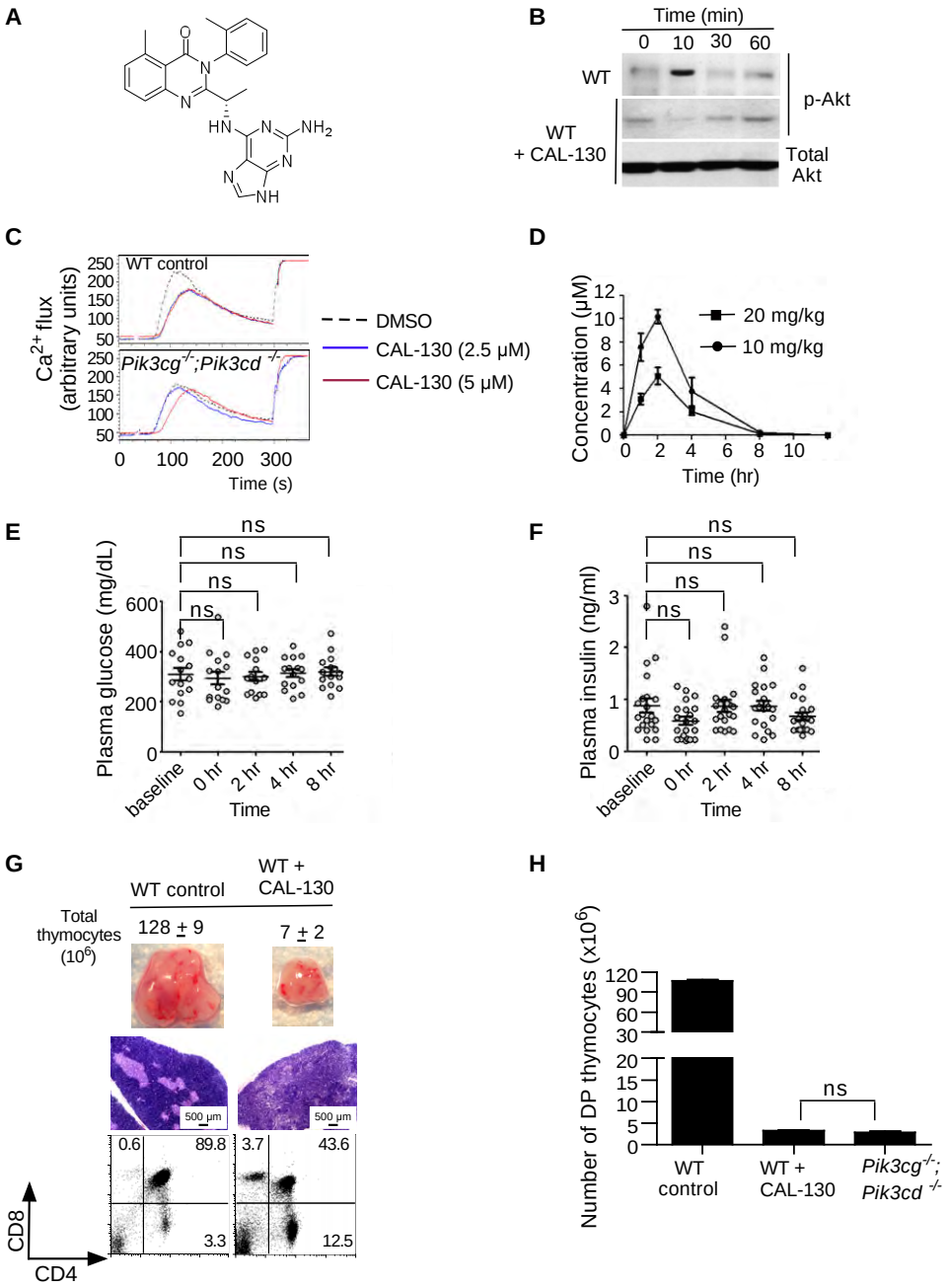

Figure 3. Inhibitory Profile of CAL-130

(A) Chemical structure of CAL-130.

(B and C) Effect of the inhibitor on (B) Akt phosphorylation (Ser473) or (C) Ca^{2+} flux in purified thymocytes from WT or *Pik3cg*$^{-/-}$;*Pik3cd*$^{-/-}$ animals in response to TCR crosslinking. Data are representative of three separate experiments.

(D) Plasma concentrations of CAL-130 in mice after a single oral dose (n = 4).

(E and F) Plasma glucose (E) and corresponding insulin levels (F) in WT mice before and after receiving a single dose of inhibitor (10 mg kg^{-1}). $p > 0.5$ for glucose and $p > 0.2$ for insulin as compared to baseline (n = 15 mice per time point; ns, not significant).

(G) Phenotypic analyses of thymi from mice treated with either CAL-130 (10 mg kg^{-1} every 8 hr) or vehicle control for 7 days. The panels are representative of data from five animals in each group.

(H) Total DP thymocyte count in the same animals in (G). Results are compared to PI3Kγ/δ double-knockout mice. Data represent the mean ± SD.

See also Figure S1.

Table 1. P110 Catalytic Domain Selectivity of CAL-130 as Assessed by Ambit KinomeScan Screening

Ambit Gene Symbol	Control Binding (%)	Ambit Gene Symbol	Control Binding (%)
PIK3CA	12	PIK3CG	3.2
PIK3CB	10	PIK3CD	0.2

CAL-130 (10 μM) was evaluated for its ability to prevent tagged kinases from interacting with immobilized "bait" ligand (Fabian et al., 2005; Karaman et al., 2008). Results are reported as percentage (%) of control binding, where lower numbers indicate stronger interactions with the tagged kinase. Values >35% are considered "no hits." PI3Kδ had the lowest percentage of control binding at 0.2% followed by PI3Kγ at 3.2%, indicating a high probability of a potent interaction. A total of 353 kinases were assessed in the screen (Table S1).

Reliance of PTEN Null Human T-ALL on PI3Kγ and PI3Kδ

To test whether CAL-130 may have similar effects on human tumors, we first analyzed the response of T-ALL cell lines to the compound. Incubation of cultured cells with CAL-130, but not inhibitors of either PI3Kγ or PI3Kδ, prevented proliferation and promoted apoptosis within 24 hr, which persisted over 4 days of treatment (Figures 5A, 5B, and S3A–S3J). To further demonstrate that the combined activities of PI3Kγ and PI3Kδ are essential for these processes, we utilized an shRNA vector that targeted the p110γ catalytic domain in CCRF-CEM cells. Western blot analysis revealed a >95% reduction in expression of p110γ with no effect on the other isoforms (Figure 5C, inset). Subsequent incubation of these cells with the PI3Kδ-specific inhibitor IC87114 prevented proliferation and promoted apoptosis as observed for nontransfected CCRF-CEM exposed to CAL-130 (Figures 5C and 5D). In contrast, IC87114 had no major effect on cells containing empty vector alone; neither did siRNA knockdown of either p110α or p110β (Figures S3K–S3N). These observations are consistent with our in vivo studies demonstrating that PI3Kγ and PI3Kδ are strictly required for the proliferation and survival of T-ALL lymphoblasts. Moreover, blockade of these two isoforms significantly enhanced the apoptotic properties of dexamethasone, a drug of considerable importance in the treatment of various lymphoid malignancies including T-ALL (Figures 5E–5H) (Beesley et al., 2009).

It is well known that PI3K/Akt signaling pathway can play a major role in cell-cycle progression and growth of tumors by regulating the activation state of the downstream targets such as glycogen synthase kinase-3β (GSK3β) and mTOR (Schmelzle and Hall, 2000; Cohen and Frame, 2001). PI3K/Akt-mediated phosphorylation suppresses the function of the former and promotes the activity of the latter. Tumor cell survival, on the other hand, is largely mediated by the ability of this pathway to inactivate proapoptotic effectors such as the BH3-only proapoptotic protein BAD and to repress the expression of BIM, both of which participate in the mitochondria-dependent cell death pathway (Strasser et al., 2000; Duronio, 2008). Therefore, we examined the ability of CAL-130 treatment to interfere with such events. Indeed, CCRF-CEM cells exposed to increasing concentration of drug exhibited a corresponding reduction and complete abrogation of Akt (Ser473) phosphorylation at 2.5 μM (Figure 6A). Downstream targets of this protein kinase were also affected as evidenced by the reduction in phosphorylation of GSK3β and mTOR. Consistent with the importance of PI3K in tumor cell survival, CAL-130 treatment resulted in a reduction in phosphorylation of BAD, as well as an enhanced expression of its counterpart BIM (including the L and S isoforms) (Figure 6B). The latter would also explain in part the synergy between CAL-130 and dexamethasone because BIM expression is required for glucocorticoid-induced apoptosis (Erlacher et al., 2005; Wang et al., 2003).

To assess the in vivo relevance of these observations, we evaluated the ability of CAL-130 to prevent the proliferation of CCRF-CEM cells implanted subcutaneously or to prolong the survival of NOD.Cg-*Prkdc*^{scid} *Il2rg*^{tm1Wjl}/Sz that received these cells intravenously. In the former, luciferase-expressing CCRF-CEM cells were injected into the flanks of immunodeficient mice and allowed to grow for 1 week before administering vehicle control or inhibitor (10 mg kg^{-1} every 8 hr) for a total of 4 days. In the latter, treatment commenced 3 days postinjection of tumor cells for a total of 7 days. Bioimaging of subcutaneous tumors revealed a 5-fold difference in luminescence in CAL-130-treated versus vehicle control-treated animals (Figure 6C). This translated into an increase in median survival time for treated animals with systemic disease of 35 versus 23 days for mice that received vehicle control alone (Figure 6D).

Because the continued passage of rapidly growing tumor lines can result in genetic alterations distinct from the cell from which it was originally derived, we also evaluated the effect of CAL-130 on primary T-ALL samples isolated from patients with active disease. Consistent with our animal studies, human tumor cells devoid of PTEN were exquisitely sensitive to dual inhibition of PI3Kγ/δ, but not single inhibition of PI3Kδ, which resulted in a reduction in tumor cell viability as well as in Akt phosphorylation in response to treatment (Figures 7A–7C; data not shown). Interestingly, one primary sample that not only expressed PTEN (T-ALL 4) but also high levels of phospho-Akt was as responsive to CAL-130 as its PTEN null counterparts. This would suggest that T-ALL sensitivity to a PI3Kγ/δ dual inhibitor might correlate better with the degree of Akt phosphorylation rather than with PTEN expression. As observed with primary mouse T-ALL, human tumors did not appear to overexpress any of the four class I *PIK3C* isoforms (Figure 7D).

DISCUSSION

Oncogenesis is a complex and multigenic process that often involves constitutive activation of the PI3K signaling pathway. Most notably are the gain-of-function mutations frequently found in *PIK3CA*, the gene that encodes for the p110α catalytic subunit, and genetic alterations that lead to the inactivation of the tumor suppressor gene *PTEN* (Samuels et al., 2004; Zunder et al., 2008; Sulis and Parsons, 2003; Salmena et al., 2008). In the latter scenario the possibility exists that the unregulated activity of any of the four class I PI3K isoforms could drive tumor development. For instance, previous reports demonstrate that PI3Kβ is essential for the induction, growth, and survival of PTEN-deficient tumors of epithelial cell origin (Jia et al., 2008; Wee et al., 2008). Moreover, it has been suggested that all class I PI3K isoforms are capable of coupling to upstream signaling pathways in which they are not normally engaged, thus compensating for inhibition/genetic deletion of a particular isoform

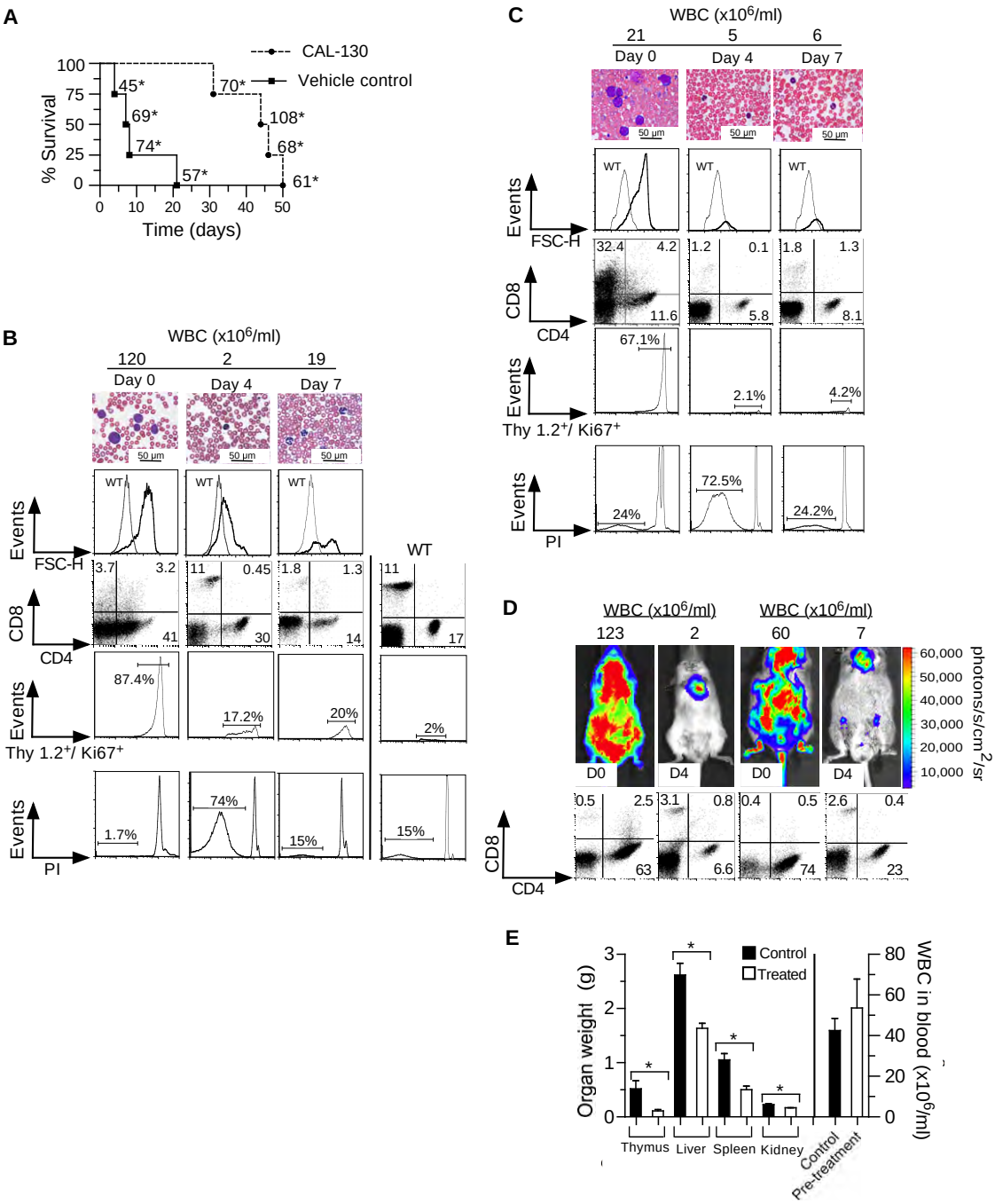

Figure 4. Combined Inhibition of p110γ and p110δ Reduces Tumor Burden and Increases Survival in Animals with PTEN Null T-ALL

(A) Kaplan-Meyer survival curve for *Lck/Pten*$^{fl/fl}$ mice diagnosed with T-ALL and immediately treated with CAL-130 for a total of 7 days. $p < 0.001$ for CAL-130 treated versus vehicle control. Numbers with an asterisk (*) represent the initial WBC count ($\times 10^6$) for each animal prior to instituting therapy.

(B and C) Peripheral blood smears and flow cytometric profiles for diseased (B) *Lck/Pten*$^{fl/fl}$ and (C) *Lck/Pten*$^{fl/fl}$;*Pik3cg*$^{-/-}$ mice just before and 4 and 7 days after initiating treatment with either CAL-130 or the PI3Kδ-specific inhibitor IC87114, respectively. The panels are representative of data from four *Lck/Pten*$^{fl/fl}$ mice and two *Lck/Pten*$^{fl/fl}$;*Pik3cg*$^{-/-}$ mice with T-ALL. Untreated WT animal is shown for comparison.

(D) Bioluminescent images and corresponding flow cytometric profiles of *Lck/Pten*$^{fl/fl}$/*Gt(ROSA)26Sor*$^{tm1(Luc)Kael}$/J animals with T-ALL immediately before and 4 days after treatment.

(E) Weights of thymi, liver, spleen, and kidneys harvested from *Lck/Pten*$^{fl/fl}$ mice with T-ALL 7 days posttreatment with either CAL-130 or vehicle control (n = 5, *$p < 0.01$ for CAL-130 treated versus vehicle control). Peripheral blood counts (WBC, right axis) represent the mean ± SD prior to treatment.

See also Figure S2.

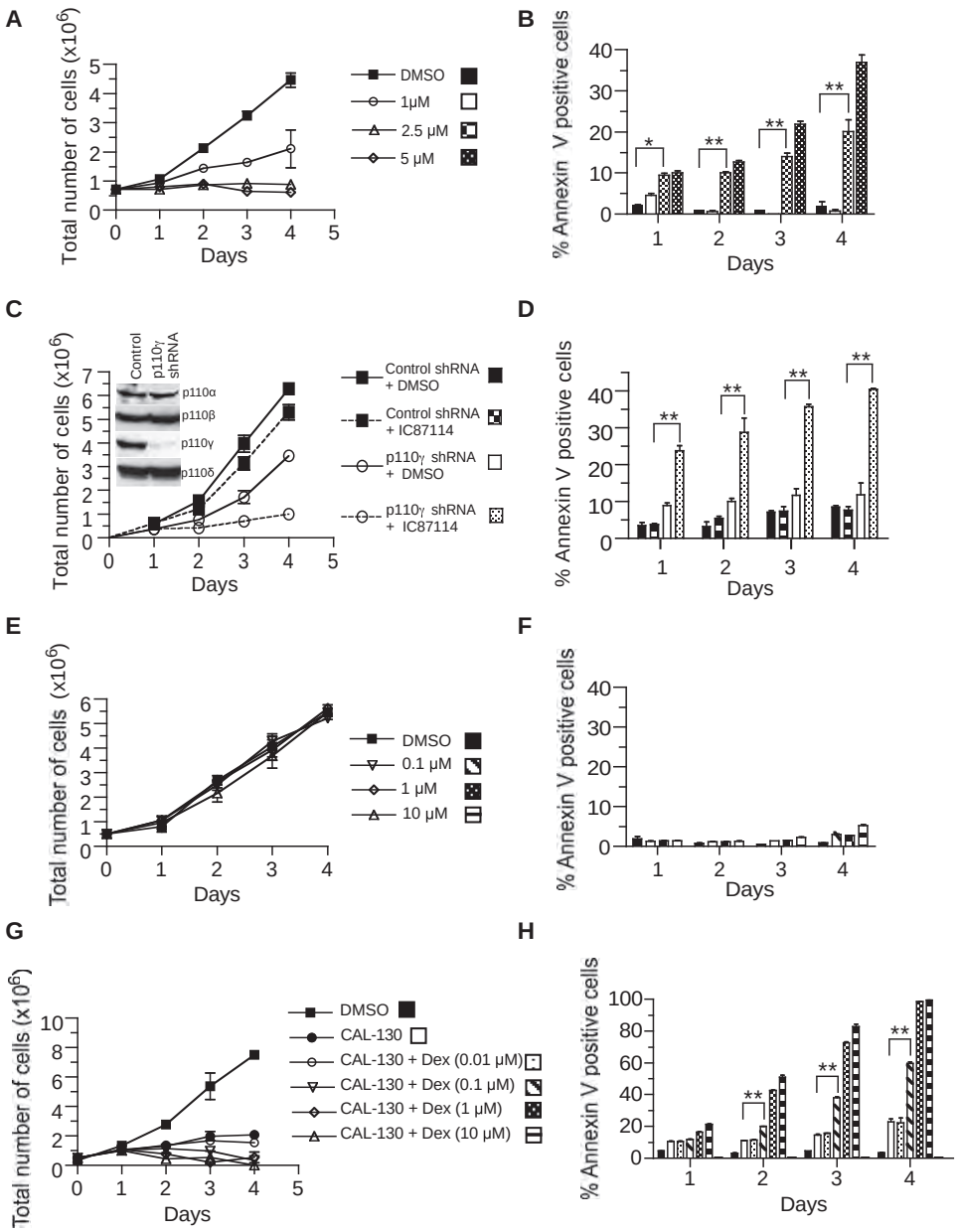

Figure 5. Contribution of PI3Kγ and PI3Kδ to the Growth and Survival of PTEN Null Human T-ALL Tumor Cell Lines

(A and B) Proliferation (A) and survival (B) of CCRF-CEM cells cultured in the presence of CAL-130 or vehicle control. *p < 0.01, **p < 0.001 for CAL-130 treated (2.5 μM) versus DMSO.

(C and D) Effect of the PI3Kδ-specific inhibitor IC87114 (10 μM) on proliferation (C) and survival (D) of CCRF-CEM cells in which p110γ expression was knocked down by shRNA transfection. **p < 0.001 for p110γ shRNA treated with IC87114 versus nonsilencing vector treated with IC87114. Inset in (C) depicts western blot analysis for p110 catalytic subunits.

(E–H) Proliferation and survival of CCRF-CEM cells cultured in the presence of dexamethasone alone (E and F) or in combination with 2.5 μM CAL-130 (G and H). **p < 0.001 for dexamethasone plus CAL-130 treated (2.5 μM) versus CAL-130 (2.5 μM) alone. Data represent the mean ± SD of experiments performed in triplicate.

See also Figure S3.

(Foukas et al., 2010). To date, to our knowledge, no conclusive evidence exists to implicate PI3Kβ or any other class I PI3K in the genesis of hematological malignancies such as T-ALL.

Our results demonstrate that in the absence of physiological regulation, the activity of either PI3Kγ or PI3Kδ is sufficient for the malignant transformation of T cell progenitors in a living animal. This is exemplified by the similar onset of disease and percent survival of mice lacking either p110γ or p110δ, and the rare incidence of tumor development in their combined absence. Moreover, pharmacological blockade of both p110γ and p110δ

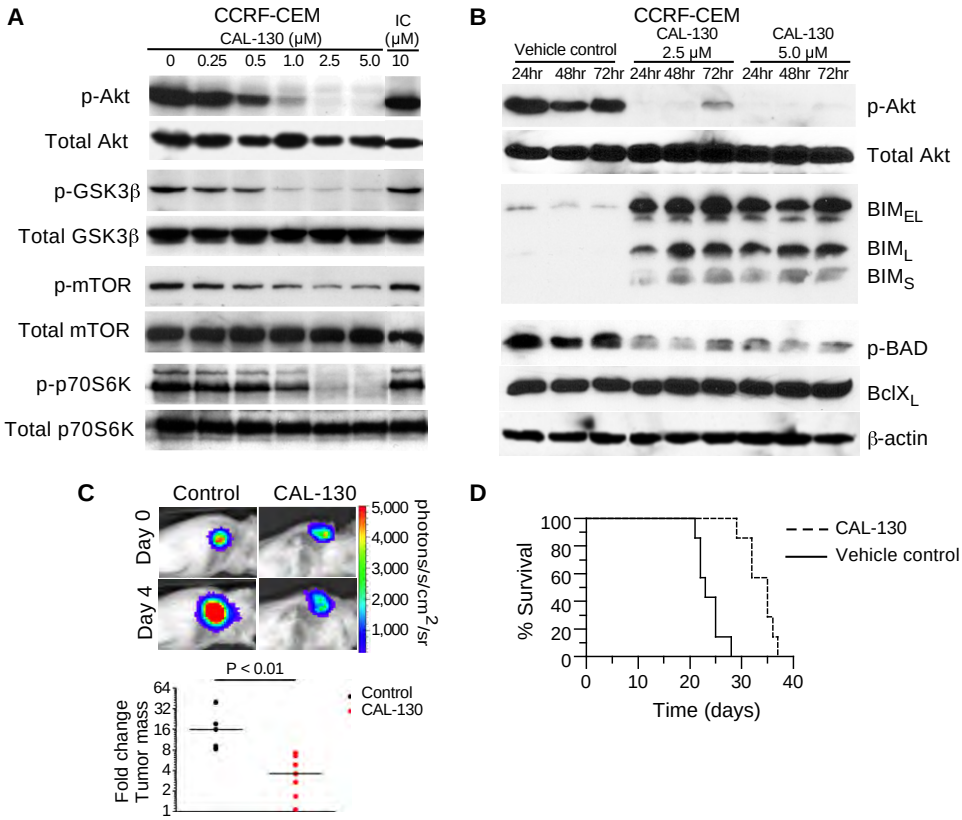

Figure 6. Effect of CAL-130 on Signaling Pathways Downstream of PI3Kγ and PI3Kδ

(A) Representative immunoblots of lysates obtained from CCRF-CEM cells treated (6 hr) with either CAL-130 or vehicle control and probed with the stated antibodies. The PI3Kδ-specific inhibitor IC87114 (IC) is shown for comparison.

(B) Representative immunoblots demonstrating activation of the proapoptotic pathway in CAL-130-treated CCRF-CEM cells.

(C) Representative bioluminescence images (upper panel) and quantification of tumor mass changes (lower panel) in mice with subcutaneous CCRF-CEM xenografts that received vehicle control or CAL-130 for 4 days (n = 7).

(D) Kaplan-Meyer analysis of overall survival of mice treated with vehicle control or CAL-130 for 7 days in a systemic CCRF-CEM xenograft model ($p < 0.01$ for CAL-130 treated versus vehicle control; n = 7 per group).

dramatically impacted on tumor cell proliferation and survival as demonstrated in CAL-130 treatment of diseased *Lck/Pten*$^{fl/fl}$ mice, IC87114 treatment of diseased *Lck/PTEN*$^{fl/fl}$;*Pik3cg*$^{-/-}$ mice, as well as CAL-130 treatment of PTEN null human T-ALL primary tumors or tumor cell lines; no such effects were observed with siRNA knockdown of either p110α or p110β, and selective blockade of PI3Kδ with IC87114 was ineffective in reducing the viability of primary human T-ALL samples. These results would suggest that propagation of upstream signaling pathways critical for the development and/or survival of PTEN null T-ALL tumors relies on PI3Kγ and PI3Kδ and that the remaining isoforms (i.e., α and β) cannot adequately compensate for their inactivity. Clearly, the same PI3K isoforms can participate in both tumorigenesis and tumor maintenance.

It has previously been established that PTEN loss is necessary but not sufficient to cause the malignant transformation of T cell progenitors (Liu et al., 2010; Guo et al., 2011). This typically requires additional genetic events such as chromosomal translocations involving the TCR α/δ locus and c-*myc* oncogene (Bernard et al., 1988; Finger et al., 1986), which are acquired during the transition from CD4$^-$CD8$^-$ DN to CD4$^+$CD8$^+$ DP development stage. Despite the presence of these strong oncogenic signals, the combined absence of PI3Kγ and PI3Kδ significantly impaired leukemogenesis, suggesting that loss of these isoforms can act as a tumorigenic bottleneck. Although it is possible that the overall reduction in CD4$^+$CD8$^+$ DP thymocyte numbers can partially account for the lower tumor incidence, we have previously shown that the transition from DN to DP thymocyte population in double-knockout mice is relatively normal (Swat et al., 2006). That is to say, there is no major deficiency in the number of early T cell progenitors that could undergo malignant transformation in the absence of PTEN activity. Yet, not only is tumorigenesis disrupted in TKO mice, but the abnormality observed in T cell development persisted as well. This is in contrast to the severe defect in thymocyte development associated with a genetic deletion of phosphoinositide-dependent kinase 1 (PDK1) (Hinton et al., 2004), a direct downstream target of class I PI3K, which can be overcome by the loss of PTEN resulting in near-normal numbers of thymocytes and peripheral T cells (Finlay et al., 2009). Similarly, PTEN deficiency can bypass a defect in either IL-7R or pre-TCR signaling, which are critical for the normal development and survival of T cells (Hagenbeek et al.,

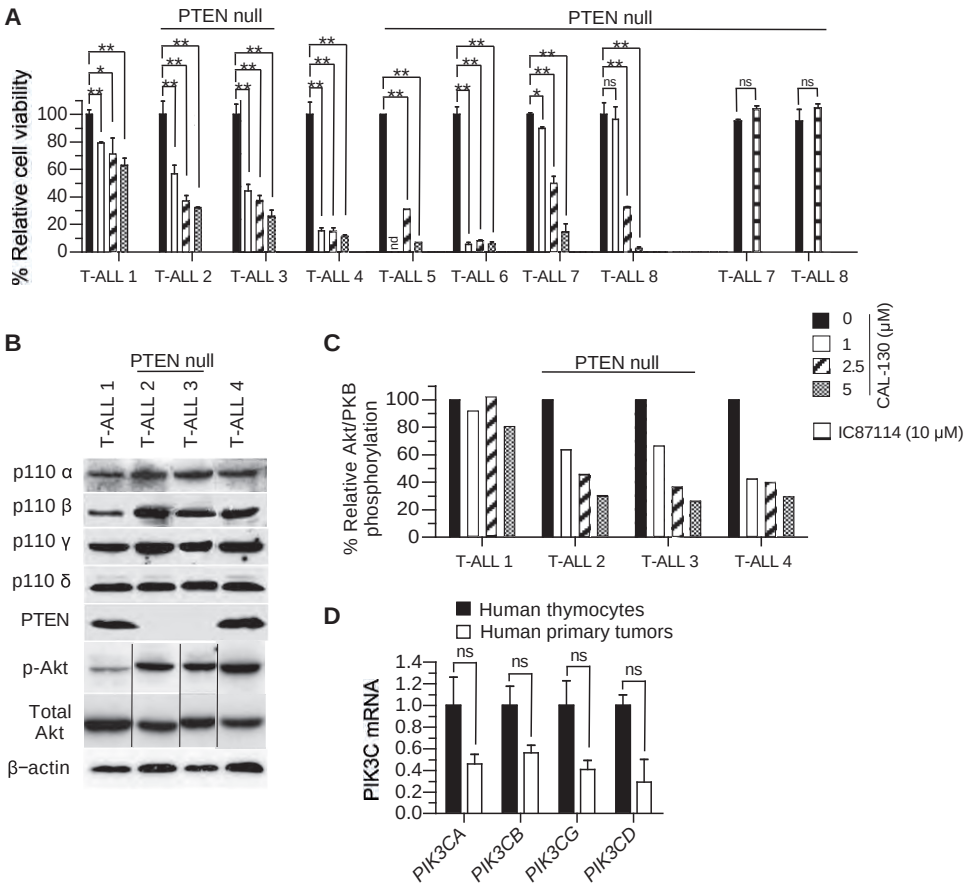

Figure 7. Susceptibility of Primary Human T-ALL Tumor Cells to Combined Inhibition of p110γ and p110δ

(A) Cell survival analyses of tumors cultured in the presence of increasing concentrations of CAL-130 for 72 hr. Percent viability indicates the proportion of live-gated cells in the treated populations relative to its vehicle control counterpart. Data represent the mean ± SD of experiments performed in duplicate or triplicate. *$p < 0.01$, **$p < 0.001$ for CAL-130 treated versus DMSO control. nd, not done; ns, not significant.

(B) Representative immunoblots of four primary human T-ALL samples to assess for expression of p110 catalytic domains and PTEN as well as phosphorylation state of Akt.

(C) Effect of CAL-130 on Akt phosphorylation on the same four representative T-ALL samples after 6 hr of treatment. Densitometry was performed on bands from immunoblots. The P-Akt signal was normalized to total Akt.

(D) Quantitative reverse-transcription PCR analysis of *PIK3C* (*A*/*B*/*G*/*D*) transcript levels in human thymocytes (n = 5) and primary human T-ALL tumors (n = 5). Error bars represent ±SD. The difference in *PIK3C* expression levels between the thymocytes and tumor cells was not statistically significant ($p > 0.05$) using a Student's t test.

2004). In stark contrast to these studies is the inability of a PTEN-deficient state to promote thymocyte proliferation and development in TKO mice. Taken together, these observations further suggest that developmental and genomic events responsible for the generation as well as the malignant transformation of T cells in the context of a PTEN-deficient state are critically reliant on proliferation and survival signals provided by PI3Kγ and PI3Kδ.

It is interesting to note that although PTEN appears to play a key role in regulating the activities of class I PI3K, it is not the only phosphatase in T cells. SHIP1 (SH2-containing inositol-5′-phosphatase) is also capable of hydrolyzing PIP3 and has been shown to play an important role in the immunoregulatory capacity and development of specific subsets of T cells (Tarasenko et al., 2007; Collazo et al., 2009). Although deletion of SHIP1 alone in T cell progenitors is not sufficient to induce leukemogenesis, low levels of this phosphatase in conjunction with PTEN inactivation have been reported in human T-ALL tumors suggesting that inactivation of both phosphatases contribute to the hyperactivation of the PI3K/Akt signaling pathway (Lo et al., 2009). Our discovery that both PI3Kγ and PI3Kδ are the engines that help drive the oncogenic process in T cell progenitors in the absence of appropriate regulation and can provide sufficient growth and survival signals necessary for tumor cell maintenance makes them attractive targets for therapy in such clinical cases. Moreover, dual inhibition of PI3Kγ and PI3Kδ in combination with conventional chemotherapies such as glucocorticoids may be of particular clinical utility in such individuals because they are more likely to fail induction chemotherapy and relapse (Gutierrez et al., 2009; Jotta et al., 2010).

It has been suggested that a complex signaling network involving PI3K exists between leukemic and supporting cells in

the tissue microenvironment that may contribute to disease progression and drug resistance (Ayala et al., 2009; Konopleva et al., 2009; Burger et al., 2009). This is exemplified by the recent observations that the PI3Kδ-specific inhibitor CAL-101 reduces levels of circulating chemokines known to contribute to tissue localization of chronic lymphocytic leukemic cells (Hoellenriegel et al., 2011). Consequently, this results in a generalized lymphocytosis during treatment of patients with this hematological malignancy. In contrast we have observed a dramatic and sustained reduction in peripheral blood T-ALL cells within hours of CAL-130 treatment of diseased *Lck/Pten*$^{fl/fl}$ mice (data not shown). That said, it is possible that paracrine and/or autocrine signaling responsible for T-ALL survival in tissues may be disrupted by simultaneously blocking the activities of PI3Kγ and PI3Kδ. Further work will be required to establish the role of these PI3K isoforms in supporting microenvironmental interactions in T-ALL.

In the broader perspective our results indicate that in the absence of PTEN-mediated regulation, distinct class I PI3K can predominate in the development and survival of tumors in a manner that is most likely to involve isoforms that normally play a critical role in the function of that particular cell type. Furthermore, we demonstrate that it is possible to target cancer cells by exploiting their "addiction" to the activity of distinct PI3K isoforms that are not themselves classical oncogenes. More generally, by identifying PI3Kγ and PI3Kδ as key therapeutic targets, it may be possible to limit toxicities that would be associated with the administration of pan-PI3K or Akt inhibitors including perturbations in insulin signaling and glucose metabolism (Crouthamel et al., 2009).

EXPERIMENTAL PROCEDURES

Cell Lines and Reagents and Antibodies

CCRF-CEM, CEM/C1, and MOLT-4 cells were obtained from ATCC and grown in RPMI-1640 medium containing 10% FBS and antibiotics. Antibodies to Akt (catalog #9272), phospho-Akt (S473, clone 193H12), phospho-mTOR (S2448, catalog #2971S), mTOR (catalog #2972), phospho-GSK3α/β (S21/9, catalog #9331S), GSK-3β (clone 27C10), phospho-p70S6K (Thr389, catalog #9205S), p70S6K (catalog #9202), and β-actin (catalog #4967S) were from Cell Signaling Technology. Antibodies to class I PI3K subunits were as follows: p110α (catalog #4255) from Cell Signaling Technology; p110β (clone Y384) from Millipore and mouse p110β from Santa Cruz Biotechnology (catalog #sc-602); p110γ (clone H1) from Jena Biosciences; and p110δ (clone H-219) from Santa Cruz Biotechnology. Antibodies to PTEN (clone 6H2.1) were from Cascade Bioscience. For flow cytometry, antibodies were obtained from BD Biosciences: CD3ε-Alexa 488 (clone 145-2C11), CD4-APC (clone RM4-5), CD8-PerCP-Cy5.5 (clone 53-6.7), CD90.2-APC (Thy-1.2, clone 53-2.1), Ki67-FITC (clone B56), and Annexin V-APC. Antibodies to Bim, phospho-Bad, Bad, and BclX_L were from Cell Signaling Technology (proapoptotic sampler kit #9942S).

The shRNA construct for p110γ in the pLKO.1 vector was obtained from Sigma-Aldrich (MISSION shRNA Plasmid DNA; clone ID: NM_002649.2-4744s1c1; TRC number: TRCN0000196870). siRNA constructs for p110α (ON-TARGET plus SMARTpool #L-003018-00) and p110β (ON-TARGET plus SMARTpool # L-003019-00) were obtained from Dharmacon (Thermo Scientific).

Primary Leukemia Samples

Cryopreserved samples were provided by collaborating institutions in the United States (Department of Pediatrics, Columbia Presbyterian Hospital and Departments of Medicine and Pathology, Vanderbilt University), The Netherlands (Erasmus MC-Sophia Children's Hospital), and Italy (Hemato-Oncology Laboratory, Department of Pediatrics, University of Padua). All samples were collected with informed consent and under the supervision of the Medical Ethics Committee of the Erasmus Medical Center, the Columbia University Medical Center Institutional Review Board, the Vanderbilt University Medical Center Institutional Review Board, and the Acute Lymphoblastic Leukemia Strategic Scientific Committee.

Cell Counts, Cell Proliferation, and Cell Viability Assay

Cell counts for mice thymi were determined as previously described by Swat et al. (2006). Cell proliferation of CCRF-CEM cells or shRNA-transfected CCRF-CEM cells, in presence or absence of appropriate drug, was followed by cell counting of samples in triplicate using a hemocytometer and trypan blue. For apoptosis determinations of untransfected or shRNA-transfected CCRF-CEMs, cells were stained with APC-conjugated Annexin-V (BD Biosciences) in Annexin Binding Buffer (Miltyeni Biotec) and analyzed by flow cytometry. For primary T-ALL samples, cell viability was assessed using the BD Cell Viability kit (BD Biosciences) coupled with the use of fluorescent-counting beads as previously described by Armstrong et al. (2009). For this, cells were plated with MS5-DL1 stroma cells, and after 72 hr following drug treatment, cells were harvested and stained with an APC-conjugated anti-human CD45 followed by a staining with the aforementioned kit according to the manufacturer's instructions.

CAL130 IC_{50}

CAL-130 is a derivative of IC87114, the synthesis of which has been previously described by Sadhu et al. (2003). IC_{50} values for CAL-130 inhibition of PI3K isoforms were determined in ex vivo PI3 kinase assays using recombinant PI3K. A ten-point kinase inhibitory profile was determined with ATP at a concentration consistent with the K_M for each enzyme (Puri et al., 2004).

Calcium Flux Measurements in Thymocytes

Ca^{2+} flux measurements in single-cell suspensions of mouse thymocytes were performed as previously described by Swat et al. (2006). Drug inhibition of Ca^{2+} flux was measured after 30 min preincubation with CAL-130 at room temperature of dye-loaded cells. Percent overall change in Ca^{2+} flux is reported as $(Ca^{2+}\ flux_{peak} - Ca^{2+}\ flux_{baseline}/Ca^{2+}flux_{ionomycin} - Ca^{2+}\ flux_{baseline}) \times 100$.

Flow Cytometry for Cell Surface Staining and Apoptosis

For cell surface staining in mouse whole blood, following incubation with appropriate antibodies, blood was processed using the BD Bioscience BD FACS Lysing Solution according to the manufacturer's instructions. For intracellular staining of Ki67, immediately after RBC lysis with the BD FACS Lysing solution, cells were permeabilized without washing with 0.025% Tween 20 in lysing solution for an additional 15 min, washed, and then incubated with Ki67 antibodies. For thymocytes, single-cell suspensions of thymocytes were isolated and stained with the appropriate antibodies as previously described by Swat et al. (2006).

Histological and Immunohistochemical Study of Tissue Samples

Formalin-fixed paraffin-embedded 5 μm tissue sections were stained with hematoxylin and eosin for histopathological diagnosis. For immunohistochemistry we performed anti-CD3 (rabbit polyclonal; Dako) staining on tissue sections after antigen retrieval by microwave heating in citrate buffer (pH 6.0). After epitope recovery, slides were incubated with antibody (anti-CD3 1:50) overnight at room temperature before antigen detection with diaminobenzidine (DAB) using a Ventana automated staining platform (Ventana).

Western Blotting

Cell lysates (from cell lines or thymocytes) were prepared on ice in M-PER Mammalian Protein Extraction reagent (Pierce) containing a cocktail of protease and phosphatase inhibitors as previously described by Swat et al. (2006). Equal amounts of total protein from lysates were subjected to SDS-PAGE, transferred to PVDF membrane (Immobilon-P; Millipore), and membranes were probed by overnight incubation with appropriate primary antibodies. Bound antibodies were visualized with HRP-conjugated secondary antibodies and ECL chemistry (SuperPico West; Pierce).

shRNA and siRNA Knockdown

CCRF-CEMs were transfected using the Amaxa Human T cell Nucleofecor kit (Lonza) according to the manufacturer's optimized protocol kit for this cell line. For shRNA knockdown of p110γ, CCRF-CEMs (2×10^6 cells) were transfected with 2 μg of purified plasmid DNA, and clones were selected by high dilution in puromycin used at a concentration predetermined by a killing curve. Expression of p110γ and p110δ was determined by western blotting.

For siRNA knockdown of p110α or p110β, CCRF-CEMs (2×10^6 cells) were transfected with 300 nM of siRNA construct. After a brief recovery period, cells were diluted to between 1 and 2×10^5/ml and grown for further 48 hr for cell counting, flow cytometry, and western blotting.

Mice and Animal Procedures

All mice were kept in a specific pathogen-free facility at Columbia University Medical Center. All mice studies and breeding were carried out under the approval of Institutional Animal Care and Use Committee of Columbia University. NOD.Cg-*Prkdc*^{scid} *Il2rg*^{tm1Wjl}/Sz mice for xenograft experiments and *Gt(ROSA)26Sor*$^{tm1(Luc)Kael}$/J for bioimaging studies were obtained from The Jackson Laboratory. Mice deficient for *Pten* in the T cell lineage were generated by crossing *Lck-cre* with floxed *Pten* (Hennet et al., 1995; Trotman et al., 2003). P110γ$^{-/-}$ and p110δ$^{-/-}$ mice have been previously described by Swat et al. (2006). These animals were intercrossed with *Lck-cre/Pten*$^{fl/fl}$ animals to generate mice homozygous mutant for either p110γ or p110δ and *Pten* or homozygous mutant for p110γ, 110δ, and *Pten*.

For subcutaneous xenograft experiments, luminescent CCRF-CEM (CEM-luc) cells were generated by lentiviral infection with FUW-luc and selection with neomycin. Luciferase expression was verified with the Dual-Luciferase Reporter Assay kit (Promega). We injected 2.5×10^6 CEM-luc cells embedded in Matrigel (BD Biosciences) in the flank of NOD.Cg-*Prkdc*^{scid} *Il2rg*^{tm1Wjl}/Sz mice. After 1 week, mice were treated by oral gavage with vehicle (0.5% methyl cellulose, 0.1% Tween 80), or CAL-130 (10 mg kg^{-1}) every 8 hr daily for 4 days, and then tumors were imaged as follows: mice anesthetized by isoflurane inhalation were injected intraperitoneally with D-luciferin (50 mg kg^{-1}; Xenogen). Photonic emission was imaged with the In Vivo Imaging System (IVIS; Xenogen). Tumor bioluminescence was quantified by integrating the photonic flux (photons per second) through a region encircling each tumor using the Living Image software package (Xenogen). Administration of D-luciferin and detection of tumor bioluminescence in *Lck/Pten*$^{fl/fl}$*/Gt(ROSA)26Sor*$^{tm1(Luc)Kael}$/J mice were performed in a similar manner.

For intravenous xenograft transplantation, 5×10^6 CCRF-CEM cells were injected intravenously in 14 NOD.Cg-*Prkdc*^{scid} *Il2rg*^{tm1Wjl}/Sz mice. After 3 days, mice were segregated into two treatment groups that received either CAL-130 or vehicle by oral gavage as described above for 7 days. Mice in both groups were then followed until moribund (and euthanized).

Plasma Levels of CAL130, Glucose, and Insulin

For CAL-130 level determinations, animals received a single oral dose (10 or 20 mg kg^{-1}) of inhibitor. Plasma was collected at 0, 2, 4, 8, and 12 hr and subjected to high-performance liquid chromatography-MS/MS (sensitivity 1 ng/ml). The concentration of CAL-130 in plasma was determined using a standard curve (analyte peak area versus concentration) generated with calibration standard pools. Values represent the mean (±SD) for four animals per group.

Plasma glucose and insulin levels were determined following a single oral dose of CAL-130 (10 mg kg^{-1}). Blood was collected into K_2EDTA tubes by cardiac puncture at baseline and 0, 2, 4, and 8 hr post-dose, and plasma samples were frozen at −80°C until analysis. The insulin and glucose levels were determined by using an Ultra Sensitive Mouse Insulin ELISA Kit (Crystal Chem) or WaveSense Presto Blood Glucose Monitoring System (Agamatrix, Boston), respectively.

Statistical Analyses

Statistical analyses were performed using Student's t test (GraphPad Prism software). Kaplan-Meier survival curves were analyzed using a log rank test (GraphPad Prism software). Values were considered significant at $p < 0.05$.

SUPPLEMENTAL INFORMATION

Supplemental Information includes three figures, one table, and Supplemental Experimental Procedures and can be found with this article online at doi:10.1016/j.ccr.2012.02.029.

ACKNOWLEDGMENTS

We thank Andrew Kung for providing the FUW luciferase vector, Jerry Evarts for supplying CAL-130, Juan Carlos Zuniga-Pflucker for providing the OP9-DL1 cells, Richard Friedman for statistical analyses, Kui Tan and Mikin Patel for genotyping and animal husbandry, and Timothy Wang for critical review of the manuscript. This work was supported by the DOD (Grant PR093714 to T.G.D. and A.F.), the Leukemia & Lymphoma Society Translational Research Program (Grant 140229 to T.G.D. and A.F.), and the Leukemia & Lymphoma Society Scholar Award (to A.F.). B.J.L. and A.K. are employees of the company (Gilead Sciences) that manufactured CAL-130.

Received: August 10, 2011
Revised: December 26, 2011
Accepted: February 24, 2012
Published: April 16, 2012

REFERENCES

Armstrong, F., Brunet de la Grange, P., Gerby, B., Rouyez, M.C., Calvo, J., Fontenay, M., Boissel, N., Dombret, H., Baruchel, A., Landman-Parker, J., et al. (2009). NOTCH is a key regulator of human T-cell acute leukemia initiating cell activity. Blood *113*, 1730–1740.

Ayala, F., Dewar, R., Kieran, M., and Kalluri, R. (2009). Contribution of bone microenvironment to leukemogenesis and leukemia progression. Leukemia *23*, 2233–2241.

Beesley, A.H., Firth, M.J., Ford, J., Weller, R.E., Freitas, J.R., Perera, K.U., and Kees, U.R. (2009). Glucocorticoid resistance in T-lineage acute lymphoblastic leukaemia is associated with a proliferative metabolism. Br. J. Cancer *100*, 1926–1936.

Bernard, O., Larsen, C.J., Hampe, A., Mauchauffé, M., Berger, R., and Mathieu-Mahul, D. (1988). Molecular mechanisms of a t(8;14)(q24;q11) translocation juxtaposing c-myc and TcR-alpha genes in a T-cell leukaemia: involvement of a V alpha internal heptamer. Oncogene *2*, 195–200.

Burger, J.A., Ghia, P., Rosenwald, A., and Caligaris-Cappio, F. (2009). The microenvironment in mature B-cell malignancies: a target for new treatment strategies. Blood *114*, 3367–3375.

Cantley, L.C. (2002). The phosphoinositide 3-kinase pathway. Science *296*, 1655–1657.

Carnero, A., Blanco-Aparicio, C., Renner, O., Link, W., and Leal, J.F. (2008). The PTEN/PI3K/AKT signalling pathway in cancer, therapeutic implications. Curr. Cancer Drug Targets *8*, 187–198.

Cohen, P., and Frame, S. (2001). The renaissance of GSK3. Nat. Rev. Mol. Cell Biol. *2*, 769–776.

Collazo, M.M., Wood, D., Paraiso, K.H., Lund, E., Engelman, R.W., Le, C.T., Stauch, D., Kotsch, K., and Kerr, W.G. (2009). SHIP limits immunoregulatory capacity in the T-cell compartment. Blood *113*, 2934–2944.

Crouthamel, M.C., Kahana, J.A., Korenchuk, S., Zhang, S.Y., Sundaresan, G., Eberwein, D.J., Brown, K.K., and Kumar, R. (2009). Mechanism and management of AKT inhibitor-induced hyperglycemia. Clin. Cancer Res. *15*, 217–225.

Duronio, V. (2008). The life of a cell: apoptosis regulation by the PI3K/PKB pathway. Biochem. J. *415*, 333–344.

Erlacher, M., Michalak, E.M., Kelly, P.N., Labi, V., Niederegger, H., Coultas, L., Adams, J.M., Strasser, A., and Villunger, A. (2005). BH3-only proteins Puma and Bim are rate-limiting for gamma-radiation- and glucocorticoid-induced apoptosis of lymphoid cells in vivo. Blood *106*, 4131–4138.

Fabian, M.A., Biggs, W.H., 3rd, Treiber, D.K., Atteridge, C.E., Azimioara, M.D., Benedetti, M.G., Carter, T.A., Ciceri, P., Edeen, P.T., Floyd, M., et al. (2005). A

small molecule-kinase interaction map for clinical kinase inhibitors. Nat. Biotechnol. *23*, 329–336.

Finger, L.R., Harvey, R.C., Moore, R.C., Showe, L.C., and Croce, C.M. (1986). A common mechanism of chromosomal translocation in T- and B-cell neoplasia. Science *234*, 982–985.

Finlay, D.K., Sinclair, L.V., Feijoo, C., Waugh, C.M., Hagenbeek, T.J., Spits, H., and Cantrell, D.A. (2009). Phosphoinositide-dependent kinase 1 controls migration and malignant transformation but not cell growth and proliferation in PTEN-null lymphocytes. J. Exp. Med. *206*, 2441–2454.

Foukas, L.C., Berenjeno, I.M., Gray, A., Khwaja, A., and Vanhaesebroeck, B. (2010). Activity of any class IA PI3K isoform can sustain cell proliferation and survival. Proc. Natl. Acad. Sci. USA *107*, 11381–11386.

Guo, W., Lasky, J.L., Chang, C.J., Mosessian, S., Lewis, X., Xiao, Y., Yeh, J.E., Chen, J.Y., Iruela-Arispe, M.L., Varella-Garcia, M., and Wu, H. (2008). Multi-genetic events collaboratively contribute to Pten-null leukaemia stem-cell formation. Nature *453*, 529–533.

Guo, W., Schubbert, S., Chen, J.Y., Valamehr, B., Mosessian, S., Shi, H., Dang, N.H., Garcia, C., Theodoro, M.F., Varella-Garcia, M., and Wu, H. (2011). Suppression of leukemia development caused by PTEN loss. Proc. Natl. Acad. Sci. USA *108*, 1409–1414.

Gutierrez, A., Sanda, T., Grebliunaite, R., Carracedo, A., Salmena, L., Ahn, Y., Dahlberg, S., Neuberg, D., Moreau, L.A., Winter, S.S., et al. (2009). High frequency of PTEN, PI3K, and AKT abnormalities in T-cell acute lymphoblastic leukemia. Blood *114*, 647–650.

Hagenbeek, T.J., and Spits, H. (2008). T-cell lymphomas in T-cell-specific Pten-deficient mice originate in the thymus. Leukemia *22*, 608–619.

Hagenbeek, T.J., Naspetti, M., Malergue, F., Garçon, F., Nunès, J.A., Cleutjens, K.B., Trapman, J., Krimpenfort, P., and Spits, H. (2004). The loss of PTEN allows TCR alphabeta lineage thymocytes to bypass IL-7 and Pre-TCR-mediated signaling. J. Exp. Med. *200*, 883–894.

Hennet, T., Hagen, F.K., Tabak, L.A., and Marth, J.D. (1995). T-cell-specific deletion of a polypeptide N-acetylgalactosaminyl-transferase gene by site-directed recombination. Proc. Natl. Acad. Sci. USA *92*, 12070–12074.

Hickey, F.B., and Cotter, T.G. (2006). BCR-ABL regulates phosphatidylinositol 3-kinase-p110gamma transcription and activation and is required for proliferation and drug resistance. J. Biol. Chem. *281*, 2441–2450.

Hinton, H.J., Alessi, D.R., and Cantrell, D.A. (2004). The serine kinase phosphoinositide-dependent kinase 1 (PDK1) regulates T cell development. Nat. Immunol. *5*, 539–545.

Hoellenriegel, J., Meadows, S.A., Sivina, M., Wierda, W.G., Kantarjian, H., Keating, M.J., Giese, N., O'Brien, S., Yu, A., Miller, L.L., et al. (2011). The phosphoinositide 3′-kinase delta inhibitor, CAL-101, inhibits B-cell receptor signaling and chemokine networks in chronic lymphocytic leukemia. Blood *118*, 3603–3612.

Huang, W.C., and Hung, M.C. (2009). Induction of Akt activity by chemotherapy confers acquired resistance. J. Formos. Med. Assoc. *108*, 180–194.

Jackson, S.P., Schoenwaelder, S.M., Goncalves, I., Nesbitt, W.S., Yap, C.L., Wright, C.E., Kenche, V., Anderson, K.E., Dopheide, S.M., Yuan, Y., et al. (2005). PI 3-kinase p110beta: a new target for antithrombotic therapy. Nat. Med. *11*, 507–514.

Ji, H., Rintelen, F., Waltzinger, C., Bertschy Meier, D., Bilancio, A., Pearce, W., Hirsch, E., Wymann, M.P., Rückle, T., Camps, M., et al. (2007). Inactivation of PI3Kgamma and PI3Kdelta distorts T-cell development and causes multiple organ inflammation. Blood *110*, 2940–2947.

Jia, S., Liu, Z., Zhang, S., Liu, P., Zhang, L., Lee, S.H., Zhang, J., Signoretti, S., Loda, M., Roberts, T.M., and Zhao, J.J. (2008). Essential roles of PI(3)K-p110beta in cell growth, metabolism and tumorigenesis. Nature *454*, 776–779.

Jotta, P.Y., Ganazza, M.A., Silva, A., Viana, M.B., da Silva, M.J., Zambaldi, L.J., Barata, J.T., Brandalise, S.R., and Yunes, J.A. (2010). Negative prognostic impact of PTEN mutation in pediatric T-cell acute lymphoblastic leukemia. Leukemia *24*, 239–242.

Kang, S., Denley, A., Vanhaesebroeck, B., and Vogt, P.K. (2006). Oncogenic transformation induced by the p110beta, -gamma, and -delta isoforms of class I phosphoinositide 3-kinase. Proc. Natl. Acad. Sci. USA *103*, 1289–1294.

Karaman, M.W., Herrgard, S., Treiber, D.K., Gallant, P., Atteridge, C.E., Campbell, B.T., Chan, K.W., Ciceri, P., Davis, M.I., Edeen, P.T., et al. (2008). A quantitative analysis of kinase inhibitor selectivity. Nat. Biotechnol. *26*, 127–132.

Katso, R., Okkenhaug, K., Ahmadi, K., White, S., Timms, J., and Waterfield, M.D. (2001). Cellular function of phosphoinositide 3-kinases: implications for development, homeostasis, and cancer. Annu. Rev. Cell Dev. Biol. *17*, 615–675.

Konopleva, M., Tabe, Y., Zeng, Z., and Andreeff, M. (2009). Therapeutic targeting of microenvironmental interactions in leukemia: mechanisms and approaches. Drug Resist. Updat. *12*, 103–113.

Larson Gedman, A., Chen, Q., Kugel Desmoulin, S., Ge, Y., LaFiura, K., Haska, C.L., Cherian, C., Devidas, M., Linda, S.B., Taub, J.W., and Matherly, L.H. (2009). The impact of NOTCH1, FBW7 and PTEN mutations on prognosis and downstream signaling in pediatric T-cell acute lymphoblastic leukemia: a report from the Children's Oncology Group. Leukemia *23*, 1417–1425.

Liu, X., Karnell, J.L., Yin, B., Zhang, R., Zhang, J., Li, P., Choi, Y., Maltzman, J.S., Pear, W.S., Bassing, C.H., and Turka, L.A. (2010). Distinct roles for PTEN in prevention of T cell lymphoma and autoimmunity in mice. J. Clin. Invest. *120*, 2497–2507.

Lo, T.C., Barnhill, L.M., Kim, Y., Nakae, E.A., Yu, A.L., and Diccianni, M.B. (2009). Inactivation of SHIP1 in T-cell acute lymphoblastic leukemia due to mutation and extensive alternative splicing. Leuk. Res. *33*, 1562–1566.

Maser, R.S., Choudhury, B., Campbell, P.J., Feng, B., Wong, K.K., Protopopov, A., O'Neil, J., Gutierrez, A., Ivanova, E., Perna, I., et al. (2007). Chromosomally unstable mouse tumours have genomic alterations similar to diverse human cancers. Nature *447*, 966–971.

Okkenhaug, K., and Vanhaesebroeck, B. (2003). PI3K in lymphocyte development, differentiation and activation. Nat. Rev. Immunol. *3*, 317–330.

Palomero, T., Dominguez, M., and Ferrando, A.A. (2008). The role of the PTEN/AKT Pathway in NOTCH1-induced leukemia. Cell Cycle *7*, 965–970.

Puri, K.D., Doggett, T.A., Douangpanya, J., Hou, Y., Tino, W.T., Wilson, T., Graf, T., Clayton, E., Turner, M., Hayflick, J.S., and Diacovo, T.G. (2004). Mechanisms and implications of phosphoinositide 3-kinase δ in promoting neutrophil trafficking into inflamed tissue. Blood *103*, 3448–3456.

Sadhu, C., Masinovsky, B., Dick, K., Sowell, C.G., and Staunton, D.E. (2003). Essential role of phosphoinositide 3-kinase δ in neutrophil directional movement. J. Immunol. *170*, 2647–2654.

Safran, M., Kim, W.Y., Kung, A.L., Horner, J.W., DePinho, R.A., and Kaelin, W.G., Jr. (2003). Mouse reporter strain for noninvasive bioluminescent imaging of cells that have undergone Cre-mediated recombination. Mol. Imaging *2*, 297–302.

Salmena, L., Carracedo, A., and Pandolfi, P.P. (2008). Tenets of PTEN tumor suppression. Cell *133*, 403–414.

Samuels, Y., Wang, Z., Bardelli, A., Silliman, N., Ptak, J., Szabo, S., Yan, H., Gazdar, A., Powell, S.M., Riggins, G.J., et al. (2004). High frequency of mutations of the PIK3CA gene in human cancers. Science *304*, 554.

Schmelzle, T., and Hall, M.N. (2000). TOR, a central controller of cell growth. Cell *103*, 253–262.

Silva, A., Yunes, J.A., Cardoso, B.A., Martins, L.R., Jotta, P.Y., Abecasis, M., Nowill, A.E., Leslie, N.R., Cardoso, A.A., and Barata, J.T. (2008). PTEN posttranslational inactivation and hyperactivation of the PI3K/Akt pathway sustain primary T cell leukemia viability. J. Clin. Invest. *118*, 3762–3774.

Sopasakis, V.R., Liu, P., Suzuki, R., Kondo, T., Winnay, J., Tran, T.T., Asano, T., Smyth, G., Sajan, M.P., Farese, R.V., et al. (2010). Specific roles of the p110alpha isoform of phosphatidylinsositol 3-kinase in hepatic insulin signaling and metabolic regulation. Cell Metab. *11*, 220–230.

Strasser, A., Puthalakath, H., Bouillet, P., Huang, D.C., O'Connor, L., O'Reilly, L.A., Cullen, L., Cory, S., and Adams, J.M. (2000). The role of bim, a proapoptotic BH3-only member of the Bcl-2 family in cell-death control. Ann. N Y Acad. Sci. *917*, 541–548.

Sujobert, P., Bardet, V., Cornillet-Lefebvre, P., Hayflick, J.S., Prie, N., Verdier, F., Vanhaesebroeck, B., Muller, O., Pesce, F., Ifrah, N., et al. (2005). Essential

role for the p110delta isoform in phosphoinositide 3-kinase activation and cell proliferation in acute myeloid leukemia. Blood *106*, 1063–1066.

Sulis, M.L., and Parsons, R. (2003). PTEN: from pathology to biology. Trends Cell Biol. *13*, 478–483.

Suzuki, A., Yamaguchi, M.T., Ohteki, T., Sasaki, T., Kaisho, T., Kimura, Y., Yoshida, R., Wakeham, A., Higuchi, T., Fukumoto, M., et al. (2001). T cell-specific loss of Pten leads to defects in central and peripheral tolerance. Immunity *14*, 523–534.

Swat, W., Montgrain, V., Doggett, T.A., Douangpanya, J., Puri, K., Vermi, W., and Diacovo, T.G. (2006). Essential role of PI3Kdelta and PI3Kgamma in thymocyte survival. Blood *107*, 2415–2422.

Tarasenko, T., Kole, H.K., Chi, A.W., Mentink-Kane, M.M., Wynn, T.A., and Bolland, S. (2007). T cell-specific deletion of the inositol phosphatase SHIP reveals its role in regulating Th1/Th2 and cytotoxic responses. Proc. Natl. Acad. Sci. USA *104*, 11382–11387.

Trotman, L.C., Niki, M., Dotan, Z.A., Koutcher, J.A., Di Cristofano, A., Xiao, A., Khoo, A.S., Roy-Burman, P., Greenberg, N.M., Van Dyke, T., et al. (2003). Pten dose dictates cancer progression in the prostate. PLoS Biol. *1*, E59.

Wang, Z., Malone, M.H., He, H., McColl, K.S., and Distelhorst, C.W. (2003). Microarray analysis uncovers the induction of the proapoptotic BH3-only protein Bim in multiple models of glucocorticoid-induced apoptosis. J. Biol. Chem. *278*, 23861–23867.

Webb, L.M., Vigorito, E., Wymann, M.P., Hirsch, E., and Turner, M.J. (2005). Cutting edge: T cell development requires the combined activities of the p110gamma and p110delta catalytic isoforms of phosphatidylinositol 3-kinase. J. Immunol. *175*, 2783–2787.

Wee, S., Wiederschain, D., Maira, S.M., Loo, A., Miller, C., deBeaumont, R., Stegmeier, F., Yao, Y.M., and Lengauer, C. (2008). PTEN-deficient cancers depend on PIK3CB. Proc. Natl. Acad. Sci. USA *105*, 13057–13062.

Yuan, T.L., and Cantley, L.C. (2008). PI3K pathway alterations in cancer: variations on a theme. Oncogene *27*, 5497–5510.

Zhao, L., and Vogt, P.K. (2008). Class I PI3K in oncogenic cellular transformation. Oncogene *27*, 5486–5496.

Zunder, E.R., Knight, Z.A., Houseman, B.T., Apsel, B., and Shokat, K.M. (2008). Discovery of drug-resistant and drug-sensitizing mutations in the oncogenic PI3K isoform p110 alpha. Cancer Cell *14*, 180–192.

Appendix 2: Accepted Manuscript

Erich Piovan, Jiyang Yu, Valeria Tosello, Daniel Herranz, Alberto Ambesi-Impiombato, Ana Carolina Da Silva, Arianne Perez-Garcia, Isaura Rigo, Mireia Castillo, Stefano Indraccolo, Elisabeth Paietta, Janis Racevskis, Jacob M Rowe, Martin S Tallman, Giuseppe Basso, Jules P Meijerink, Carlos Cordon-Cardo, Andrea Califano and Adolfo A. Ferrando Direct reversal of glucocorticoid resistance by AKT inhibition in T-ALL. **Cancer Cell** *in press*

Direct reversal of glucocorticoid resistance by AKT inhibition in acute lymphoblastic leukemia

Erich Piovan[1,2,3,17], Jiyang Yu[4,5,17], Valeria Tosello[1,6], Daniel Herranz[1], Alberto Ambesi-Impiombato[1], Ana Carolina Da Silva[1], Marta Sanchez-Martin[1], Arianne Perez-Garcia[1], Isaura Rigo[1], Mireia Castillo[7], Stefano Indraccolo[2], Justin R Cross[8], Elisa de Stanchina[9], Elisabeth Paietta[10,11], Janis Racevskis[10,11], Jacob M Rowe[12], Martin S Tallman[13], Giuseppe Basso[14], Jules P Meijerink[15], Carlos Cordon-Cardo[7], Andrea Califano[1,4,5] and Adolfo A. Ferrando[1,7,16]

[1]Institute for Cancer Genetics, Columbia University, New York, NY, 10032, USA.

[2]UOC Immunologia e Diagnostica Molecolare Oncologica, Istituto Oncologico Veneto—IRCCS, Padova, Italy.

[3]Dipartimento di Scienze Chirurgiche, Oncologiche e Gastroenterologiche, Universita' di Padova, Padova, Padova, Veneto, 35128, Italy.

[4]Department of Biomedical Informatics, Columbia University, New York, NY, 10032, USA.

[5]Joint Centers for Systems Biology, Columbia University, New York, NY, 10032, USA.

[6]Istituto Oncologico Veneto, IRCCS, Padova, Veneto, 35128, Italy.

[7]Department of Pathology, Mount Sinai School of Medicine, New York, NY, 10029, USA

[8]Donald B. and Catherine C. Marron Cancer Metabolism Center, Memorial Sloan-Kettering Cancer Center, New York, NY, 10065 USA

[9]Antitumor Assessment Core Facility, Memorial Sloan-Kettering Cancer Center, New York, NY,10065 USA

[10]Department of Medicine, Albert Einstein School of Medicine, Bronx, NY, 10461, USA.

[11]New York Medical College and Albert Einstein College of Medicine, Bronx, NY, 10461, USA.

[12]Hematology Department, Shaare Zedek Hospital, Jerusalem, 91031, Israel

[13]Leukemia Service, Department of Medicine, Memorial Sloan Kettering Cancer Center, New York, NY 10065, USA

[14] Dipartimento di Salute della Donna e del Bambino, Università di Padova,via Giustiniani 3, 35128, Padova, Italy

[15]Department of Pediatric Oncology/Hematology, Erasmus MC-Sophia Children's Hospital, Rotterdam, South Holland, 010 7040704, the Netherlands.

[16]Department of Pediatrics, Columbia University Medical Center, New York, NY, 10032, USA.

[17]These authors contributed equally to this work

Contacts:
Adolfo Ferrando:
Phone: 212-8514611
E-mail: af2196@columbia.edu

Andrea Califano:
Phone:212-851-5183
E-mail: ac2248@columbia.edu

Running title: AKT inhibition reverses glucocorticoid resistance

SUMMARY

Glucocorticoid resistance is a major driver of therapeutic failure in T-cell acute lymphoblastic leukemia (T-ALL). Here we identify the AKT1 kinase as a major negative regulator of the NR3C1 glucocorticoid receptor protein activity driving glucocorticoid resistance in T-ALL. Mechanistically, AKT1 impairs glucocorticoid-induced gene expression by direct phosphorylation of NR3C1 at position S134 and blocking glucocorticoid-induced NR3C1 translocation to the nucleus. Moreover, we demonstrate that loss of PTEN and consequent AKT1 activation can effectively block glucocorticoid induced apoptosis and induce resistance to glucocorticoid therapy. Conversely, pharmacologic inhibition of AKT with MK2206 effectively restores glucocorticoid-induced NR3C1 translocation to the nucleus, increases the response of T-ALL cells to glucocorticoid therapy and effectively reverses glucocorticoid resistance *in vitro* and *in vivo*.

SIGNIFICANCE

Improving the outcomes of patients with acute lymphoblastic leukemia (ALL) will require the identification of specific molecular mechanisms driving resistance to therapy and developing new pharmacologic strategies to neutralize them. Primary resistance to glucococorticoids, defined as failure to achieve robust cytoreduction after a week of glucocorticoid therapy, is of particular importance as it is associated with very poor prognosis. Here we show that AKT1 can drive resistance to glucocorticoids via direct inhibition of the glucocorticoid receptor. Consistently, pharmacologic inhibition of AKT effectively reverses glucocorticoid resistance. These results highlight the potential role of AKT1 as therapeutic target in the treatment of glucocorticoid resistant T-ALL.

INTRODUCTION

Glucocorticoids are small lipophilic compounds derived from cortisol, a natural adrenal hormone that signals via the glucocorticoid receptor alpha, a nuclear receptor ligand-activated transcription factor encoded by the *NR3C1* gene (Schlossmacher et al., 2011). Glucocorticoids play a fundamental role in the treatment of all lymphoid tumors because of their capacity to induce apoptosis in lymphoid progenitor cells (Inaba and Pui, 2010) (Pui et al., 2011; Pui et al., 2012). The importance of glucocorticoid therapy in lymphoid malignancies is underscored by the strong association of primary glucocorticoid resistance with poor prognosis in childhood acute lymphoblastic leukemia (ALL). Thus, prednisone poor response, defined as failure to show effective cytoreduction after 7 days of glucocorticoid therapy is strongly associated with increased risk of relapse and therapeutic failure (Dordelmann et al., 1999; Inaba and Pui, 2010) and *in vitro* resistance to glucocorticoids is associated with unfavorable prognosis in this disease (Hongo et al., 1997; Inaba and Pui; Klumper et al., 1995). Primary glucocorticoid resistance is particularly frequent in T-ALL (Hongo et al., 1997; Inaba and Pui, 2010; Klumper et al., 1995), leading us to hypothesize that activation of one or more oncogenic signaling pathways implicated in T-cell transformation could be driving primary glucocorticoid resistance in T-ALL directly by interfering with glucocorticoid receptor function or indirectly via inhibition of glucocorticoid induced apoptosis. In this context, the *AKT1* gene emerged as a plausible candidate as PI3K-AKT activation plays a major role of in the pathogenesis of T-ALL, particularly in leukemias harboring mutations and deletions in the *PTEN* tumor suppressor gene (Gutierrez et al., 2009; Palomero et al., 2007). Moreover, in silico analysis of signaling factors modulating transcriptional signatures associated with glucocorticoid resistance in T-ALL pointed to a potential role of AKT1 as driver of glucocorticoid resistance in T-ALL (**Supplementary Results and Figure S1**). These results together with the association of mutational loss of *PTEN* and increased AKT1 phosphorylation with primary glucocorticoid resistance in the clinic (Bandapalli et al.; Morishita et al., 2012) and the availability of PI3K-AKT specific inhibitors in clinical trials for the treatment of human cancer, prompted us to analyze the mechanistic role of AKT1 in the control of glucocorticoid resistance in T-ALL.

RESULTS

AKT1 binds to the NR3C1 glucocorticoid receptor protein

Activation of gene expression by glucocorticoids is a multistep process that requires effective release of the glucocorticoid receptor from heat shock protein complexes, translocation to the nucleus and formation of a multiprotein transcriptional complex on the promoter of glucocorticoid target genes (Heitzer et al., 2007). To test if AKT1 can interact with and inhibit the glucocorticoid receptor protein, we transfected 293T cells with plasmid constructs driving the expression of Flag-tagged AKT1 and HA-tagged NR3C1 and isolated glucocorticoid receptor-containing protein complexes via immunoprecipitation using an anti-HA antibody. Western blot analysis demonstrated the presence of Flag-AKT1 in HA-NR3C1 immunoprecipitates, suggesting that AKT1 can interact with NR3C1 *in vivo* (**Figure 1A**). Reciprocal immunoprecipitation experiments confirmed the association between Flag-AKT1 and HA-NR3C1 (**Figure 1B**). Moreover, immunoprecipitation of NR3C1 protein complexes from the T-ALL cell lines DND41 and CCRF-CEM demonstrated that endogenous NR3C1 and AKT1 can interact in T-ALL lymphoblast cells (**Figure 1C** and **Figure S2**). In addition, immunofluorescence analysis showed colocalization of NR3C1 and AKT1 in DND41 and CCRF-CEM cells (**Figure 1D and Figure S3**). Finally, glutathione-S-transferase (GST)-pulldown assays showed that recombinant GST-NR3C1 fusion protein can directly interact with His-tagged AKT1 *in vitro* (**Figure 1E**).

AKT1 phosphorylates S134 in the NR3C1 protein

AKT1 kinase substrates are typically phosphorylated by AKT at RXRXXS/T motifs (Mok et al., 1999; Ozes et al., 1999; Zimmermann and Moelling, 1999). Phospho-AKT motif scanning analysis of NR3C1 revealed a potential AKT phosphorylation motif 131RSTS134 (**Figure 1F and Figure S4**), suggesting that the glucocorticoid receptor could be an AKT1 substrate phosphorylated at serine 134. To test this possibility, we expressed HA-tagged wild type NR3C1 (HA-NR3C1) or an HA-tagged form of the glucocorticoid receptor with a serine to alanine substitution at position 134 (HA-NR3C1 S134A) in cells infected with retroviruses expressing MYR-AKT1. Protein immunoprecipitation of NR3C1 with an antibody against HA and subsequent Western blot analysis with an antibody recognizing the phospho-RXXS/T AKT phosphorylation motif showed the presence of a HA-NR3C1 phospho-AKT band in cells expressing the wild type glucocorticoid receptor, but not in cells expressing the HA-NR3C1 S134A mutant (**Figure 1G**). Consistently, *in vitro* kinase assays in which we analyzed the capacity of the AKT1 kinase to phosphorylate the wild type or S134A glucocorticoid receptor proteins demonstrated that AKT1 can effectively phosphorylate recombinant wild type NR3C1 protein *in vitro*,

but not the serine 134 to alanine NR3C1 mutant protein (**Figure 1H**). Mass spectrometry analysis of HA-NR3C1 protein isolated from MYR-AKT1 expressing cells demonstrated the presence of serine phosphorylation at position 134 of the glucocorticoid receptor (**Figure 1I,J**), which was effectively abrogated (control S134P:non-P = 0.47; MK2206 S134P:non-P = 0.03; **Table S1**) upon treatment with MK2206, a highly potent and selective inhibitor of AKT (Hirai et al.). Finally, and most notably, western blot analysis with the AKT phosphorylation motif antibody showed decreased AKT phosphorylated NR3C1 in NR3C1 immunoprecipitates from CCRF-CEM T-ALL cells upon AKT inhibition with MK2206 (**Figure 1K**).

AKT signaling inhibits NR3C1 nuclear translocation following glucocorticoid treatment

After establishing the interaction and phosphorylation of the glucocorticoid receptor by AKT1 we sought to elucidate the relevance of the NR3C1 S134 phosphorylation for glucocorticoid receptor function. Glucocorticoid induced cytoplasmic-nuclear shuttling is strictly required for glucocorticoid receptor activity, which functions as a ligand activated transcription factor (Heitzer et al., 2007). U2OS cells, which express undetectable levels of endogenous NR3C1 (**Figure S5**), showed cytoplasmic localization of retrovirally expressed HA-tagged glucocorticoid receptor protein, which was completely relocalized to the nucleus upon dexamethasone treatment (**Figure 2A**). Notably, expression of MYR-AKT1 in these cells resulted in impaired nuclear relocalization of NR3C1 after dexamethasone treatment (**Figure 2B**). In addition, and in contrast with wild type glucocorticoid receptor, the NR3C1 S134A mutant protein showed increased nuclear localization in basal conditions and effective nuclear relocalization upon dexamethasone treatment (**Figure 2C**), even upon expression of MYR-AKT1 (**Figure 2D**). Next we analyzed the capacity of the MK2206 AKT inhibitor to modulate glucocorticoid induced translocation of NR3C1 to the nucleus in T-ALL cells. CCRF-CEM and MOLT3, two PTEN null, glucocorticoid resistant T-ALL cell lines expressing high levels of AKT activation, showed cytoplasmic localization of NR3C1 in basal conditions, which was only partially relocalized to the nucleus upon dexamethasone treatment (**Figure 2E**, **Figure S6**). Inhibition of AKT with MK2206 effectively enhanced glucocorticoid-induced translocation of the NR3C1 protein to the nucleus in these cells (**Figure 2E**, **Figure S6**). Notably, similar results were obtained in primary T-ALL lymphoblasts in which inhibition of AKT with MK2206 increased the nuclear translocation of the NR3C1 protein following glucocorticoid treatment (**Figure 2F**).

Transcriptionally, MYR-AKT1 impaired the capacity of NR3C1 to activate a luciferase reporter construct under the control of a synthetic glucocorticoid response element (**Figure 3A**). Consistently, AKT activation via MYR-AKT1 expression or PTEN knockdown in DND41 and KOPTK1 T-ALL cells impaired key effector responses mediating glucocorticoid induced cell death including glucocorticoid receptor autoupregulation (Geng et al., 2008) and induction of *BCL2L11*, a proapototic factor essential for glucocorticoid induced cell death (Wang et al., 2003) (**Figure 3B,C; Figures S7 and S8**). Consistently, glucorticoid induced apoptosis was significantly blunted in DND41 and KOPTK1 MYR-AKT expressing cells compared with controls (**Figure S9**). Next, and to best analyze the potential impact of mutational loss of PTEN in T-ALL on the global transcriptional program induced by glucocorticoids, we performed microarray gene expression analysis of DND41 shRNA control and PTEN shRNA knockdown cells treated with dexamethasone. In agreement with a global inhibition of glucocorticoid receptor activity by AKT, microarray analysis of gene expression changes induced by dexamethasone treatment showed complete abrogation of glucocorticoid induced signatures upon activation of AKT1 via *PTEN* shRNA knockdown (**Figure 3D**). Moreover, GSEA analysis of genes regulated by glucocorticoids in primary leukemia samples (Schmidt et al., 2006) showed a marked enrichment in DND41 control cells treated with dexamethasone compared with dexamethasone-treated *PTEN* shRNA knockdown samples (**Figure 3E**).

Pharmacologic inhibition of AKT reverses glucocorticoid resistance *in vitro* and *in vivo*

To test the therapeutic role of AKT inhibition in the treatment of glucocorticoid resistant leukemias we first treated CCRF-CEM cells a PTEN-null glucocorticoid resistant T-ALL cell line with dexamethasone and MK2206. In these experiments AKT1 inhibition of CCRF-CEM lymphoblasts with MK2206 effectively restored glucocorticoid induced apoptosis and reversed glucocorticoid resistance *in vitro* (**Figure 4A**). Similar results were obtained in the glucocorticoid resistant MOLT3 and PF382 T-ALL cell lines (**Figure S10**). Analysis of an extended panel of cell lines including B precursor ALL, diffuse B cell lymphoma and multiple myeloma lines showed additive effects with this combination (**Figures S11-S13**), suggesting that the synergistic interaction between glucocorticoids and AKT inhibition may be most prominently relevant in the context of T-ALL.

Next we analyzed the effects of MK2206 and glucocorticoid *in vivo* in a xenograft model of glucocorticoid-resistant T-ALL. CCRF-CEM cells expressing the luciferase gene were injected intravenously in

immunodeficient NOG mice and tumor engraftment was assessed by *in vivo* bioimaging at day 18. Animals harboring homogeneous tumor burdens were treated with vehicle only (DMSO), MK2206, dexamethasone or MK2206 plus dexamethasone for 3 days. In this experiment, animals treated with dexamethasone or MK2206 showed progressive tumor growth similar to that observed in vehicle-treated controls, while mice treated with MK2206 plus dexamethasone had significant antitumor responses (**Figure 4B**; $P = 0.031$). Following these results we evaluated the response to the combination treatment MK2206 plus dexamethasone in primary T-ALL lymphoblasts. Towards this goal we established viable *in vitro* cultures of T-ALL leukemia samples supported by bone marrow MS5 stroma cells expressing the Delta like 1 NOTCH1 ligand (Armstrong et al., 2009). Treatment of T-ALL primary leukemia cultures with MK2206 plus dexamethasone in combination showed significantly increased antileukemic effects compared with treatment with dexamethasone or MK2206 alone (**Figure 4C,D** and **Figure S14**). Notably, the antileukemic effects of MK2206 plus dexamethasone were prominent in tumor samples with PTEN loss (TALL#6, TALL#9 and T-ALL#28), but were also realized in PTEN-expressing tumors with moderate levels of AKT1 activation (T-ALL #19, TALL#37 and T-ALL#39) (**Figure S15**).

To further test the efficacy of this treatment combination *in vivo* we established leukemia xenografts in NOD rag gamma immunodeficient mice using three independent glucocorticoid resistant primary T-ALL samples infected with lentiviruses expressing the luciferase gene. Animals harboring homogeneous tumor burdens by *in vivo* bioimaging were treated with vehicle only (DMSO), MK2206, dexamethasone or MK2206 plus dexamethasone. In this experiment, mice treated with dexamethasone or MK2206 showed progressive tumor growth similar to that observed in vehicle-treated controls, while mice treated with MK2206 plus dexamethasone showed significant antitumor responses (**Figure 5**). In these experiments analysis of AKT1 phosphorylation showed effective suppression of AKT1 signaling in mice treated with MK2206 and MK2206 plus dexamethasone *in vivo* (**Figure S16**). Moreover, expression analysis of the GILZ-TSC22D3 glucocorticoid receptor target (Ayroldi et al., 2007; D'Adamio et al., 1997; Riccardi et al., 1999), showed increased glucocorticoid response and apoptosis in leukemia infiltrated tissues of mice treated with MK2206 plus dexamethasone in combination (**Figure S16**). Pharmacokinetic analysis of MK2206 and dexamethasone ruled out that this effect could be mediated by decreased clearance of dexamethasone as the pharmacokinetic

profile of this glucocorticoid was identical in animals treated with dexamethasone alone and mice treated with MK2206 plus dexamethasone in combination (**Figure S17**). In addition, even though we observed a modest decrease in MK2206 half life in mice treated with dexamethasone plus MK2206 (**Figure S17)**, AKT inhibitor levels obtained in animals treated with MK2206 as single agent already result in complete suppression of AKT activation *in vivo* (**Figure S16**), supporting that this pharmacokinetic interaction does not account for the increased antileukemic responses observed in mice treated with dexamethasone plus MK2206.

Finally, we generated a mouse leukemia model in which glucocorticoid resistance is specifically driven by genetic loss of *Pten* using a well established retroviral transduction and bone marrow transplantation protocol (Chiang et al., 2008). In this model, transplantation of tamoxifen-inducible conditional *Pten* knockout (Rosa26TMCre *Pten*$^{flox/flox}$) hematopoietic progenitors infected with retroviruses expressing a mutant constitutively active form of the NOTCH1 receptor (*NOTCH1* L1601P ΔPEST) resulted in the development of NOTCH1 driven T-ALL tumors as previously described (Chiang et al.). Next we infected *NOTCH1* Rosa26TMCre *Pten*$^{flox/flox}$ T-ALL lymphoblasts with a luciferase expressing retrovirus and transplanted them into secondary recipients which were treated with vehicle only or tamoxifen in order to generate *Pten*-non-deleted and *Pten*-deleted isogenic tumors, respectively. Treatment of *Pten*-non-deleted tumor bearing mice with dexamethasone showed a significant improvement in survival compared with vehicle only treated controls ($P < 0.01$) (**Figure 6A**). In contrast, and consistent with a role of *Pten* loss and AKT1 activation in promoting glucocorticoid resistance, all mice harboring *Pten*-deleted tumors failed to respond to dexamethasone treatment and showed no survival differences compared to vehicle treated controls (**Figure 6B**).

To test the efficacy of MK2206 and glucocorticoids in combination we treated mice transplanted with *NOTCH1*-induced *Pten*-deleted murine tumors expressing luciferase in secondary recipients, with vehicle only (DMSO), MK2206, dexamethasone or MK2206 plus dexamethasone and monitored their response to therapy by *in vivo* bioimaging. Animals treated with dexamethasone or MK2206 in this experiment showed progressive tumor growth similar to that observed in vehicle-treated controls, while mice treated with MK2206 plus dexamethasone showed significant antitumor responses (**Figure 6C,D**; $P < 0.001$) which translated in significantly improved survival in this group (**Figure 6E**; $P < 0.001$). As before, analysis of AKT1 phosphorylation showed effective suppression of AKT1 signaling in mice treated with MK2206 and MK2206

plus dexamethasone *in vivo* (**Figure S18**) while GILZ-TSC22D3 expression analysis showed increased glucocorticoid response and apoptosis in tumor cells from animals treated with MK2206 plus dexamethasone in combination (**Figure S18**).

Finally, we analyzed the role of NR3C1 S134 phosphorylation in the therapeutic response to glucocorticoids and the effects of *Pten* loss in glucocorticoid therapy in this model. Retroviral expression of the glucocorticoid receptor in *Pten* non-deleted lymphoblasts (**Figure S19**) enhanced the response of NOTCH1-induced leukemias to glucocorticoid treatment; an effect that was effectively abrogated upon *Pten* loss (**Figure 6F**). In contrast, expression of the AKT-resistant NR3C1 S134A mutant protein was equally effective at increasing the antileukemic effects of glucocorticoids in *Pten* non-deleted and *Pten* null lymphoblasts (**Figure 6G**). Overall, these results support that pharmacologic inhibition of AKT can effectively enhance glucocorticoid response and reverse glucocorticoid resistance in T-ALL.

DISCUSSION

Glucocorticoids were the first group of drugs introduced in the treatment of acute lymphoblastic leukemia and have remained at the core of the treatment of lymphoid malignancies for over 50 years. Over the last four decades, the use of glucocorticoids in combination chemotherapy has led to significant progress in the treatment of leukemias and lymphomas. Notwithstanding, 25% of children with T-ALL, fail to achieve a sustained response and ultimately die because of relapsed, refractory disease (Freyer et al., 2011; Ko et al., 2010; Tallen et al., 2010). Clinical outcomes in adult T-ALL are substantially worse, with only about 50% of the patients achieving long-term remissions (Marks et al., 2009). In this context, primary resistance to glucocorticoids is a major clinical problem as failure to achieve an adequate initial response to glucocorticoid monotherapy is associated with high rates of relapse and poor prognosis (Dordelmann et al., 1999; Inaba and Pui, 2010).

Numerous mechanisms have been proposed to explain the lack of effective glucocorticoid induced apoptosis in prednisone poor responders (Bhadri et al., 2012). However, and despite much research over the last two decades, the molecular basis of primary glucocorticoid resistance in ALL remain poorly understood. Given that primary glucocorticoid resistance is a cell intrinsic property of leukemia lymphoblasts present before exposure to glucocorticoid therapy, we proposed that primary oncogenic signaling pathways involved in leukemia

transformation could also function as negative upstream regulators of the glucocorticoid receptor driving this phenotype. The identification of AKT1 as a driver of glucocorticoid resistance in T-ALL is perfectly consistent with this model. Notably, direct activation of AKT1 can drive T-cell transformation (Kharas et al., 2010); activation of PI3K-AKT signaling as result of deletions and mutations in *PTEN* (Gutierrez et al.; Palomero et al., 2007) is highly prevalent in T-ALL; and *PTEN* mutations are associated with primary glucocorticoid resistance in the clinic (Bandapalli et al.).

Mechanistically, we show that AKT1 can induce glucocorticoid resistance by phosphorylation of the glucocorticoid receptor in position S134, which impairs the nuclear relocalization of the glucocorticoid receptor protein and blocks transcriptional regulation of glucocorticoid target genes. However, it should be noted that additional mechanisms downstream of AKT1 in addition to direct inactivation of the glucocorticoid receptor can also promote resistance to glucocorticoid therapy by promoting cell growth, metabolism and survival in T-ALL. In this regard, mTOR phosphorylation by AKT impairs glucocorticoid induced apoptosis by increasing the expression of MCL1 (Wei et al., 2006). In addition, AKT phosphorylation inhibits BAD mediated apoptosis (Bornhauser et al., 2007; Datta et al., 1997; del Peso et al., 1997); AKT-mediated phosphorylation of XIAP prevents the autoubiquitination and subsequent degradation of this antiapoptotic factor (Bornhauser et al., 2007; Dan et al., 2004); and increased metabolism induced by AKT activation can antagonize metabolic inhibition induced by glucocorticoids (Beesley et al., 2009). The convergent effects of direct (shown here) and indirect mechanisms downstream of AKT1 antagonizing the antileukemic effects of glucocorticoids further support the role of the PI3K-AKT pathway as therapeutic target for the reversal of primary glucocorticoid resistance in T-ALL.

EXPERIMENTAL PROCEDURES

INHIBITORS AND DRUGS

MK2206 or 8-[4- (1-aminocyclobutyl)phenyl]-9-phenyl-1,2,4-triazolo[3,4-f] [1,6]naphthyridin-3 (2H)-one hydrochloride [1:1] was from Selleck Chemicals LLC. Dexamethasone and 4-Hydroxytamoxifen were from Sigma-Aldrich.

TARGETED siRNA SCREEN

DND41 cells were electroporated with smartpool siRNAs (Dharmacon) targeting candidate regulators of glucocorticoid resistance or an inactive siRNA control using the SF Cell line 96-well Nucleofector Kit (Lonza). Twenty-four hours after electroporation, cells were treated with dexamethasone (1 μM) for 48h. Apoptosis was analyzed by FACS using the PE AnnexinV Apoptosis Kit I (BD Biosciences).

MICROARRAY EXPRESSION ANALYSIS OF GLUCOCORTICOID RESPONSE

DND41 shRNA LUC and DND41 PTEN shRNA cell were treated with vehicle only (DMSO) or dexamethasone (1μM) for 24 hours in triplicate. RNA was isolated, labeled and hybridized to the HumanHT-12 v4 Expression BeadChip (Illumina) using standard procedures. Raw gene expression data was log transformed and quantile normalized using MATLAB. Differentially regulated genes in DND41 shRNA LUC vs DND41 PTEN shRNA upon dexamethasone treatment with a fold change > 2 were selected by t-test. Glucocorticoid regulated transcripts (t-test $P<0.01$ and fold change >1.25) in primary ALL were identified from processed expression data obtained from peripheral blood lymphoblasts from 13 pediatric ALL patients after 24 hours of treatment with glucocorticoids (Schmidt et al., 2006). Enrichment of these glucocorticoid signature genes in shRNA PTEN vs shRNA LUC dexamethasone treated samples normalized to DMSO controls was analyzed by GSEA using the t-test metric comparing and 1,000 permutations of the genes.

LUCIFERASE REPORTER ASSAYS

We performed NR3C1 reporter assays using the Cignal GRE Reporter (luc) Kit (SABiosciences).

***IN VITRO* KINASE ASSAYS**

Flag-tagged recombinant GST-NR3C1 and GST-NR3C1 S134A mutant proteins were incubated with recombinant active His-AKT1 protein (Millipore) in kinase buffer (Cell Signaling) containing γ-32P-ATP and analyzed by autoradiography after SDS-PAGE.

MASS SPECTROMETRY

HA-NR3C1 protein was immunoprecipitated from U2OS cells stably expressing HA-tagged human NR3C1 and Myr-AKT with anti-HA antibody conjugated beads (Sigma), electrophoresed on a 3-8% Tris-Acetate gel, stained with Simply Blue Stain (Invitrogen), excised, reduced with DTT, alkylated with iodoacetamide and digested with trypsin and analyzed for phosphorylated peptides by nanoLC-ESI-MS/MS. MS/MS spectra were processed using ProteinLynx from the MassLynx 4.0 software and searched against the Swiss-Prot protein

database using Mascot (www.matrixscience.com) with differential modifications for Ser/Thr/Tyr phosphorylation (+79.97).

To test the effects of AKT1 inhibition in NR3C1 S134 phosphorylation we treated U2OS cells stably expressing HA-tagged human NR3C1 and the constitutively active Myr-AKT with MK2206 or DMSO (10 μM, 5 hours). We immunoprecipitated HA-NR3C1 protein with anti-HA antibody conjugated beads (Sigma). Immnuopurified HA-NR3C1 was then electrophoresed on a 4-12% Bis-Tris gel, stained with Simply Blue Stain (Invitrogen), digested with trypsin and analyzed for the phosphorylation status at residue S134 by microcapillary LC-MS/MS.

IMMUNOFLUORESCENCE

We analyzed U2OS cells stably expressing wild type NR3C1 or the S134A NR3C1 by NR3C1 immunofluorescence (1:500; Santa Cruz Biotechnology), followed by Alexa Fluor 594 (1:1000; Invitrogen) staining and confocal microscopy. In colocalization studies, T-ALL cell lines were immunostained with rabbit antibodies against NR3C1 (1:300; Santa Cruz Biotechnology) and a mouse antibody against AKT (1:100)(Cell Signaling, 2920) using anti-rabbit Alexa Fluor 594 (1:500; Invitrogen) and anti-mouse Alexa Fluor 488 (1:500; Invitrogen) as secondary antibodies. We stained nuclei with TO-PRO3 reagent (Invitrogen) and visualized them by confocal imaging on a Zeiss LSM510-NLO microscope.

MICE

Animal procedures were approved by the Columbia University IACUC. Rosa26 Cre-Tam mice expressing a tamoxifen-inducible form of the Cre recombinase from the ubiquitous *Rosa26* locus (Guo et al., 2007) and *Pten* conditional knockout mice (*Pten*^{fl}) have been previously described (Trotman et al., 2003). To generate *NOTCH1*-induced T-ALL tumors in mice we performed retroviral transduction of bone marrow cells with an activated form of the *NOTCH1* oncogene (NOTCH1 L1601P ΔPEST) and transplanted them via intravenous injection into lethally irradiated recipients as previously described (Chiang et al., 2008). Primary human T-ALL xenografts experiments were generated via intravenous injection of human T-ALL lymphoblasts into NOD rag gamma mice. We evaluated disease progression and therapy response by *in vivo* bioimaging with the In Vivo Imaging System (IVIS, Xenogen), human CD45 analysis by flow cytometry and analysis of luciferase activity in bone marrow and spleen.

STATISTICAL ANALYSES

We performed statistical analysis by Student's *t*-test and Wilcoxon signed-rank test. We considered results with $P < 0.05$ as statistically significant. Survival in animal experiments was represented with Kaplan–Meier curves and significance was estimated with the log-rank test (Prism GraphPad).

ACCESION NUMBERS

Microarray gene expression data is available in Gene Expression Omnibus (accession numbers GSE41062, GSE32215, GSE2677 and GSE10609).

SUPPLEMENTAL INFORMATION

Supplemental information includes Supplementary Results, Extended Experimental Procedures, nineteen figures and one table.

ACKNOWLEDGEMENTS

This work was supported by the National Institutes of Health (grant R01CA129382 to A.A.F.; U24 CA114737 to E.P.; RC2 CA148308 to A.C. and A.F.), the Stand Up To Cancer Innovative Research Award (A.A.F.), the Chemotherapy Foundation (A.A.F.), the Leukemia & Lymphoma Society Scholar Award (A.A.F.), a Leukemia & Lymphoma Society SCOR Grant (A.A.F.), and the ECOG Leukemia Tissue Bank. We are grateful to A. Kung for the FUW-luc vector, J. Aster for the MigR1-*NOTCH1* L1601PΔP vector, P. P. Pandolfi for the *Pten*^{fl} conditional knockout mouse, T. Ludwig for the *Rosa26* Cre-Tam mouse, S. Minuzzo for generating T-ALL xenografts, L. Xu for help in animal procedures, M. A. Gawinowicz from the Proteomics Share Resource at the Herbert Irving Comprehensive Cancer Center at Columbia University for assistance in mass spectrometry analysis and R. Baer for helpful discussions and revision of the manuscript.

FIGURE LEGENDS

Figure. 1. AKT1 interacts with the glucocorticoid receptor protein and regulates NR3C1 S134 phosphorylation

(A) Western blot analysis of AKT1 and activated AKT1 after NR3C1 immunoprecipitation in 293T cells expressing Flag-tagged AKT1 and HA-tagged NR3C1. (B) NR3C1 western blot analysis after AKT1 immunoprecipitation in 293T cells expressing Flag-tagged AKT1 and HA-tagged NR3C1. (C) Western blot analysis of AKT1 after NR3C1 protein immunoprecipitation in DND-41 T-ALL cells. (D) Immunofluorescence colocalization analysis of AKT (green) and NR3C1 (red) proteins in DND41 cells. Cell nuclei stained with TO-PRO3 are shown in blue. (E) Analysis of AKT1-NR3C1 interaction via Western blot analysis of protein complexes recovered after NR3C1-GST pull down of recombinant His-tagged AKT1. (F) Partial alignment of the glucocorticoid receptor protein sequences flanking S134. (G) Western blot analysis of NR3C1 phosphorylation using an antibody against the AKT phospho-motif in NR3C1 protein immunoprecipitates from U2OS cells expressing MYR-AKT1 together with HA-NR3C1 or HA-NR3C1 S134A. (H) *In vitro* kinase analysis of AKT1 phosphorylation of recombinant NR3C1 (GST-NR3C1) and NR3C1 S134A mutant (GST-NR3C1 S134A) proteins. Top panel shows P32 autoradiography after SDS-PAGE and corresponding protein loading is shown at the bottom. (I) ESI-MS/MS spectrum of monophosphorylated peptide STpS134VPENPK (S-132 to K-140) obtained after trypsin digestion of NR3C1 isolated from cells expressing constitutively active AKT1. (J) Collision induced dissociation of the molecular ion, [M+2H]2+ at m/z 519.72 (M = 1037.42 Da) corresponding to S134. Characteristic b- and y-fragment ions including y7 which contains pSer and features the loss of 98 Da (elimination of phosphoric acid) are shown. (K) Western blot analysis of NR3C1 phosphorylation using an anti AKT phospho-motif antibody in NR3C1 immunoprecipitates from CCRF-CEM cells expressing HA-NR3C1 treated with vehicle or the MK2206 AKT inhibitor.

Figure. 2. AKT1-mediated S134 phosphorylation of the NRC3C1 protein impairs dexamethasone-induced glucocorticoid receptor nuclear translocation

(A) Confocal microscopy analysis and quantitation of the distribution of NR3C1 cellular localization in U2OS cells expressing HA-NRC31 in basal conditions (DMSO) and after dexamethasone (Dexa; 1 μM) stimulation. (B) NR3C1 cellular localization in U2OS cells expressing HA-NRC31 and MYR-AKT1 in basal conditions and after dexamethasone stimulation. (C) Cellular localization of NR3C1 in U2OS cells expressing the HA-NRC31 S134A mutant in basal conditions and after dexamethasone stimulation. (D) Cellular localization of the HA-NRC31 S134A protein in U2OS cells expressing MYR-AKT1 in basal conditions and after dexamethasone

stimulation. (E) Cellular localization analysis of NR3C1 via nuclear and cytoplasmic cell fractionation and analysis of AKT1 signaling in cell lysates from CCRF-CEM T-ALL cells treated with vehicle only (DMSO), dexamethasone (Dexa; 1 μM), the MK2206 AKT inhibitor (1 μM) and MK2206 plus dexamethasone (1 μM each). (F) Cellular localization analysis of NR3C1 via Western blot analysis of nuclear and cytoplasmic cell fractions in cell lysates from primary T-ALL lymphoblasts. Tubulin and MAX proteins are shown as controls for cytosolic and nuclear fractions. C: cytoplasmic fraction; N: nuclear fraction. Data in A-D are represented as mean ± s.d.

Figure 3. AKT activation inhibits glucocorticoid-induced gene expression.

(A) Luciferase reporter analysis of dexamethasone-induced glucocorticoid receptor transactivation in U2OS cells expressing MYR-AKT1 compared with GFP only expressing controls using a synthetic glucocorticoid response element reporter. (B) Western blot analysis of PTEN expression and AKT activation in DND41 T-ALL cells infected with lentiviruses expressing a PTEN shRNA construct (shRNA PTEN) or a control shRNA targeting the *Renilla* luciferase gene (shRNA LUC). (C) RT-PCR analysis of glucocorticoid regulated transcripts in control and PTEN knockdown DND41 cells treated with vehicle (DMSO) only or 1 μM dexamethasone (Dexa). (D) Heat map representation of the top differentially expressed genes between control DND41 cells treated with vehicle only (Control) *vs.* 1 μM dexamethasone (Dexa) and corresponding transcript levels in control and dexamethasone treated PTEN knockdown cells. The scale bar shows color coded differential expression with red indicating higher levels and blue lower levels of expression. (E) GSEA analysis of genes regulated by glucocorticoids in ALL patients undergoing glucocorticoid therapy in DND41 shRNA LUC dexamethasone treated cells compared with DND41 shRNA PTEN dexamethasone treated cells. Data in A and C are represented as mean ± s.d.

Figure. 4. Pharmacologic inhibition of AKT with MK2206 reverses glucocorticoid resistance

(A) Representative plots of apoptosis and cell viability quantification in CCRF-CEM T-ALL cells treated with vehicle only, MK2206 (100 nM), dexamethasone (Dexa; 1 μM) or dexamethasone plus MK2206 (Dexa + MK2206; 1 μM and 100 nM, respectively) in combination *in vitro*. (B) Tumor load quantification *in vivo* by bioluminescence imaging and analysis of luciferase activity and human CD45 expressing cells in the bone marrow of CCRF-CEM T-ALL xenografts treated with vehicle only, MK2206 (10 mg kg^{-1} via oral gavage twice a

day), dexamethasone (5 mg kg^{-1} via intraperitoneal injection) or MK2206 (10 mg kg^{-1} twice a day) plus dexamethasone (5 mg kg^{-1}). (C) Representative plots and quantification of cell viability in primary T-ALL samples treated with vehicle only, MK2206 (100 nM-10 μM), dexamethasone (10 nM-1 μM) alone and dexamethasone (10 nM-1 μM) plus MK2206 (100 nM-10 μM) in combination. Percentages of viable (PI −), and non-viable (PI +) cells are indicated. Bar graphs represent mean ± s.d.

Figure 5. Pharmacologic inhibition of AKT reverses glucocorticoid resistance in primary human T-ALL *in vivo*

(A-C) Representative examples of tumor load analysis via *in vivo* by bioluminescence imaging in mice xenopgrafted with three independent human T-ALLs treated with vehicle only, MK2206 (10 mg kg^{-1} twice a day), dexamethasone (5 mg kg^{-1}) or MK2206 (10 mg kg^{-1} twice a day) plus dexamethasone (5 mg kg^{-1}). (D-F) Quantitative analysis of tumor load and therapy response based on luciferase activity. (G-I) Representative images of spleens in primary T-ALL xenografted mice at the end of treatment. (J-L) Quantitative analysis of tumor burden estimated by spleen weight in primary T-ALL xenografted mice at the end of treatmet. (M-O) Quanttative analysis of tumor burden estimated by luciferase counts in bone marrow in primary T-ALL xenografted mice at the end of treatment. Scale bar: 2 cm. Bar graphs in M-O represent mean ± s.d.

Figure 6. Pharmacologic inhibition of AKT reverses glucocorticoid resistance in a mouse model of glucorticoid resistant T-ALL

(A, B) Kaplan-Meier curve in mice treated with dexamethasone (Dexa) or vehicle (Control) after allograft transplantation of *Pten*-non-deleted [–Tmx (*Pten*$^{f/f}$)] or *Pten*-deleted [+Tmx (*Pten*$^{-/-}$)] *NOTCH1*-induced T-ALL tumor cells. Arrows indicate drug treatment. (C, D) Representative images, changes in bioluminescence by *in vivo* imaging and analysis of treatment response in mice allografted with *NOTCH1* induced *Pten* deleted mouse leukemia cells treated with vehicle only, MK2206 (10 mg kg^{-1} via oral gavage twice a day), dexamethasone (Dexa; 5 mg kg^{-1}) or MK2206 (10 mg kg^{-1} twice a day) plus dexamethasone (5 mg kg^{-1}) (Dexa + MK2206). (E) Kaplan-Meier overall survival curve in mice allografted with *NOTCH1* induced *Pten* deleted mouse leukemia cells and treated with vehicle only (control), MK2206 (10 mg kg^{-1} via oral gavage twice a day), dexamethasone (Dexa; 5 mg kg^{-1}) or MK2206 (10 mg kg^{-1} twice a day), plus dexamethasone (5 mg kg^{-1}) (Dexa + MK2206). (F,G) Quantification of glucocorticoid-induced loss of viability in *NOTCH1* induced *Pten* non

deleted [–Tmx (*Pten* f/f)] or *Pten* deleted [+Tmx (*Pten* –/–)] mouse leukemia cells infected with retroviruses expressing the wild type glucocorticoid receptor NR3C1 (MSCV HA-NR3C1) or the S134A glucocorticoid receptor NR3C1 mutant protein (MSCV HA-NR3C1 S134A). Data in F and G are represented as mean ± s.d.

REFERENCES

Armstrong, F., Brunet de la Grange, P., Gerby, B., Rouyez, M. C., Calvo, J., Fontenay, M., Boissel, N., Dombret, H., Baruchel, A., Landman-Parker, J.*, et al.* (2009). NOTCH is a key regulator of human T-cell acute leukemia initiating cell activity. Blood *113*, 1730-1740.

Ayroldi, E., Zollo, O., Bastianelli, A., Marchetti, C., Agostini, M., Di Virgilio, R., and Riccardi, C. (2007). GILZ mediates the antiproliferative activity of glucocorticoids by negative regulation of Ras signaling. The Journal of clinical investigation *117*, 1605-1615.

Bandapalli, O. R., Zimmermann, M., Kox, C., Stanulla, M., Schrappe, M., Ludwig, W. D., Koehler, R., Muckenthaler, M. U., and Kulozik, A. E. (2013). NOTCH1 activation clinically antagonizes the unfavorable effect of PTEN inactivation in BFM-treated children with precursor T-cell acute lymphoblastic leukemia. Haematologica *98*, 928-936.

Beesley, A. H., Firth, M. J., Ford, J., Weller, R. E., Freitas, J. R., Perera, K. U., and Kees, U. R. (2009). Glucocorticoid resistance in T-lineage acute lymphoblastic leukaemia is associated with a proliferative metabolism. British journal of cancer *100*, 1926-1936.

Bhadri, V. A., Trahair, T. N., and Lock, R. B. (2012). Glucocorticoid resistance in paediatric acute lymphoblastic leukaemia. Journal of paediatrics and child health *48*, 634-640.

Bornhauser, B. C., Bonapace, L., Lindholm, D., Martinez, R., Cario, G., Schrappe, M., Niggli, F. K., Schafer, B. W., and Bourquin, J. P. (2007). Low-dose arsenic trioxide sensitizes glucocorticoid-resistant acute lymphoblastic leukemia cells to dexamethasone via an Akt-dependent pathway. Blood *110*, 2084-2091.

Chiang, M. Y., Xu, L., Shestova, O., Histen, G., L'Heureux, S., Romany, C., Childs, M. E., Gimotty, P. A., Aster, J. C., and Pear, W. S. (2008). Leukemia-associated NOTCH1 alleles are weak tumor initiators but accelerate K-ras-initiated leukemia. The Journal of clinical investigation *118*, 3181-3194.

D'Adamio, F., Zollo, O., Moraca, R., Ayroldi, E., Bruscoli, S., Bartoli, A., Cannarile, L., Migliorati, G., and Riccardi, C. (1997). A new dexamethasone-induced gene of the leucine zipper family protects T lymphocytes from TCR/CD3-activated cell death. Immunity *7*, 803-812.

Dan, H. C., Sun, M., Kaneko, S., Feldman, R. I., Nicosia, S. V., Wang, H. G., Tsang, B. K., and Cheng, J. Q. (2004). Akt phosphorylation and stabilization of X-linked inhibitor of apoptosis protein (XIAP). The Journal of biological chemistry *279*, 5405-5412.

Datta, S. R., Dudek, H., Tao, X., Masters, S., Fu, H., Gotoh, Y., and Greenberg, M. E. (1997). Akt phosphorylation of BAD couples survival signals to the cell-intrinsic death machinery. Cell *91*, 231-241.

del Peso, L., Gonzalez-Garcia, M., Page, C., Herrera, R., and Nunez, G. (1997). Interleukin-3-induced phosphorylation of BAD through the protein kinase Akt. Science *278*, 687-689.

Dordelmann, M., Reiter, A., Borkhardt, A., Ludwig, W. D., Gotz, N., Viehmann, S., Gadner, H., Riehm, H., and Schrappe, M. (1999). Prednisone response is the strongest predictor of treatment outcome in infant acute lymphoblastic leukemia. Blood *94*, 1209-1217.

Freyer, D. R., Devidas, M., La, M., Carroll, W. L., Gaynon, P. S., Hunger, S. P., and Seibel, N. L. (2011). Postrelapse survival in childhood acute lymphoblastic leukemia is independent of initial treatment intensity: a report from the Children's Oncology Group. Blood *117*, 3010-3015.

Geng, C. D., Schwartz, J. R., and Vedeckis, W. V. (2008). A conserved molecular mechanism is responsible for the auto-up-regulation of glucocorticoid receptor gene promoters. Molecular endocrinology *22*, 2624-2642.

Guo, K., McMinn, J. E., Ludwig, T., Yu, Y. H., Yang, G., Chen, L., Loh, D., Li, C., Chua, S., Jr., and Zhang, Y. (2007). Disruption of peripheral leptin signaling in mice results in hyperleptinemia without associated metabolic abnormalities. Endocrinology *148*, 3987-3997.

Gutierrez, A., Sanda, T., Grebliunaite, R., Carracedo, A., Salmena, L., Ahn, Y., Dahlberg, S., Neuberg, D., Moreau, L. A., Winter, S. S., *et al.* (2009). High frequency of PTEN, PI3K, and AKT abnormalities in T-cell acute lymphoblastic leukemia. Blood *114*, 647-650.

Heitzer, M. D., Wolf, I. M., Sanchez, E. R., Witchel, S. F., and DeFranco, D. B. (2007). Glucocorticoid receptor physiology. Reviews in endocrine & metabolic disorders *8*, 321-330.

Hirai, H., Sootome, H., Nakatsuru, Y., Miyama, K., Taguchi, S., Tsujioka, K., Ueno, Y., Hatch, H., Majumder, P. K., Pan, B. S., and Kotani, H. (2010). MK-2206, an allosteric Akt inhibitor, enhances antitumor efficacy by standard chemotherapeutic agents or molecular targeted drugs in vitro and in vivo. Molecular cancer therapeutics *9*, 1956-1967.

Hongo, T., Yajima, S., Sakurai, M., Horikoshi, Y., and Hanada, R. (1997). In vitro drug sensitivity testing can predict induction failure and early relapse of childhood acute lymphoblastic leukemia. Blood *89*, 2959-2965.

Inaba, H., and Pui, C. H. (2010). Glucocorticoid use in acute lymphoblastic leukaemia. The lancet oncology *11*, 1096-1106.

Kharas, M. G., Okabe, R., Ganis, J. J., Gozo, M., Khandan, T., Paktinat, M., Gilliland, D. G., and Gritsman, K. (2010). Constitutively active AKT depletes hematopoietic stem cells and induces leukemia in mice. Blood *115*, 1406-1415.

Klumper, E., Pieters, R., Veerman, A. J., Huismans, D. R., Loonen, A. H., Hahlen, K., Kaspers, G. J., van Wering, E. R., Hartmann, R., and Henze, G. (1995). In vitro cellular drug resistance in children with relapsed/refractory acute lymphoblastic leukemia. Blood *86*, 3861-3868.

Ko, R. H., Ji, L., Barnette, P., Bostrom, B., Hutchinson, R., Raetz, E., Seibel, N. L., Twist, C. J., Eckroth, E., Sposto, R.*, et al.* (2010). Outcome of patients treated for relapsed or refractory acute lymphoblastic leukemia: a Therapeutic Advances in Childhood Leukemia Consortium study. Journal of clinical oncology : official journal of the American Society of Clinical Oncology *28*, 648-654.

Marks, D. I., Paietta, E. M., Moorman, A. V., Richards, S. M., Buck, G., DeWald, G., Ferrando, A., Fielding, A. K., Goldstone, A. H., Ketterling, R. P.*, et al.* (2009). T-cell acute lymphoblastic leukemia in adults: clinical features, immunophenotype, cytogenetics, and outcome from the large randomized prospective trial (UKALL XII/ECOG 2993). Blood *114*, 5136-5145.

Mok, C. L., Gil-Gomez, G., Williams, O., Coles, M., Taga, S., Tolaini, M., Norton, T., Kioussis, D., and Brady, H. J. (1999). Bad can act as a key regulator of T cell apoptosis and T cell development. The Journal of experimental medicine *189*, 575-586.

Morishita, N., Tsukahara, H., Chayama, K., Ishida, T., Washio, K., Miyamura, T., Yamashita, N., Oda, M., and Morishima, T. (2012). Activation of Akt is associated with poor prognosis and chemotherapeutic resistance in pediatric B-precursor acute lymphoblastic leukemia. Pediatric blood & cancer *59*, 83-89.

Ozes, O. N., Mayo, L. D., Gustin, J. A., Pfeffer, S. R., Pfeffer, L. M., and Donner, D. B. (1999). NF-kappaB activation by tumour necrosis factor requires the Akt serine-threonine kinase. Nature *401*, 82-85.

Palomero, T., Sulis, M. L., Cortina, M., Real, P. J., Barnes, K., Ciofani, M., Caparros, E., Buteau, J., Brown, K., Perkins, S. L.*, et al.* (2007). Mutational loss of PTEN induces resistance to NOTCH1 inhibition in T-cell leukemia. Nature medicine *13*, 1203-1210.

Pui, C. H., Carroll, W. L., Meshinchi, S., and Arceci, R. J. (2011). Biology, risk stratification, and therapy of pediatric acute leukemias: an update. Journal of clinical oncology : official journal of the American Society of Clinical Oncology *29*, 551-565.

Pui, C. H., Mullighan, C. G., Evans, W. E., and Relling, M. V. (2012). Pediatric acute lymphoblastic leukemia: where are we going and how do we get there? Blood *120*, 1165-1174.

Riccardi, C., Cifone, M. G., and Migliorati, G. (1999). Glucocorticoid hormone-induced modulation of gene expression and regulation of T-cell death: role of GITR and GILZ, two dexamethasone-induced genes. Cell death and differentiation *6*, 1182-1189.

Schlossmacher, G., Stevens, A., and White, A. (2011). Glucocorticoid receptor-mediated apoptosis: mechanisms of resistance in cancer cells. The Journal of endocrinology *211*, 17-25.

Schmidt, S., Rainer, J., Riml, S., Ploner, C., Jesacher, S., Achmuller, C., Presul, E., Skvortsov, S., Crazzolara, R., Fiegl, M.*, et al.* (2006). Identification of glucocorticoid-response genes in children with acute lymphoblastic leukemia. Blood *107*, 2061-2069.

Tallen, G., Ratei, R., Mann, G., Kaspers, G., Niggli, F., Karachunsky, A., Ebell, W., Escherich, G., Schrappe, M., Klingebiel, T.*, et al.* (2010). Long-term outcome in children with relapsed acute lymphoblastic leukemia after time-point and site-of-relapse stratification and intensified short-course multidrug chemotherapy: results of trial ALL-REZ BFM 90. Journal of clinical oncology : official journal of the American Society of Clinical Oncology *28*, 2339-2347.

Trotman, L. C., Niki, M., Dotan, Z. A., Koutcher, J. A., Di Cristofano, A., Xiao, A., Khoo, A. S., Roy-Burman, P., Greenberg, N. M., Van Dyke, T.*, et al.* (2003). Pten dose dictates cancer progression in the prostate. PLoS biology *1*, E59.

Wang, Z., Malone, M. H., He, H., McColl, K. S., and Distelhorst, C. W. (2003). Microarray analysis uncovers the induction of the proapoptotic BH3-only protein Bim in multiple models of glucocorticoid-induced apoptosis. The Journal of biological chemistry *278*, 23861-23867.

Wei, G., Twomey, D., Lamb, J., Schlis, K., Agarwal, J., Stam, R. W., Opferman, J. T., Sallan, S. E., den Boer, M. L., Pieters, R.*, et al.* (2006). Gene expression-based chemical genomics identifies rapamycin as a modulator of MCL1 and glucocorticoid resistance. Cancer cell *10*, 331-342.

Zimmermann, S., and Moelling, K. (1999). Phosphorylation and regulation of Raf by Akt (protein kinase B). Science *286*, 1741-1744.

Figure 1

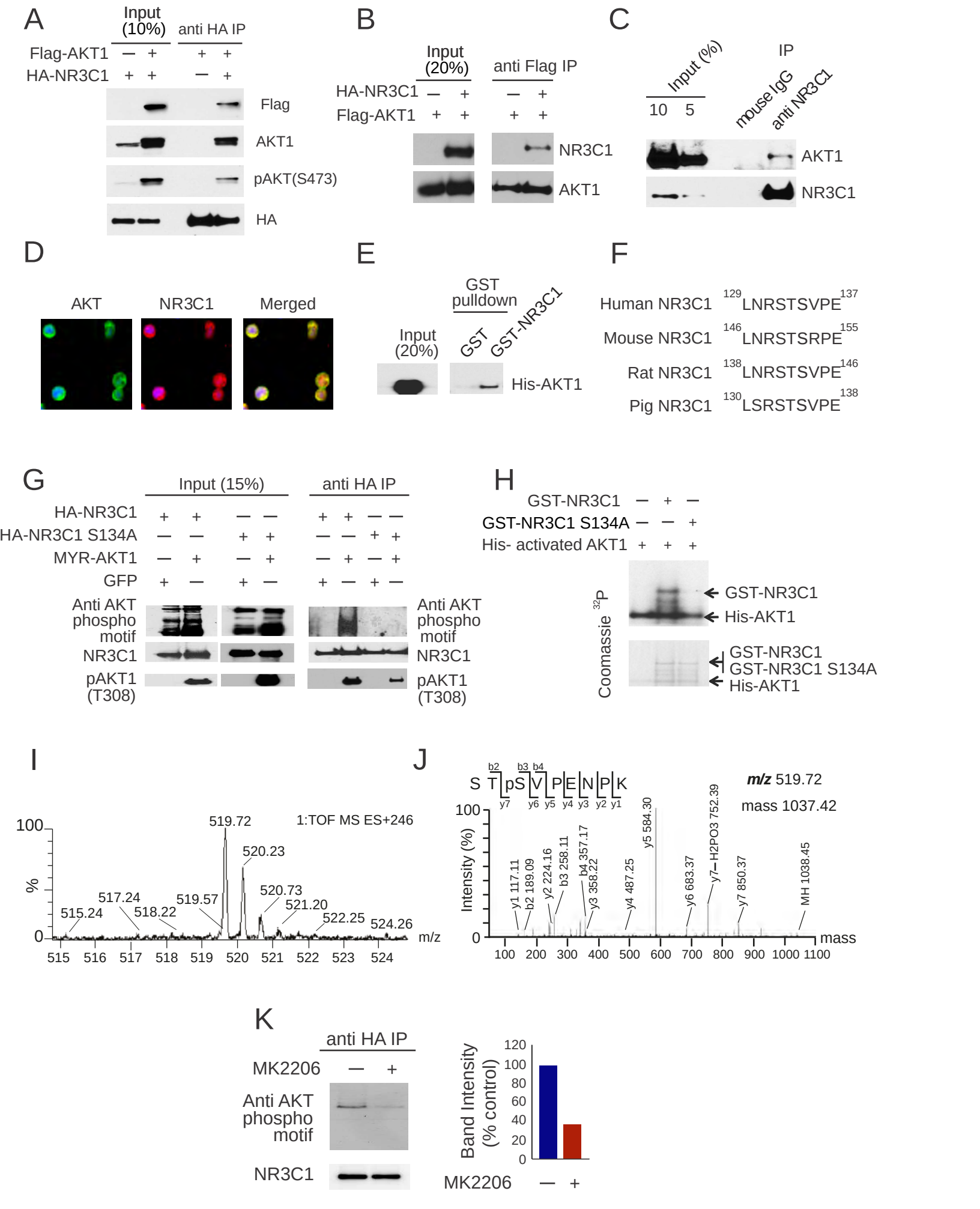
A
Input (10%)
anti HA IP
Flag-AKT1 — + + +
HA-NR3C1 + + — +
Flag
AKT1
pAKT(S473)
HA
B
Input (20%)
anti Flag IP
HA-NR3C1 — + — +
Flag-AKT1 + + + +
NR3C1
AKT1
C
Input (%)
10 5
IP
mouse IgG
anti NR3C1
AKT1
NR3C1
D
AKT
NR3C1
Merged
E
GST pulldown
Input (20%)
GST
GST-NR3C1
His-AKT1
F
Human NR3C1 129 LNRSTSVPE 137
Mouse NR3C1 146 LNRSTSRPE 155
Rat NR3C1 138 LNRSTSVPE 146
Pig NR3C1 130 LSRSTSVPE 138
G
Input (15%)
anti HA IP
HA-NR3C1 + + — — + + — —
HA-NR3C1 S134A — — + + — — + +
MYR-AKT1 — + — + — + — +
GFP + — + — + — + —
Anti AKT phospho motif
NR3C1
pAKT1 (T308)
H
GST-NR3C1 — + —
GST-NR3C1 S134A — — +
His- activated AKT1 + + +
32P
Coomassie
GST-NR3C1
His-AKT1
GST-NR3C1
GST-NR3C1 S134A
His-AKT1
I
100
%
0
519.72
1:TOF MS ES+246
520.23
517.24
519.57
520.73
521.20
515.24
518.22
522.25
524.26
m/z
515 516 517 518 519 520 521 522 523 524
J
S T pS V P E N P K
b2 b3 b4
y7 y6 y5 y4 y3 y2 y1
m/z 519.72
mass 1037.42
100
Intensity (%)
0
y1 117.11
b2 189.09
y2 224.16
b3 258.11
b4 357.17
y3 358.22
y4 487.25
y5 584.30
y6 683.37
y7–H2PO3 752.39
y7 850.37
MH 1038.45
mass
100 200 300 400 500 600 700 800 900 1000 1100
K
anti HA IP
MK2206 — +
Anti AKT phospho motif
NR3C1
Band Intensity (% control)
120
100
80
60
40
20
0
MK2206 — +

Figure 2

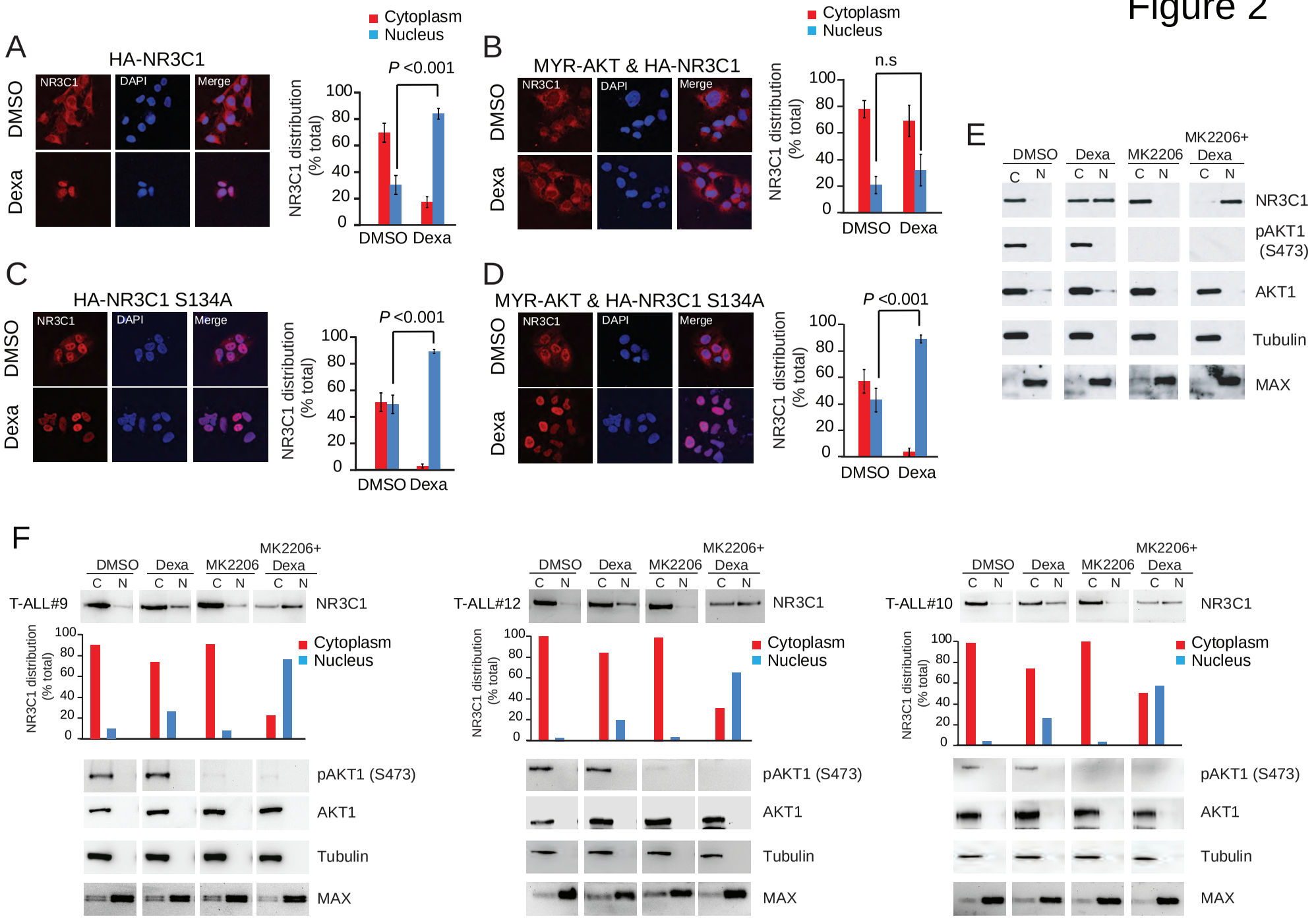
A
HA-NR3C1
DMSO
Dexa
NR3C1
DAPI
Merge
Cytoplasm
Nucleus
P <0.001
NR3C1 distribution (% total)
DMSO Dexa
B
MYR-AKT & HA-NR3C1
n.s
C
HA-NR3C1 S134A
D
MYR-AKT & HA-NR3C1 S134A
E
DMSO
Dexa
MK2206
MK2206+ Dexa
C N
NR3C1
pAKT1 (S473)
AKT1
Tubulin
MAX
F
T-ALL#9
T-ALL#12
T-ALL#10

Figure 3

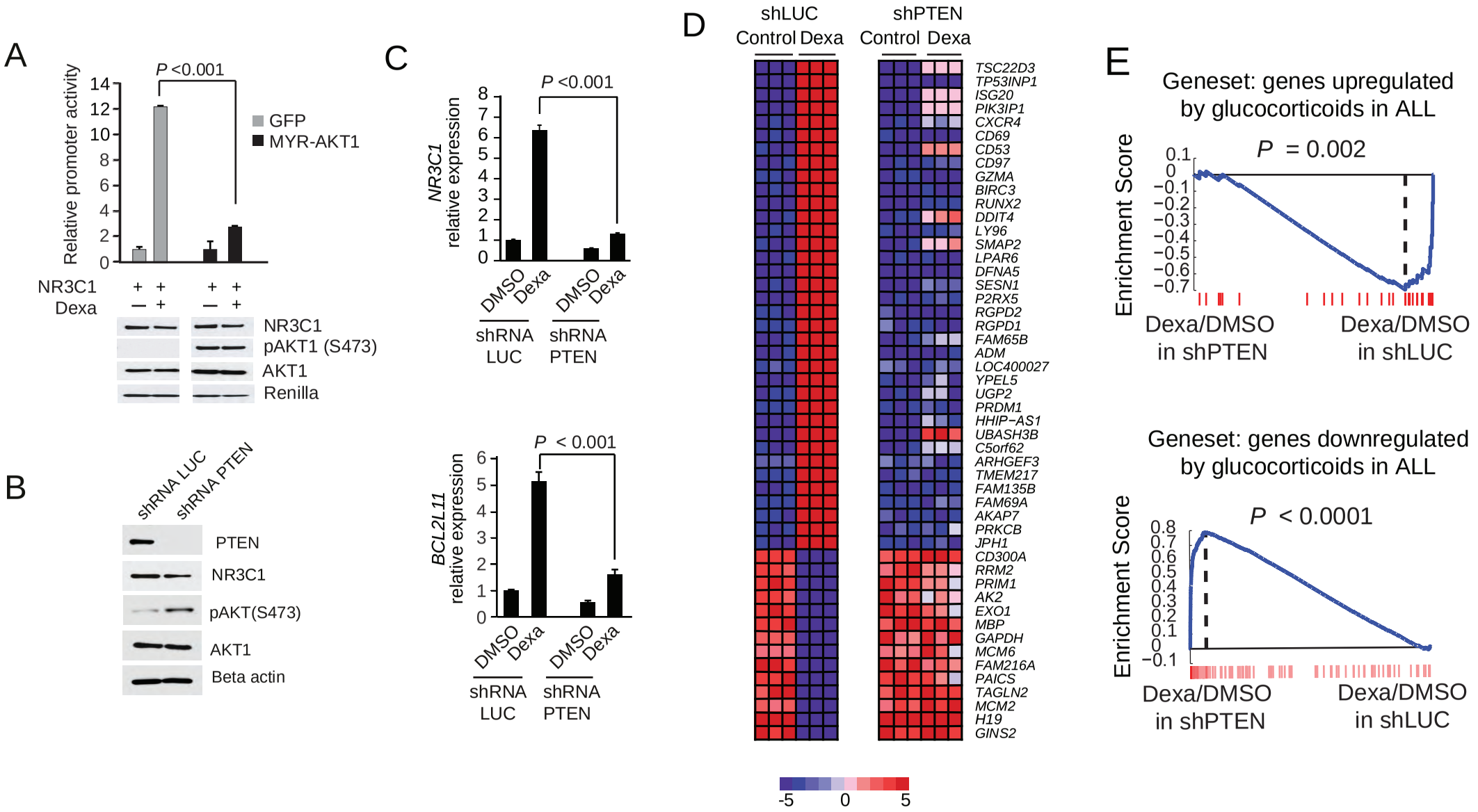
A
P <0.001
Relative promoter activity
GFP
MYR-AKT1
NR3C1
Dexa
NR3C1
pAKT1 (S473)
AKT1
Renilla
B
shRNA LUC
shRNA PTEN
PTEN
NR3C1
pAKT(S473)
AKT1
Beta actin
C
P <0.001
NR3C1 relative expression
DMSO
Dexa
shRNA LUC
shRNA PTEN
P < 0.001
BCL2L11 relative expression
D
shLUC
shPTEN
Control
Dexa
TSC22D3
TP53INP1
ISG20
PIK3IP1
CXCR4
CD69
CD53
CD97
GZMA
BIRC3
RUNX2
DDIT4
LY96
SMAP2
LPAR6
DFNA5
SESN1
P2RX5
RGPD2
RGPD1
FAM65B
ADM
LOC400027
YPEL5
UGP2
PRDM1
HHIP-AS1
UBASH3B
C5orf62
ARHGEF3
TMEM217
FAM135B
FAM69A
AKAP7
PRKCB
JPH1
CD300A
RRM2
PRIM1
AK2
EXO1
MBP
GAPDH
MCM6
FAM216A
PAICS
TAGLN2
MCM2
H19
GINS2
-5
0
5
E
Geneset: genes upregulated by glucocorticoids in ALL
P = 0.002
Enrichment Score
Dexa/DMSO in shPTEN
Dexa/DMSO in shLUC
Geneset: genes downregulated by glucocorticoids in ALL
P < 0.0001
Enrichment Score
Dexa/DMSO in shPTEN
Dexa/DMSO in shLUC

Figure4

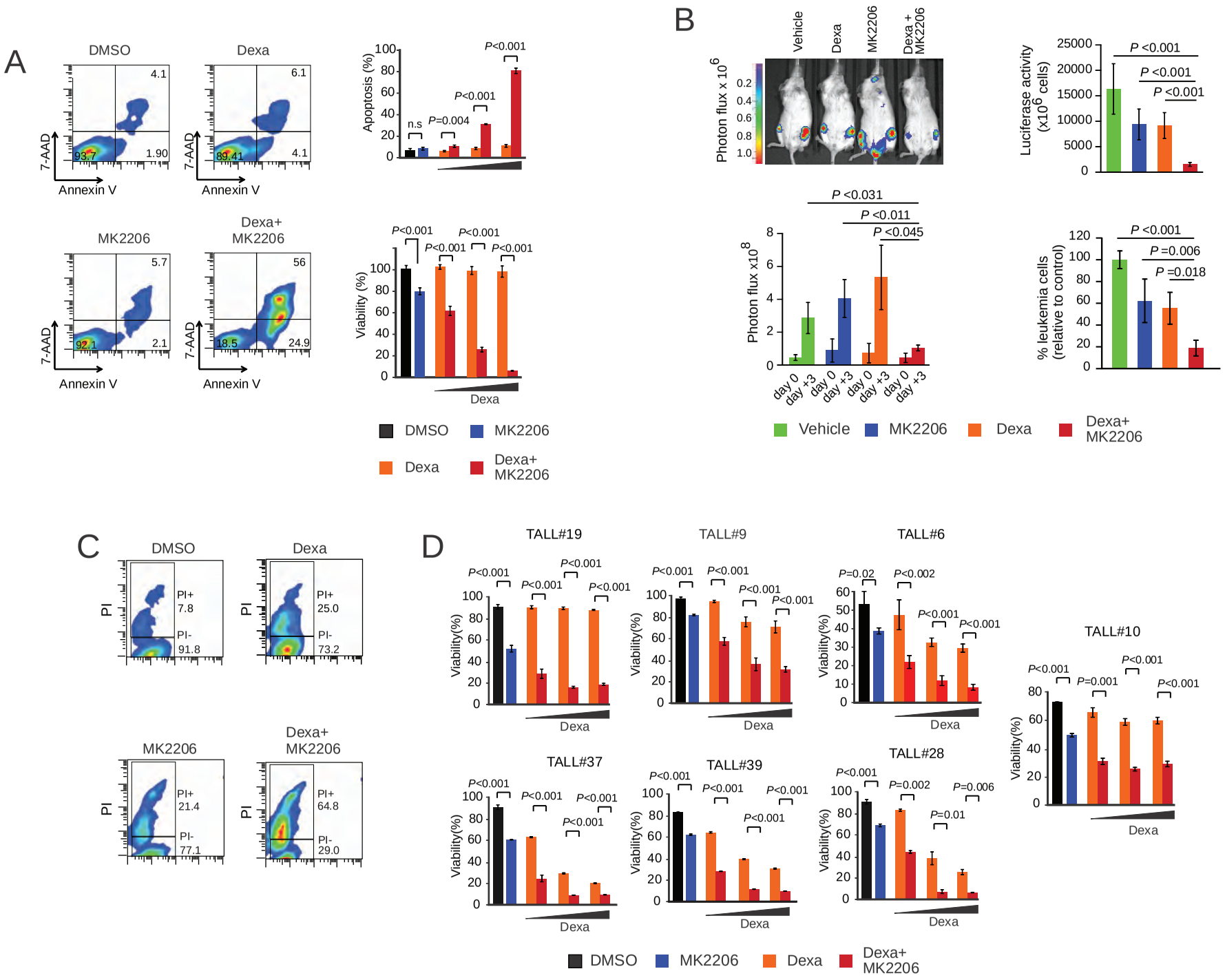
A
DMSO
Dexa
MK2206
Dexa+ MK2206
7-AAD
Annexin V
4.1
1.90
93.7
6.1
4.1
89.41
5.7
2.1
92.1
56
24.9
18.5
Apoptosis (%)
n.s
P=0.004
P<0.001
Viability (%)
Dexa
DMSO
MK2206
Dexa
Dexa+ MK2206
B
Vehicle
Dexa
MK2206
Dexa + MK2206
Photon flux x 10^6
Luciferase activity (x10^6 cells)
P <0.001
P <0.001
P <0.001
Photon flux x10^8
P <0.031
P <0.011
P <0.045
day 0
day +3
% leukemia cells (relative to control)
P <0.001
P =0.006
P =0.018
Vehicle
MK2206
Dexa
Dexa+ MK2206
C
DMSO
Dexa
MK2206
Dexa+ MK2206
PI
PI+
PI-
7.8
91.8
25.0
73.2
21.4
77.1
64.8
29.0
D
TALL#19
TALL#9
TALL#6
TALL#37
TALL#39
TALL#28
TALL#10
Viability(%)
Dexa
P<0.001
P=0.02
P<0.002
P=0.01
P=0.002
P=0.006
P=0.001
DMSO
MK2206
Dexa
Dexa+ MK2206

Figure 5

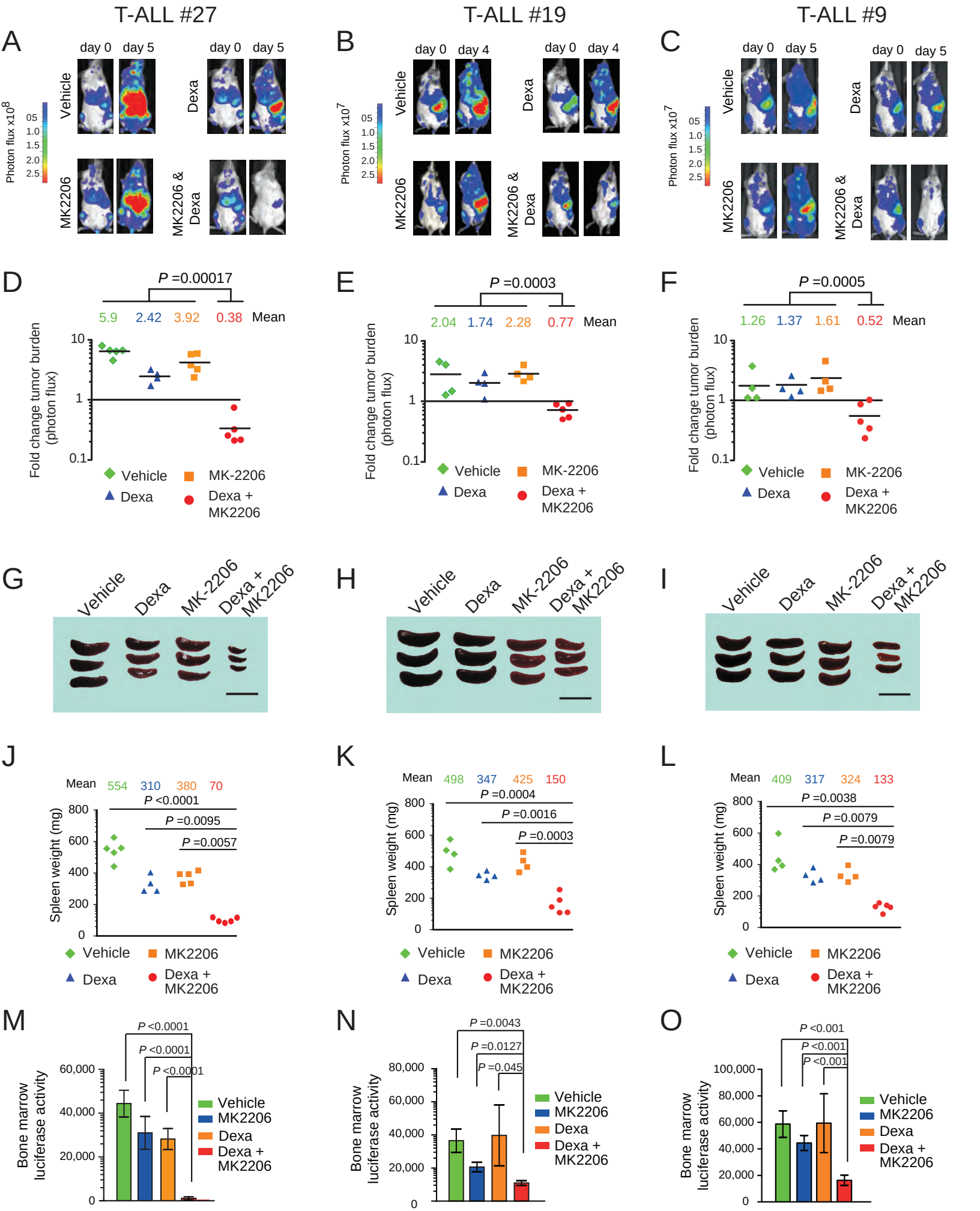
T-ALL #27
T-ALL #19
T-ALL #9
A
B
C
day 0
day 5
day 4
Vehicle
Dexa
MK2206
MK2206 & Dexa
Photon flux x10^8
Photon flux x10^7
05
1.0
1.5
2.0
2.5
D
E
F
P =0.00017
5.9 2.42 3.92 0.38 Mean
P =0.0003
2.04 1.74 2.28 0.77 Mean
P =0.0005
1.26 1.37 1.61 0.52 Mean
Fold change tumor burden (photon flux)
10
1
0.1
Vehicle
MK-2206
Dexa
Dexa + MK2206
G
H
I
Vehicle
Dexa
MK-2206
Dexa + MK2206
J
K
L
Mean 554 310 380 70
P <0.0001
P =0.0095
P =0.0057
Mean 498 347 425 150
P =0.0004
P =0.0016
P =0.0003
Mean 409 317 324 133
P =0.0038
P =0.0079
P =0.0079
Spleen weight (mg)
800
600
400
200
0
Vehicle
MK2206
Dexa
Dexa + MK2206
M
N
O
P <0.0001
P <0.0001
P <0.0001
P =0.0043
P =0.0127
P =0.045
P <0.001
P <0.001
P <0.001
Bone marrow luciferase activity
60,000
40,000
20,000
0
80,000
100,000
Vehicle
MK2206
Dexa
Dexa + MK2206

Figure 6

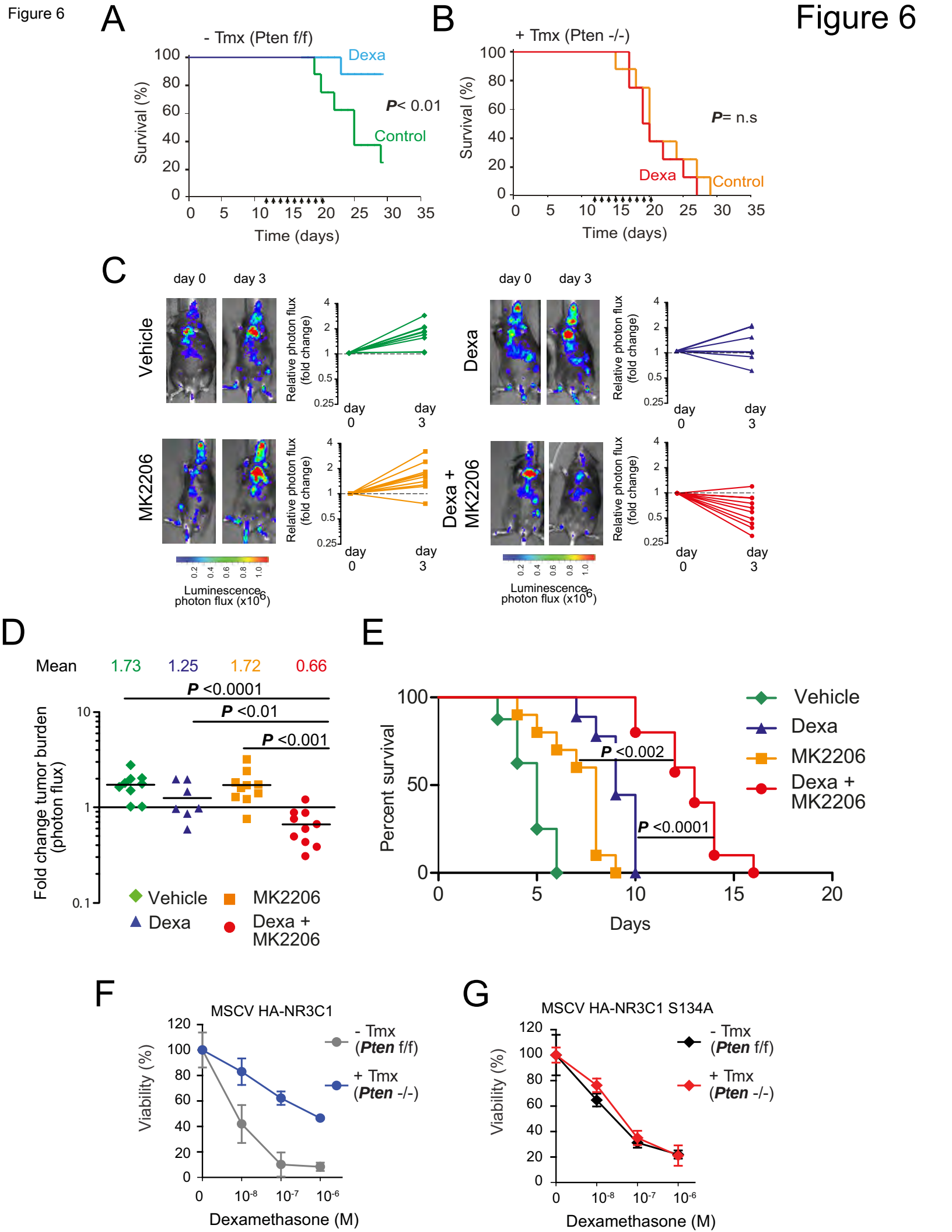
A
- Tmx (Pten f/f)
Dexa
Control
P< 0.01
Survival (%)
Time (days)
B
+ Tmx (Pten -/-)
P= n.s
Dexa
Control
Survival (%)
Time (days)
C
day 0
day 3
Vehicle
MK2206
Dexa
Dexa + MK2206
Relative photon flux (fold change)
day 0
day 3
Luminescence photon flux (x10^6)
D
Mean 1.73 1.25 1.72 0.66
P <0.0001
P <0.01
P <0.001
Fold change tumor burden (photon flux)
Vehicle
Dexa
MK2206
Dexa + MK2206
E
Percent survival
P <0.002
P <0.0001
Days
Vehicle
Dexa
MK2206
Dexa + MK2206
F
MSCV HA-NR3C1
Viability (%)
- Tmx (Pten f/f)
+ Tmx (Pten -/-)
Dexamethasone (M)
G
MSCV HA-NR3C1 S134A
Viability (%)
- Tmx (Pten f/f)
+ Tmx (Pten -/-)
Dexamethasone (M)

Direct reversal of glucocorticoid resistance by AKT inhibition in T-ALL

Erich Piovan, Jiyang Yu, Valeria Tosello, Daniel Herranz, Alberto Ambesi-Impiombato, Ana Carolina Da Silva, Marta Sanchez Martin, Arianne Perez-Garcia, Isaura Rigo, Mireia Castillo, Stefano Indraccolo, Justin R Cross, Elisa de Stanchina, Elisabeth Paietta, Janis Racevskis, Jacob M Rowe, Martin S Tallman, Giuseppe Basso, Jules P Meijerink, Carlos Cordon-Cardo, Andrea Califano and Adolfo A. Ferrando

Supplemental Information index **Page**

Supplemental Text and Figures

Click here to download Supplemental Text and Figures: SupplementaryMaterial.pdf

Direct reversal of glucocorticoid resistance by AKT inhibition in T-ALL

Erich Piovan, Jiyang Yu, Valeria Tosello, Daniel Herranz, Alberto Ambesi-Impiombato, Ana Carolina Da Silva, Arianne Perez-Garcia, Isaura Rigo, Mireia Castillo, Stefano Indraccolo, Elisabeth Paietta, Janis Racevskis, Jacob M Rowe, Martin S Tallman, Giuseppe Basso, Jules P Meijerink, Carlos Cordon-Cardo, Andrea Califano and Adolfo A. Ferrando

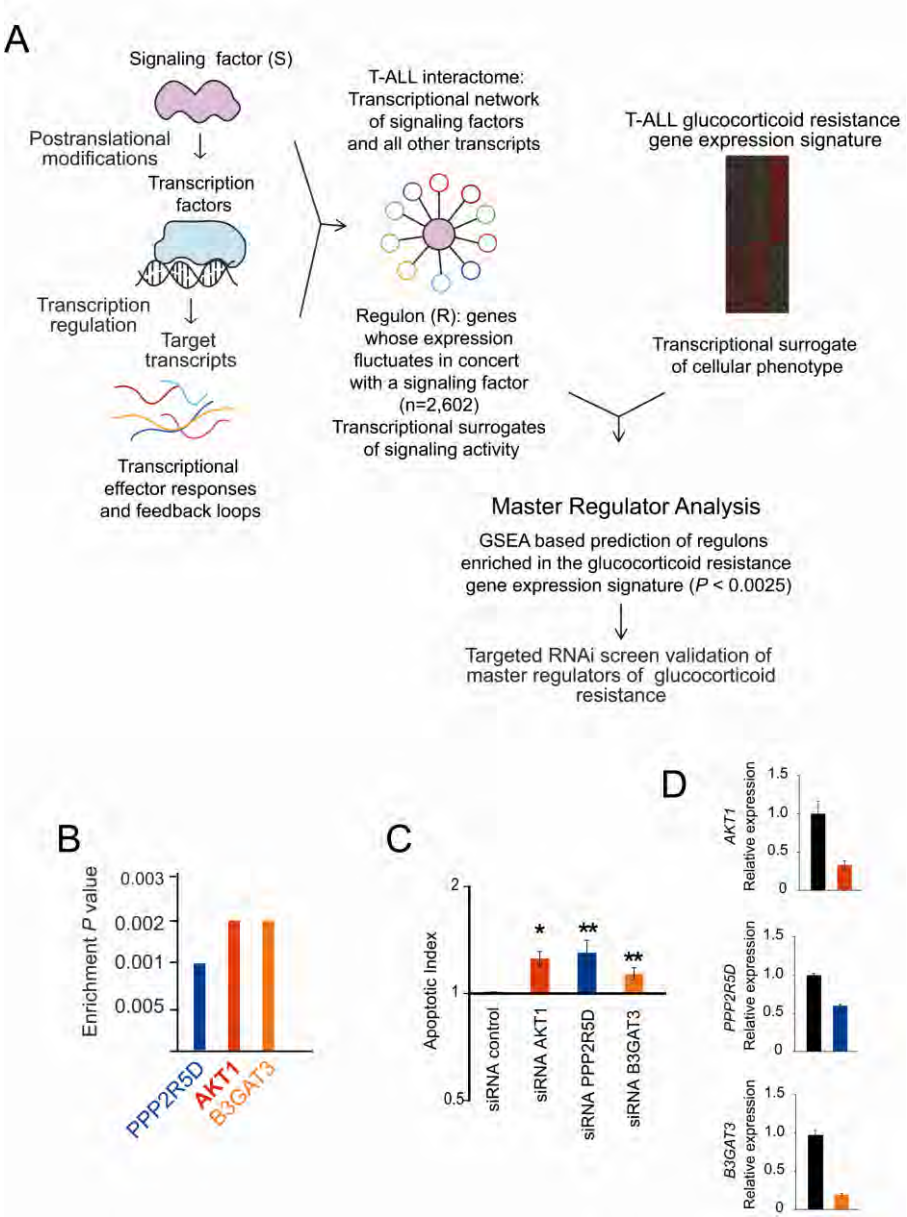

Figure S1. Figure 1. Master Regulator Analysis identifies modulators of glucocorticoid resistance in T-ALL. (A) Schematic representation of the principles and analytical approach for the identification of signaling factors involved in glucocorticoid resistance in T-ALL. Signaling molecules (S) controlling the activity of transcription factors are indirect transcriptional regulators. Reverse engineering of transcriptional networks can identify sets of genes (S-regulons, R_S) whose expression

fluctuates as a function of the activity of signaling factors. Gene expression profiling of glucocorticoid sensitive and resistant T-ALL samples identifies a transcriptional signature associated with glucocorticoid resistance. The Master Regulator Analysis step uses Gene Set Enrichment Analysis to identify signaling molecules whose associated regulons are enriched or depleted in the glucocorticoid resistant signature. (B) Master Regulator Analysis P values of validated signaling factors associated with glucocorticoid resistance. (C) Apoptosis analysis in DND41 T-ALL cells electroporated with siRNA pools targeting validated candidate regulators of glucocorticoid resistance treated with dexamethasone. The apoptotic index indicates apoptotic cell number in gene specific siRNA dexamethasone treated samples relative to siRNA control dexamethasone treated cells. *, P <0.01; **, P <0.05. (D) Quantitative RT-PCR analysis of siRNA knockdown. Data in C and D are represented as mean ± s.d.

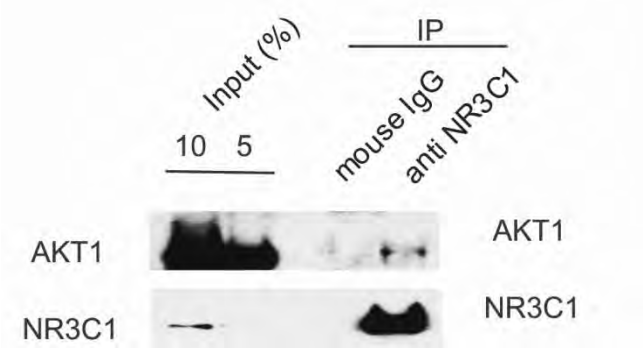

Figure S2. AKT1 directly interacts with the glucocorticoid receptor in T-ALL cells. Western blot analysis of AKT1 after NR3C1 protein immunoprecipitation in CCRF-CEM cells.

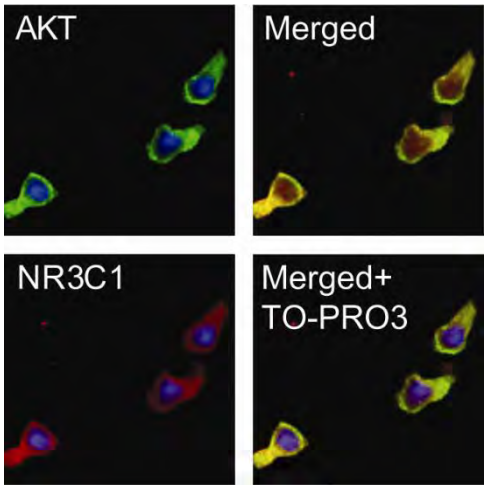

Figure S3. AKT1 colocalizes with NR3C1 in T-ALL cells. Immunofluorescence colocalization analysis of AKT (green) and NR3C1 (red) proteins in CCRF-CEM cells. Cell nuclei stained with TO-PRO3 are shown in blue.

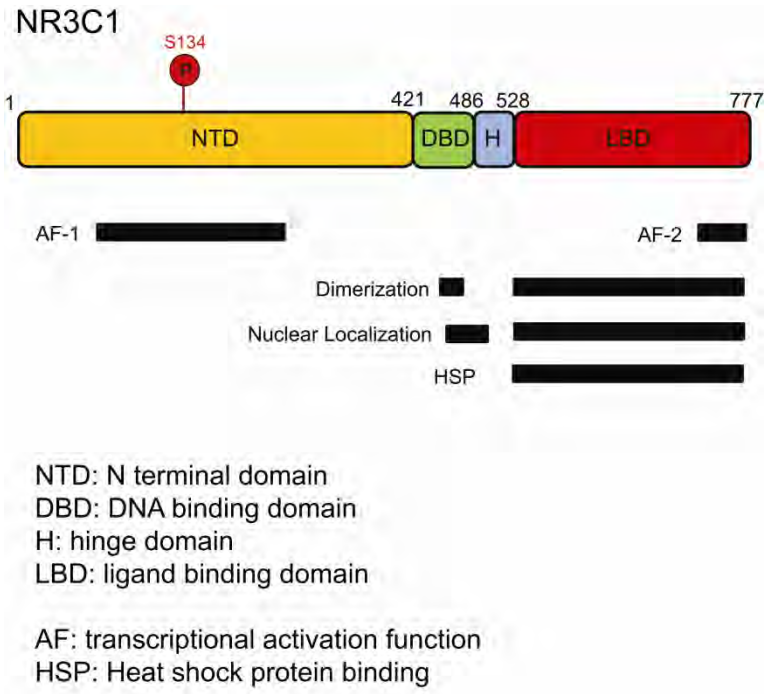

Figure S4. Schematic representation of the NR3C1 structure indicating functional and structural domains and the position of the S134 AKT phosphorylation site.

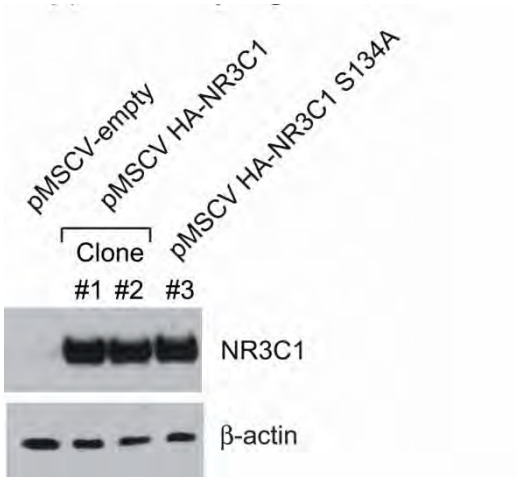

Figure S5. U2OS cells do not express detectable levels of endogenous NR3C1. Western blot analysis of NR3C1 expression in U2OS cells infected with pMSCV empty vector, pMSCV-HA NR3C1 or pMSCV-HA NR3C1 S134A retroviruses.

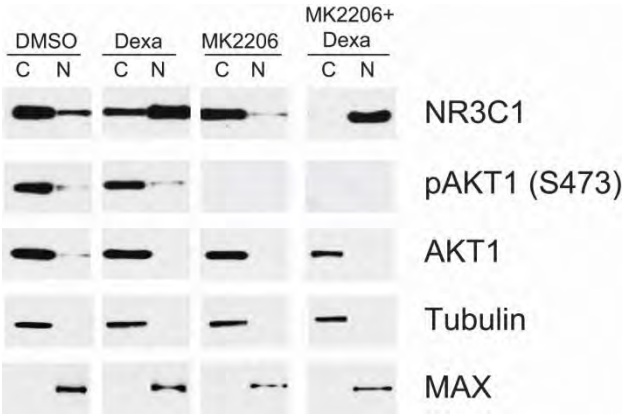

Figure S6. AKT1-mediated phosphorylation of the NR3C1 protein impairs dexamethasone-induced glucocorticoid receptor nuclear translocation in MOLT3 T-ALL cells. Cellular localization analysis of NR3C1 via nuclear and cytoplasmic cell fractionation and analysis of AKT1 signaling in cell lysates from MOLT-3 T-ALL cells treated with vehicle only (DMSO), dexamethasone (Dexa; 1μM), the MK2206 AKT inhibitor (0.5 μM) and MK2206 (0.5 μM) plus dexamethasone (1 μM). Tubulin and MAX proteins are shown as controls for cytosolic and nuclear fractions, respectively. C: cytoplasmic fraction; N: nuclear fraction.

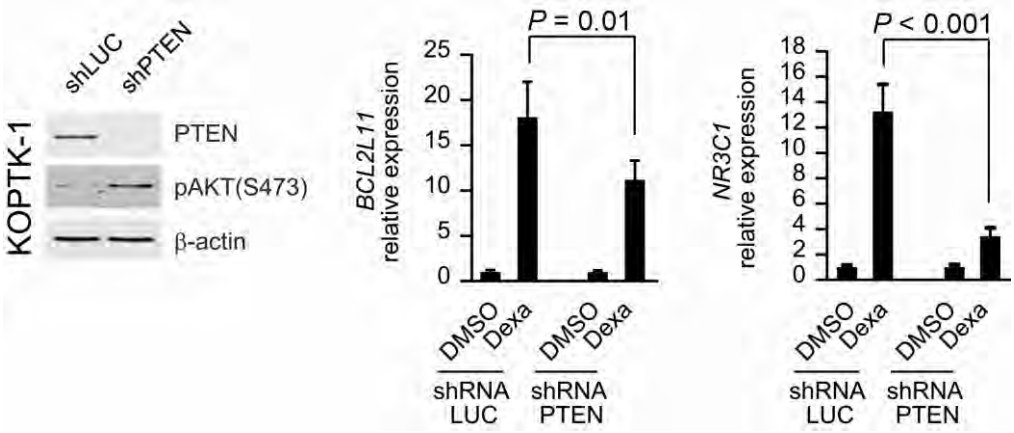

Figure S7. PTEN knock down impairs glucocorticoid transcriptional response in KOPTK1 T-ALL cells. Western blot analysis of PTEN expression and AKT activation in control (shRNA LUC) and PTEN (shRNA PTEN) knockdown KOPTK1 T-ALL cells. RT-PCR analysis of *BCL2L11* and *NR3C1* expression in KOPTK1 control and PTEN knockdown cells treated with vehicle only (DMSO) or 1 μM dexamethasone (Dexa).

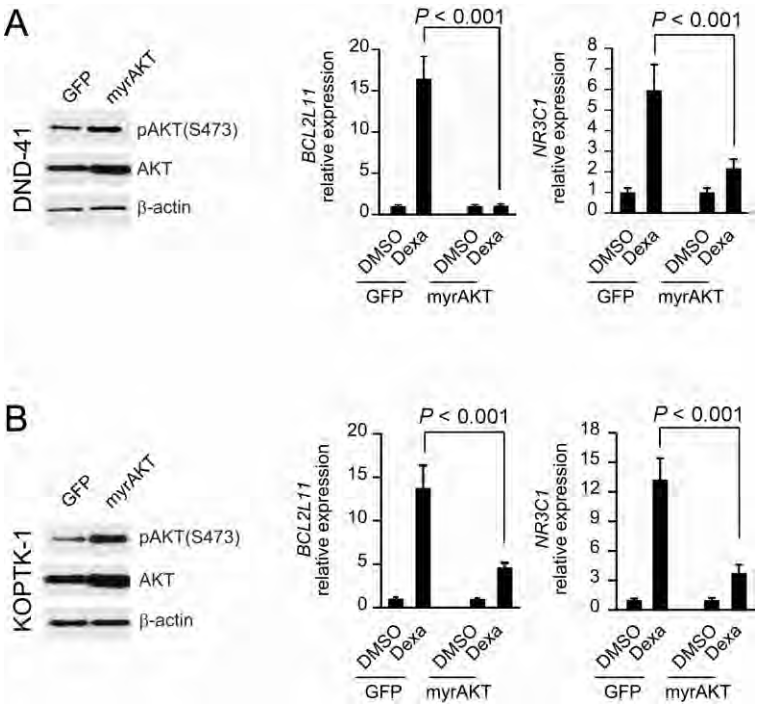

Figure S8. MYR-AKT expression impairs glucocorticoid transcriptional response in T-ALL cells. **A** Western blot analysis of AKT expression and AKT activation in control (GFP) and MYR-AKT1 (myrAKT) expressing DND41 T-ALL cells. RT-PCR analysis of *BCL2L11* and *NR3C1* expression in control and MYR-AKT1 expressing cells treated with vehicle only (DMSO) or 1 μM dexamethasone (Dexa). **B** Western blot analysis of AKT expression and AKT activation in control (GFP) and MYR-AKT1 (myrAKT) expressing KOPTK1 T-ALL cells. RT-PCR analysis of *BCL2L11* and *NR3C1* expression in control and MYR-AKT1 expressing cells treated with vehicle only (DMSO) or 1 μM dexamethasone (Dexa).

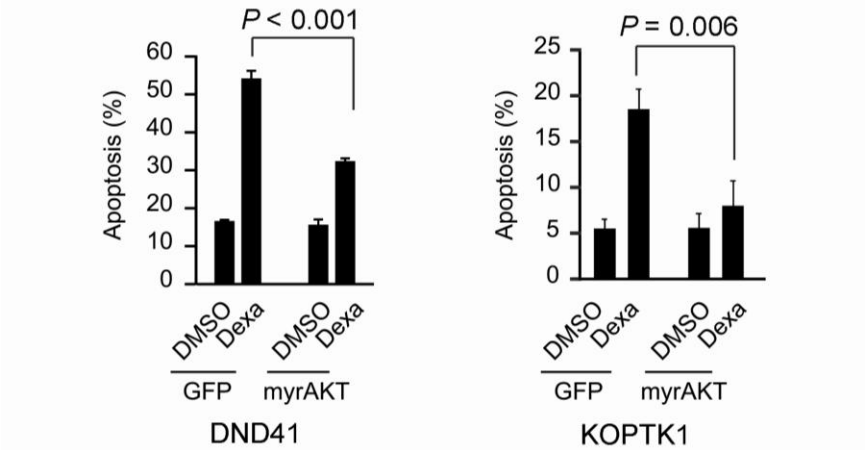

Figure S9. MYR-AKT expression impairs glucocorticoid induced apoptosis in T-ALL cells. Apoptosis quantification in DND41 and KOPTK1 T-ALL cells infected with control (GFP) and MYR-AKT1 (myrAKT) expressing retroviruses after treatment with vehicle only (DMSO) or 1 μM dexamethasone (Dexa).

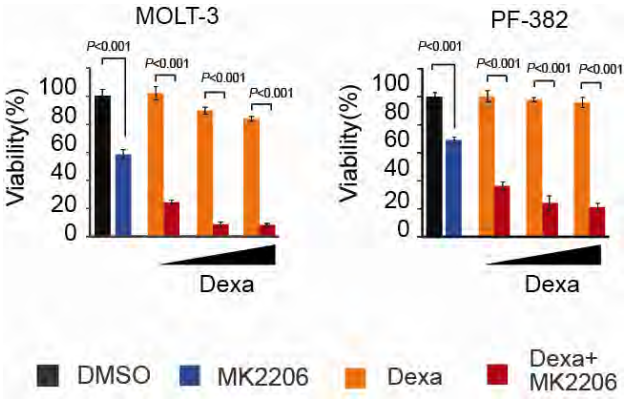

Figure S10. Pharmacological inhibition of AKT reverses glucocorticoid resistance in T-ALL cell lines. Analysis of cell viability in T-ALL cell lines treated for 72 hours with vehicle only, MK2206 (1 μM) and dexamethasone (10 nM-1 μM) alone or dexamethasone (10 nM-1 μM) plus MK2206 (1 μM) in combination.

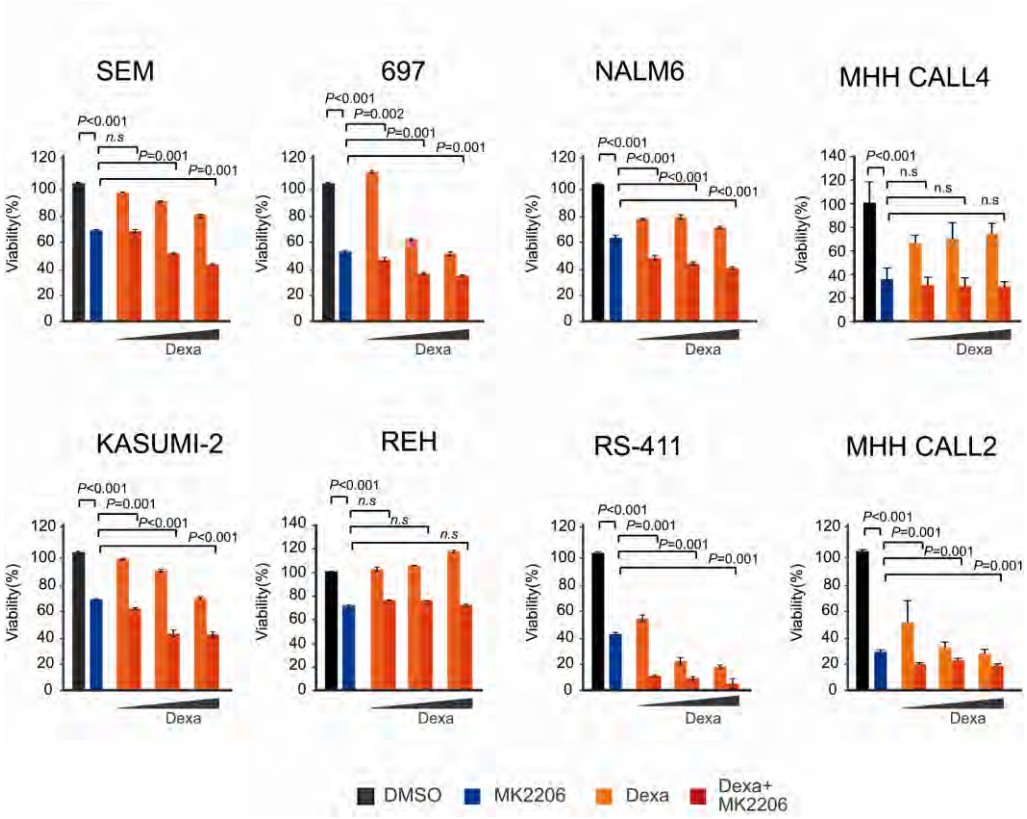

Figure S11. Inhibition of AKT and dexamethasone treatment in B precursor ALL. Analysis of cell viability in B precursor ALL cell lines treated with vehicle only, MK2206 (1 μM) and dexamethasone (10 nM-1 μM) alone or dexamethasone (10 nM-1 μM) plus MK2206 (1 μM) in combination.

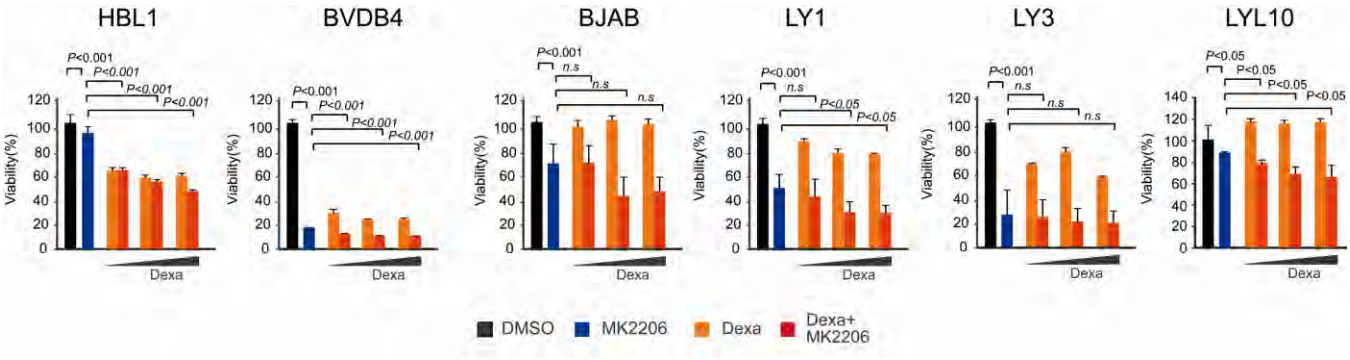

Figure S12. Inhibition of AKT and dexamethasone treatment in diffuse large B cell lymphoma. Analysis of cell viability in diffuse large B cell lymphoma cell lines treated with vehicle only, MK2206 (1 μM) and dexamethasone (10 nM-10 μM) alone or dexamethasone (10 nM-10 μM) plus MK2206 (1 μM) in combination.

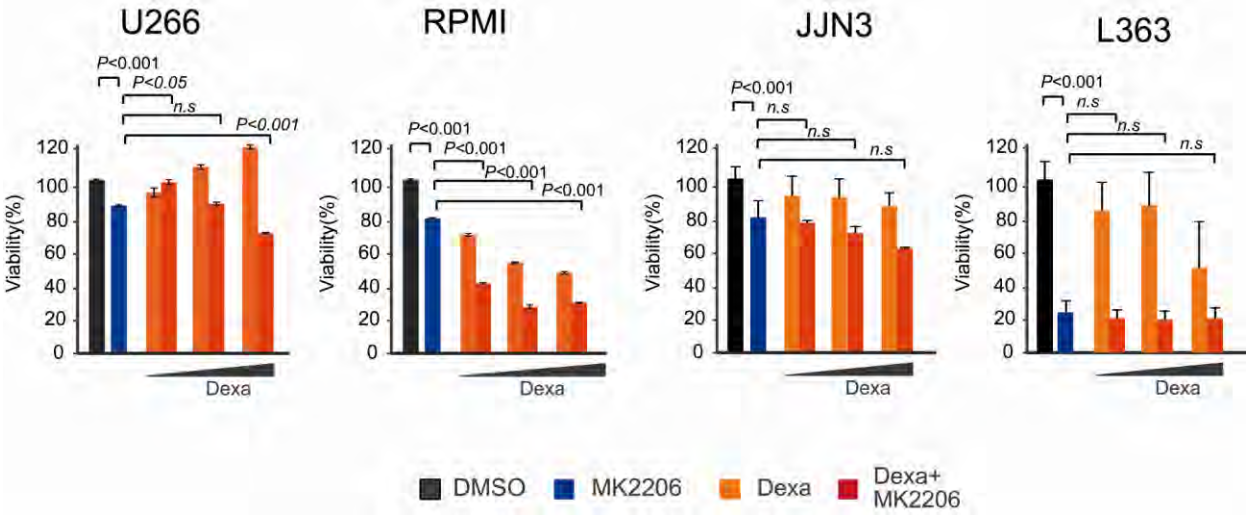

Figure S13. Inhibition of AKT and dexamethasone treatment in multiple myeloma. Analysis of cell viability in multiple myeloma cell lines treated with vehicle only, MK2206 (1 μM) and dexamethasone (10 nM-10 μM) alone or dexamethasone (10 nM-10 μM) plus MK2206 (1 μM) in combination.

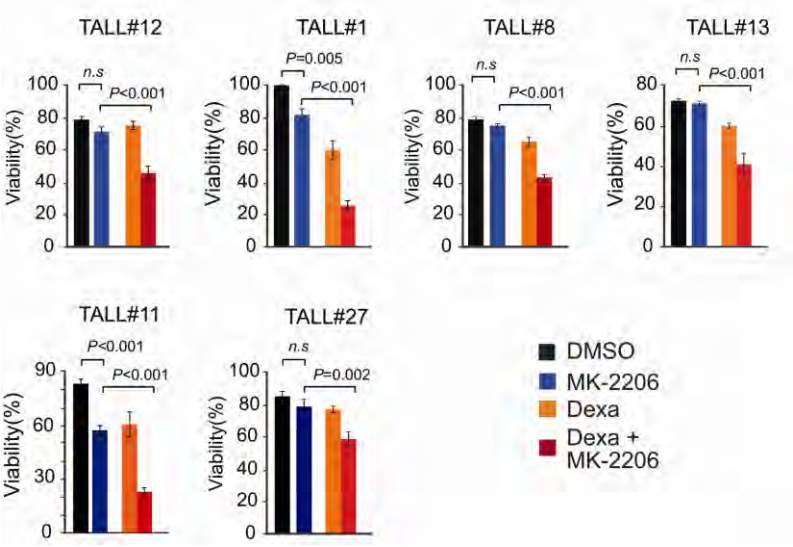

Figure S14. Pharmacological inhibition of AKT *in vitro* reverses glucocorticoid resistance in primary human T-ALL xenografts. Analysis of cell viability in primary T-ALL samples treated for 72 hours with vehicle only, MK2206 (100 nM-1 μM) and dexamethasone (100 nM-1 μM) alone or dexamethasone (100 nM-1 μM) plus MK2206 (100 nM-1μ M) in combination.

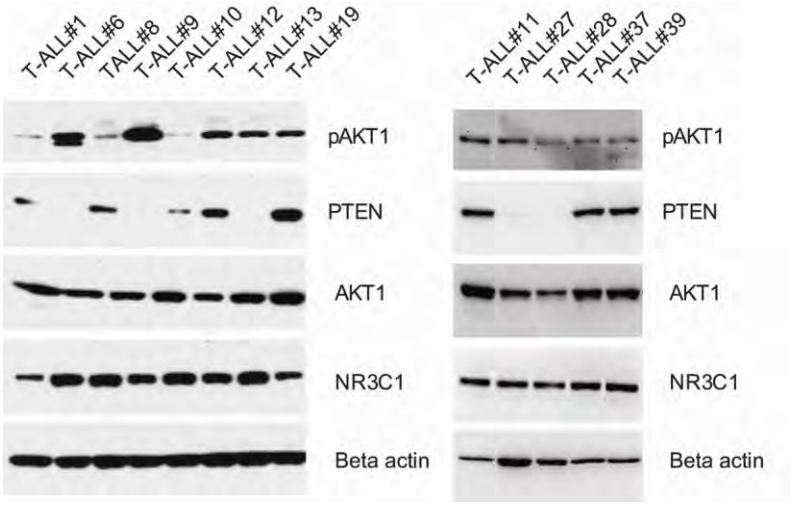

Figure S15. Western Blot analysis of AKT activation, PTEN and NR3C1 expression in T-ALL primary patient samples.

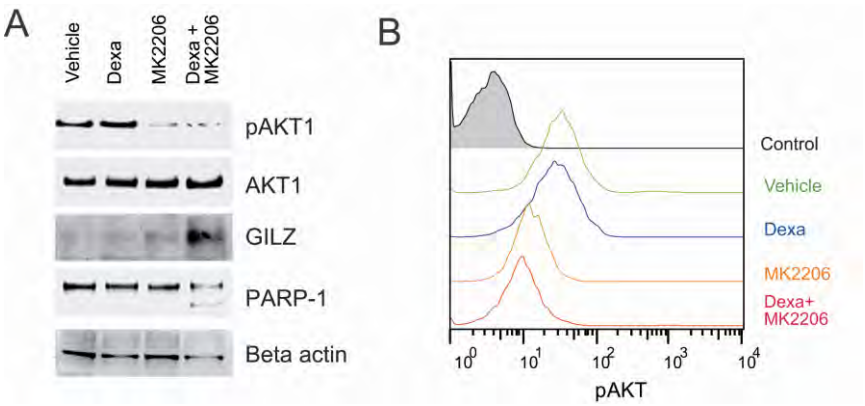

Figure S16. Pharmacodynamic response of human T-ALL cells to MK2206 and dexamethasone treatment. (A) Western blot analysis of AKT phosphorylation, glucocorticoid induced GILZ upregulation, and apoptosis (PARP cleavage) in spleen T-ALL lymphoblasts from mice xenografted with human T-ALL#9 cells and treated with control (Vehicle), dexamethasone, MK2206 and dexamethasone plus MK2206. (B) AKT phosphoflow analysis in peripheral blood in mice xenografted with human T-ALL#9 cells and treated with control (Vehicle), dexamethasone, MK2206 and dexamethasone plus MK2206.

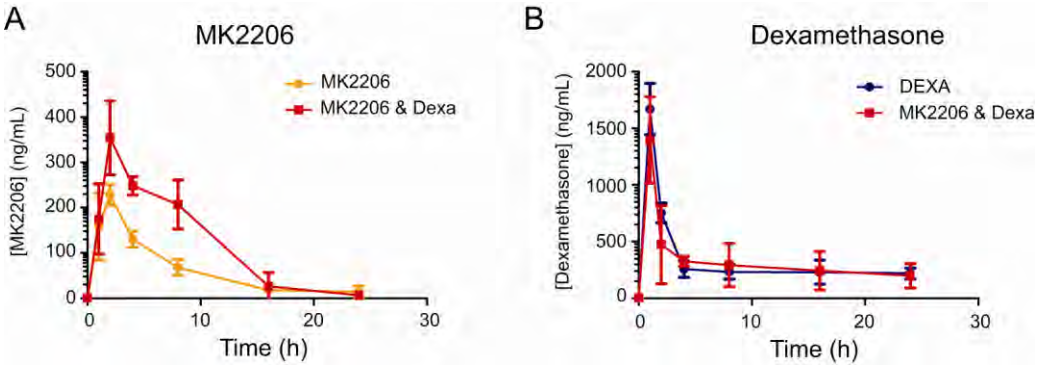

Figure S17. Pharmacokinetic analysis of MK2206 and dexamethasone. (A) Quantiative analysis of MK2206 concentrations in plasma from mice treated with MK2206 alone and MK plus dexamethasone. (B) Quantiative analysis of dexamethasone concentrations in plasma from mice treated with MK2206 alone and MK plus dexamethasone. Data shows average measurements of triplicate biological replicas. Error bars indicate s.d.

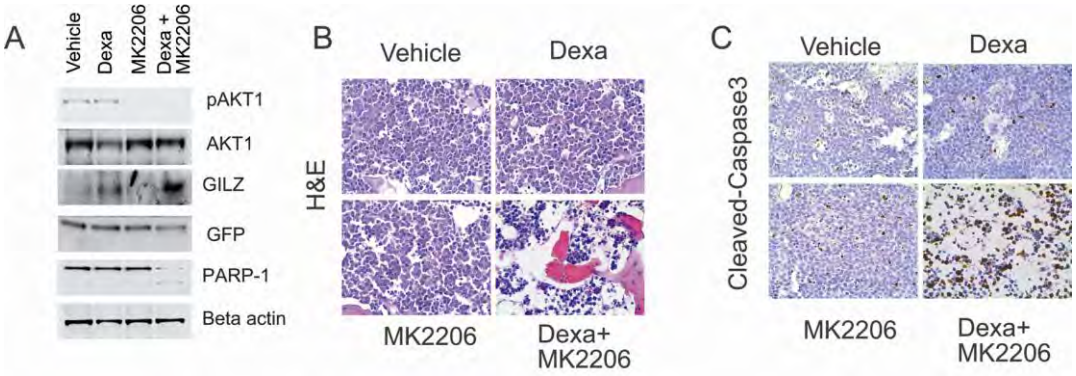

Figure S18. Pharmacodynamic response of mouse NOTCH1-induced Pten null T-ALL cells to MK2206 and dexamethasone treatment. (A) Western blot analysis of AKT phosphorylation, glucocorticoid induced GILZ upregulation, and apoptosis (PARP cleavage) in spleen T-ALL lymphoblasts from mice xenografted with NOTCH1-induced Pten null T-ALL cells and treated with control (Vehicle), dexamethasone, MK2206 and dexamethasone plus MK2206. (B) Histological analysis of bone marrow tissue in mice mice xenografted with NOTCH1-induced Pten null T-ALL cells and treated with control (Vehicle), dexamethasone, MK2206 and dexamethasone plus MK2206. (C) Immunohistochemical analysis of apoptosis (cleaved caspase 3 staining) in mice xenografted with NOTCH1-induced Pten null T-ALL cells and treated with control (Vehicle), dexamethasone, MK2206 and dexamethasone plus MK2206.

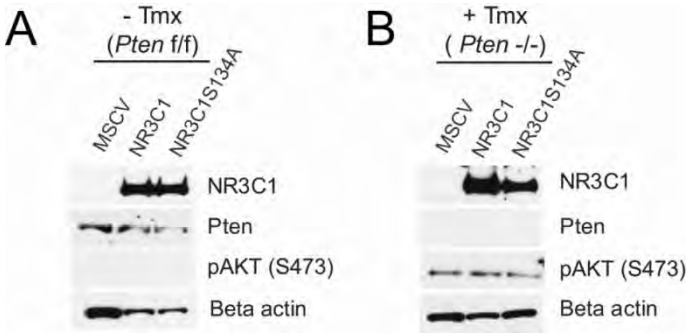

Figure S19. Overexpression of NR3C1 and NR3C1 S134A mutant in primary murine leukemia cells. (A) Western blot analysis determining the retroviral expression of NR3C1 or NR3C1 S134A in *Pten* non-deleted [–Tmx (*Pten*$^{f/f}$)] and (B) *Pten* deleted [+Tmx (*Pten*$^{-/-}$)] *NOTCH1*-induced T-ALL mouse leukemia cells. Beta actin is shown as loading control.

Table S1. Mass spectrometry analysis of NR3C1 S134 phosphorylation in MYR-AKT1 expressing U2OS cells treated with vehicle only (DMSO) or the MK2206 AKT inhibitor.

	Peak Intensity ($x10^5$)	
	DMSO	**MK2206**
ST**S134**VPENPK	71.6	264.0
ST**pS134**VPENPK	33.7	8.3
Ratio ST**pS134**VPENPK/ST**S134**VPENPK	0.47	0.03

SUPPLEMENTARY RESULTS

Signaling network analysis identifies AKT1 as a modulator of glucocorticoid resistance in T-ALL

Reverse engineering of transcriptional regulatory networks has emerged as a powerful tool to identify key transcription factors controlling complex physiologic processes such as germinal center formation during B-cell development (Basso et al.; Lefebvre et al.), and pathologic cellular phenotypes such as mesenchymal glioblastoma (Carro et al.) or *TLX1* induced transformation in T-ALL (Della Gatta et al.). Using this approach here we identify the AKT1 kinase, a central mediator of the phosphatidylinositol 3-kinase (PI3K) pathway, as a direct negative regulator of glucocorticoid receptor activity and a major mediator of glucocorticoid resistance in T-ALL.

We postulated that reverse engineering of the signaling networks could identify key druggable regulators of glucocorticoid resistance in T-ALL. In this analysis we used genes globally coexpressed with a signaling molecule (*S*) as surrogate readout of *S* activity (**Figure S1**) and then applied a Master Regulator Inference approach (Carro et al.; Lefebvre et al.) to identify specific signaling molecules associated with glucocorticoid resistance in T-ALL. Top scoring genes were then tested in a targeted siRNA screen for their capacity to modulate the response of T-ALL lymphoblasts to glucocorticoids. This analysis identified three genes whose inhibition can enhance glucocorticoid induced apoptosis in DND41 T-ALL cells: *PPP2R5D*, a protein phosphatase 2A regulatory B subunit; the *B3GAT3* glucuronosyl transferase 1; and *AKT1*, a central mediator in phosphatidylinositol 3-kinase (PI3K) signaling.

EXTENDED EXPERIMENTAL PROCEDURES

MASTER REGULATOR ANALYSIS OF GLUCOCORTICOID RESISTANCE

We used mRNAs globally co-expressed with a signaling molecule (*S*) as a surrogate of the activity of *S* based on the assumption that such genes are enriched for both members of the signal transduction cascade that includes *S* and targets of transcription factors regulated by *S*. To generate a T-ALL transcriptional network, we processed Human U133 Plus2.0 Affymetrix microarray gene expression data from 223 T-ALLs using GC-RMA normalization and non-specific filtering (removing probes with no Entrez id, Affymetrix control probes, and non-informative probes by IQR variance filtering with a cutoff of 0.5), to 21,054 probes in total. This large dataset is used as reference of multiple different biological conditions and transcriptional states. Each sample here has different genotype, signaling and transcriptional state. By analyzing an unbiased large collection of cases we aimed to capture as many transcriptional states and to create a network that computes the correlation of all analyzed transcripts across multiple different conditions. To build this network we used the ARACNe algorithm (Margolin et al., 2006), against 4,831 probe sets corresponding to 2,602 genes with annotated functions in signaling transduction (GO:0007165) such as kinases, phosphatases, ubiquitin ligases, etc. to establish a signaling factor-centered interactome at the transcriptional level. Use of ARACNe is justified to find minimal regulatory paths, i.e., to eliminate most indirect interactions in signal transduction analysis. This produces a minimal representation such that if any interaction were removed, information transfer in the system could no longer be explained. The parameters of the algorithm were configured as below: *P*-value threshold $P = 1e{-}7$, DPI tolerance e = 0, and number of bootstraps $NB = 100$. We used the adaptive partitioning algorithm for mutual information estimation.

Then, to address our specific question we moved from this large unselected sample collection to a selected group of 22 glucocorticoid resistant and 10 glucocorticoid sensitive T-ALLs. By performing differential gene expression analysis between glucocorticoid resistant and glucocorticoid sensitive in this well annotated group of cases we obtained a rank of genes whose expression varies across these two conditions. Finally, we used the MARINa algorithm to interrogate the ARACNe-inferred signaling network (generated from the large unselected group of cases) to identify candidate regulators of glucocorticoid resistance (in the context of the glucocorticoid sensitivity/resistance annotated samples). In this analysis, for each signaling gene (*S)*, we generated a putative *S*-regulon (*RS)*, from the T-ALL signaling interactome by selecting the first neighbors of *S* (as computed in the ARACNe network). Next, we used Gene Set Enrichment Analysis (GSEA) to test the differential enrichment of the *RS* regulons in the rank of genes differentially expressed between glucocorticoid sensitive and glucocorticoid resistant samples (Carro et al.). For GSEA method we applied 'maxmean' statistic (Efron and Tibshirani, 2007) to score the enrichment of the gene set in the glucocorticoid resistant *vs.* glucocorticoid sensitive leukemias and used sample permutation to build the null distribution for statistical significance. To generate robust signatures, we only used signaling proteins with more than 50 genes in their *S*-regulon. *P*-values were corrected using Efron's procedure (Efron and Tibshirani, 2007).

CELL LINES AND PRIMARY LEUKEMIA SAMPLES

(HEK) 293T, U2OS (HTB-96), DND41, CCRF-CEM, MOLT3, MOLT4, PF382, SEM, 697, NALM6, MHH CALL4, KASUMI2, REH, RS-411, MHH CALL2, HBL1, BVDB4, BJAB, LY1, LY3, LYL10, U266, RPMI, JJN3 AND L363 cell lines were cultured in standard conditions in media supplemented with fetal bovine serum. T-ALL samples were provided by Columbia Presbyterian Hospital, the Eastern Cooperative Oncology Group (ECOG), University of Padova and Hospital Central de Asturias with informed consent and under the supervision of the Columbia University Medical Center IRB committee. Primary T-ALL cells were cultured *in vitro* with MS5-DL1 stromal cells as previously described (Armstrong et al., 2009) and expanded *in vivo* via intravenous injection in NOD rag gamma (NOD.Cg-Rag1tm1Mom Il2rgtm1Wjl/SzJ) immunodeficient mice.

WESTERN BLOTTING AND IMMUNOPRECIPITATION

Western blot and immunoprecipitation were performed using standard procedures. Antibodies against glucocorticoid receptor (E-20), tubulin (TU-02), beta actin (C-11), GILZ (FL-1341) and MAX (C-17) were from Santa Cruz Biotechnology. Antibodies recognizing phospho-AKT Ser473 (9271), phospho-AKT Thr308 (9275), AKT (9272, 2920), cleaved Caspase 3 (9661), PARP-1 (9542) and phospho-(Ser/Thr) Akt substrate (9614) were from Cell Signaling Technologies. For immunoprecipitation of endogenous NR3C1 bound proteins in T-ALL cells we used a mouse antibody against NR3C1 (Abcam). Green Fluorescent antibody was from Invitrogen (A11122), HA epitope antibody was from Roche, FLAG epitope antibody from Sigma and an antibody against PTEN (clone 6H2.1) was obtained from Cascade Biosciences.

PHOSPHOFLOW ANALYSIS

For analysis of phosphosignalling, whole blood samples (100µl) were fixed in 4% formaldehyde for 15 min. Red blood cells were lysed and samples were permeabilized with 0.1% Triton-X in PBS. After

washing in incubation buffer (PBS-0.5% BSA), cells were resuspended in 50% Methanol in PBS. Cells were then stained with anti-pAKT (S473) Alexa-Fluor 647 (4075; Cell Signaling Technologies) or Alexa-Fluor 488 (4071; Cell Signaling Technologies) conjugated antibodies. The samples were collected on a FACSCalibur (BD Biosciences) using Cell Quest software (BD Biosciences), and analysed with FlowJo.

CELLULAR FRACTIONATION

We prepared cytoplasmic and nuclear extracts using the nuclear extraction kit (Active Motif) according to the manufacturer's recommendations.

***IN VITRO* GST PULL DOWN PROTEIN INTERACTION ASSAYS**

GST-NR3C1 and GST-NR3C1 S134A were bound to glutathione-agarose beads (Immobilized glutathione; Thermo scientific), incubated with Histidine-tagged activated AKT1 (His-AKT1, Millipore) in GST-lysis buffer (20 mM Tris-HCl, 200 mM NaCl, 1mM EDTA, 0.5% NP-40 and protease inhibitors) washed and analyzed by Western blot.

LUCIFERASE REPORTER ASSAYS

We performed NR3C1 reporter assays in U2OS cells stably expressing haemagglutinin (HA) tagged wild type NR3C1 and infected with retroviruses expressing EGFP (pMSCV IRES GFP) or myristoylated AKT1 and GFP (pMSCV MYR-AKT1 IRES GFP) using the Cignal GRE Reporter (luc) Kit (SABiosciences) .

CELL PROLIFERATION AND VIABILITY ASSAYS

We analyzed cell line viability using the Cell Proliferation Kit I (MTT; Roche) or Cell Proliferation Reagent WST-1 (Roche) and apoptosis with the PE AnnexinV Apoptosis Kit I (BD Biosciences). For primary T-ALL samples, we assessed cell viability using the BD Cell Viability kit (BD Biosciences) and fluorescent counting beads. In these experiments, 2×10^5 leukemic cells were plated with 4×10^4 MS5-DL1 stroma cells into 24-well plates and treated after 24 hours with vehicle only (DMSO), dexamethasone (10 nM -1μM), MK2206 (0.1 μM -10μM) or the combination dexamethasone (10 nM - 1μM) plus MK2206 (0.1 μM -10μM) for 3 days.

RECOMBINANT PROTEIN PRODUCTION

GST-NR3C1 and GST-NR3C1 S134A proteins were expressed in BL21 bacteria transformed with pGEX4T-1 NR3C1 and pGEX4T-1 NR3C1 S134A vectors and purified using glutathione-Sepharose 4B beads (Amersham Biosciences) following standard procedures.

MICE

All animals were maintained in specific pathogen-free facilities at the Irving Cancer Research Center at Columbia University Medical Campus. Animal procedures were approved by the Columbia University IACUC. Rosa26 Cre-Tam mice expressing a tamoxifen-inducible form of the Cre recombinase from the ubiquitous *Rosa26* locus (Guo et al., 2007) and *Pten* conditional knockout mice (*Pten*^{fl}) have been previously described (Trotman et al., 2003). To generate *NOTCH1*-induced T-ALL tumors in mice we performed retroviral transduction of bone marrow cells with an activated form of the *NOTCH1* oncogene (NOTCH1 L1601P ΔPEST) and transplanted them via intravenous injection into lethally irradiated recipients as previously described (Chiang et al., 2008). Leukemia cells from primary transplant

recipients were infected with retroviral particles (MigR1 Cherry-LUC), expressing a fusion protein between the red cherry fluorescent protein and luciferase and re-injected in sub-lethally irradiated mice (4 Gy). We treated secondary recipients with tamoxifen (5mg/mouse by intra-peritoneal injection) (n=16), to induce deletion of the *Pten* locus or vehicle only (n=16). We treated *Pten*-non-deleted animals (n=8) and *Pten*-deleted mice (n=8) with vehicle (DMSO), or with escalating daily doses of 1mg kg^{-1}, 2 mg kg^{-1} and 5 mg kg^{-1} of dexamethasone. Each dose of dexamethasone was administered for three consecutive days.

The efficacy of glucocorticoids and AKT inhibition with MK2206 in NOTCH1 induced *Pten* deleted tumors was analyzed in secondary recipient mice transplanted with *Pten* deleted *NOTCH1* L1601P ΔPEST CHERRY-luciferase expressing cells. In this experiment, groups of 7-10 mice per group were treated with daily doses of vehicle (DMSO), dexamethasone (5 mg kg^{-1} via intraperitoneal injection), MK2206 (10 mg kg^{-1} via oral gavage twice a day) or dexamethasone (5 mg kg^{-1}) plus MK2206 (10 mg kg^{-1}) for 7 days. CCRF-CEM xenografts were generated by tail vein injection in 7 to 9-week-old female NOD/*scid*/IL-2Rγ null mice (Taconic Farms). We divided mice with homogeneous tumor burdens with vehicle (DMSO), dexamethasone (5 mg kg^{-1} via intraperitoneal injection), MK2206 (10 mg kg^{-1} via oral gavage twice a day) or dexamethasone (5 mg kg^{-1}) plus MK2206 (10 mg kg^{-1}) for three days.

For pharmacodynamics studies, xenografts (primary TALL xenograft #9 and *NOTCH1*-induced Pten deleted mouse T-ALL) were established as described above. When extensive disease was established (20-40 days post-injection), mice were randomized and treated with vehicle (DMSO), dexamethasone (5 mg kg^{-1} via intraperitoneal injection), MK2206 (10 mg kg^{-1} via oral gavage twice a day) or dexamethasone (5 mg kg^{-1}) plus MK2206 (10 mg kg^{-1}) for 1 day. Four hours after the final dose, the mice were bled and euthanized. Infiltrated tissues were snap frozen in liquid nitrogen, homogenized in lysis buffer and processed for Western blot analysis. In some experiments infiltrated tissues were also fixed in formalin and processed for immunohistochemistry (IHC).

In primary xenograft experiments we infected leukemic cells with lentiviral particles expressing the mCHERRY fluorescent protein and luciferase (FUW-CHERRY-puro-LUC) and injected them intravenously into NOD rag gamma mice. We treated groups of 4-5 animals with vehicle (DMSO), dexamethasone (5 mg kg^{-1} via intraperitoneal injection), MK2206 (10 mg kg^{-1} via oral gavage twice a day) or dexamethasone (5 mg kg^{-1}) plus MK2206 (10 mg kg^{-1}).

We evaluated disease progression and therapy response by *in vivo* bioimaging with the In Vivo Imaging System (IVIS, Xenogen), human CD45 analysis by flow cytometry and analysis of luciferase activity in bone marrow and spleen.

IMMUNOHISTOCHEMISTRY

We performed anti cleaved Caspase 3 (9661;Cell Signaling Technologies) -immunostaining on formalin-fixed paraffin-embedded tissue sections after antigen retrieval by microwave heating in citrate buffer (pH 6.0). After epitope recovery slides were incubated with antibody anti cleaved caspase 3 (1:300 dilution) overnight at 4ºC. Next, slides were incubated with biotinylated immunoglobulins specific to rabbit at a 1:1000 dilution (Vector Laboratories) for 30 min, followed by avidin-biotin peroxidase complexes at a 1:25 dilution (Vector Laboratories) for 30 min. Diaminobenzidine was used as the chromogen and hematoxylin as a nuclear counterstain.

PHARMACOKINETIC ANALYSIS

MK2206 was formulated in 30% captisol in water and Dexamethasone as a 20 mg/ml solution in 100% DMSO, which was subsequently diluted to 0.5 mg/ml in 0.5% methyl cellulose. We used 6 week old C57 BL/6 male mice divided in the following treatment groups: (1) DMSO 3 mice ip QD x 5; (2) MK-2206 18 mice 10 mg/kg po BID x 5 days (9 doses total); (3) Dexamethasone 18 mice 5 mg/kg i.p. QD x 5 days (5 doses total); (4) MK-2206 + 18 mice 10 mg/kg po BID x 5 days (9 doses total); Dexamethasone 5 mg/kg i.p. QD x 5 days (5 doses total); (5) Untreated 3 mice. Time-points of analysis included 1 hr only after last dosing for Group 1 & Group 5; and 1 h, 2 h, 4 h, 8 h, 16 h and 24 h after last dosing for Groups 2 – 4 with 3 animals-samples per time point. Blood collection was performed by cardiac puncture directly into BD Microtainer (EDTA) and plasma was separated by centrifugation immediately after collection. Drug concentrations were calculated in triplicate by LC-MS using serial dilutions of MK2206 and dexamethasone as reference as detailed below:

MK-2206 LC method:
LC equipment: Shimadzu LC-20AD HPLC system
Column: Agilent XDB-Phenyl, 5 µm, 4.6 x 50 mm
Mobile phase: Acetonitrile (B solvent) / 0.1 % Formic Acid in DI-H2O (A solvent);
Isocratic: B/A = 0.28/0.12, v/v.
Flow Rate: 0.4 mL/min

MK-2206 MS method:
Mass spectrometer: Sciex API 4000 Triple Quadrupole LC/MS/MS
Ion Spray Voltage: -4200 V
Declustering Potential: -84 V
Entrance Potential: -10
Curtain gas: N2, 16
Collision gas: N2, 4
Collision energy: -35 V
Collision Cell Exit Potential: -8.3 V
Ionization mode: Negative
Turbolon Spray Temperature: 450°C
Gas 1: N2
Flow rate: 55 L/min
Gas 2: N2
Flow rate: 55 L/min
Scan Type: MRM mode
SRM transition: MK-2206: m/z 406.3 → m/z 378.1

Dexamethasone LC method:
LC equipment: Shimadzu LC-20AD HPLC system
Column: Agilent XDB-Phenyl, 5 µm, 4.6 x 50 mm
Mobile phase: Acetonitrile (B solvent) / 0.1 % Formic Acid in DI-H2O (A solvent);
Antitumor Assessment Core Laboratory - 3 - Cell Metabolism Core Laboratory
Isocratic: B/A = 0.36/0.04, v/v.
Flow Rate: 0.4 mL/min

Dexamethasone MS method:

Mass spectrometer: Sciex API 4000 Triple Quadrupole LC/MS/MS
Ion Spray Voltage: 4200 V
Declustering Potential: 60 V
Entrance Potential: 10 V
Curtain gas: N2, 16
Collision gas: N2, 4
Collision energy: 30 V
Collision Cell Exit Potential: 15 V
Ionization mode: Positive
Turbolon Spray Temperature: 450°C
Gas 1: N2
Flow rate: 65 L/min
Gas 2: N2
Flow rate: 65 L/min
Scan Type: MRM mode
SRM transition: Dexamethasone: m/z 393.2 → m/z 147.1

REFERENCES

Armstrong, F., Brunet de la Grange, P., Gerby, B., Rouyez, M. C., Calvo, J., Fontenay, M., Boissel, N., Dombret, H., Baruchel, A., Landman-Parker, J.*, et al.* (2009). NOTCH is a key regulator of human T-cell acute leukemia initiating cell activity. Blood *113*, 1730-1740.

Basso, K., Margolin, A. A., Stolovitzky, G., Klein, U., Dalla-Favera, R., and Califano, A. (2005). Reverse engineering of regulatory networks in human B cells. Nat Genet *37*, 382-390.

Carro, M. S., Lim, W. K., Alvarez, M. J., Bollo, R. J., Zhao, X., Snyder, E. Y., Sulman, E. P., Anne, S. L., Doetsch, F., Colman, H.*, et al.* The transcriptional network for mesenchymal transformation of brain tumours. Nature *463*, 318-325.

Chiang, M. Y., Xu, L., Shestova, O., Histen, G., L'Heureux, S., Romany, C., Childs, M. E., Gimotty, P. A., Aster, J. C., and Pear, W. S. (2008). Leukemia-associated NOTCH1 alleles are weak tumor initiators but accelerate K-ras-initiated leukemia. J Clin Invest *118*, 3181-3194.

Della Gatta, G., Palomero, T., Perez-Garcia, A., Ambesi-Impiombato, A., Bansal, M., Carpenter, Z. W., De Keersmaecker, K., Sole, X., Xu, L., Paietta, E.*, et al.* (2012) Reverse engineering of TLX oncogenic transcriptional networks identifies RUNX1 as tumor suppressor in T-ALL. Nat Med *18*, 436-440.

Efron, B., and Tibshirani, R. (2007). On testing the significance of sets of genes. The Annals of Applied Statistics *1*, 107-129.

Guo, K., McMinn, J. E., Ludwig, T., Yu, Y. H., Yang, G., Chen, L., Loh, D., Li, C., Chua, S., Jr., and Zhang, Y. (2007). Disruption of peripheral leptin signaling in mice results in hyperleptinemia without associated metabolic abnormalities. Endocrinology.

Lefebvre, C., Lim, W. K., Basso, K., Dalla-Favera, R., and Califano, A. (2007). A context-specific network of protein-DNA and protein-protein interactions reveals new regulatory motifs in human B cells. Lecture Notes in Bioinformatics (LNCS) *4532*, 42-56.

Lefebvre, C., Rajbhandari, P., Alvarez, M. J., Bandaru, P., Lim, W. K., Sato, M., Wang, K., Sumazin, P., Kustagi, M., Bisikirska, B. C.*, et al.* (2010) A human B-cell interactome identifies MYB and FOXM1 as master regulators of proliferation in germinal centers. Mol Syst Biol *6*, 377.

Margolin, A. A., Nemenman, I., Basso, K., Wiggins, C., Stolovitzky, G., Dalla Favera, R., and Califano, A. (2006). ARACNE: an algorithm for the reconstruction of gene regulatory networks in a mammalian cellular context. BMC Bioinformatics *7 Suppl 1*, S1-7.

Trotman, L. C., Niki, M., Dotan, Z. A., Koutcher, J. A., Di Cristofano, A., Xiao, A., Khoo, A. S., Roy-Burman, P., Greenberg, N. M., Van Dyke, T.*, et al.* (2003). Pten dose dictates cancer progression in the prostate. PLoS Biol *1*, E59.

Supporting Data
Figures

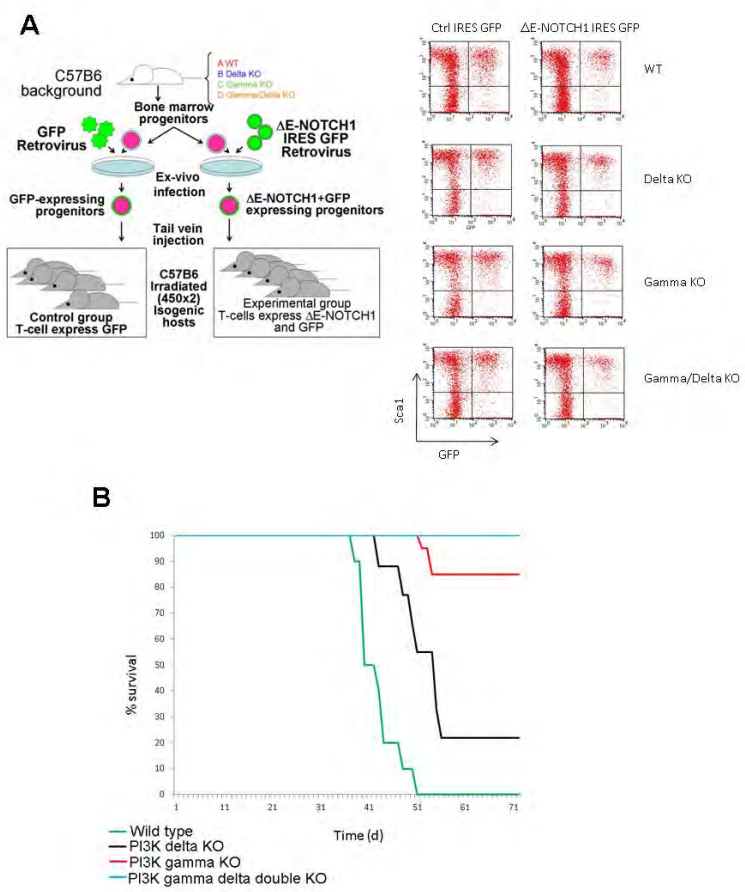

Figure 1: Genetic ablation of PI3K gamma and Pi3K delta abrogates the oncogenic effects of activated NOTCH1. To test the effects of PI3K gamma and Pi3K delta in tumor initiation induced by NOTCH we used a bone marrow transduction transplantation system (A). Hematopoyetic progenitors from wild type PI3K gamma, Pi3K delta and double PI3K gamma Pi3K delta knockout mice were infected with retroviruses driving the expression of a strong constitutively active form of NOTCH1 (Delta E NOTCH). Flow cytometry analysis showed no differences in the efficiency of the infections between different genotypes. Isogenic mice were transplanted with infected hematopoietic progenitors and monitored for leukemia development and survival (B) Mice transplanted with wild type NOTCH infected progenitors rapidly developed fatal leukemia. In contrast loss of PI3K delta and PI3K gamma completely impaired the oncogenic effects of NOTCH1($P<0.001$). Mice transplanted with Pi3K delta or Pi3K gamma only deficient cells showed delayed tumor initiation and lower disease penetrance ($P<0.001$).

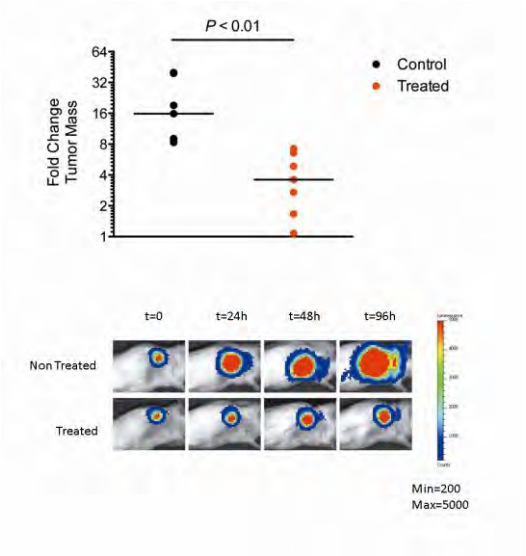

Figure 2: In vivo therapeutic response to CAL130 in CCRF CEM cells. To test the therapeutic effects of CAL130 in vivo we first tested the activity of this drug against CCRF CEM cell in a subcutaneous xenograft experiment. CCRF-CEM T-ALL cells expressing the luciferase gene were injected subcutaneously in NOD-SCID mice and animals were treated with vehicle only or CAL130. In vivo bioimaging was used to analyze therapeutic response. Animals treated with CAL130 demonstrated a strong antileukemic response to the inhibition of PI3KG and PI3KD. Treatment with CAL130 showed a statistical significant antileukemic effect in this model.

Figure 3: Dose response engraftment of CCRF-CEM T-ALL cells in NOD-SCID mice. NOD-SCID mice were sublethally radiated and challenged with serial dilutions of CCRF-CEM T-ALL cells expressing the luciferase gene (CCRF-CEM LUC) via intravenous injection. In vivo bioimaging was performed at 1 week intervals after transplant to monitor engraftment and disease progression. The results of this experiment were used to calibrate the xenograft dose and to time the treatment schedule for experimental therapeutic analysis of CAL130 in vivo.

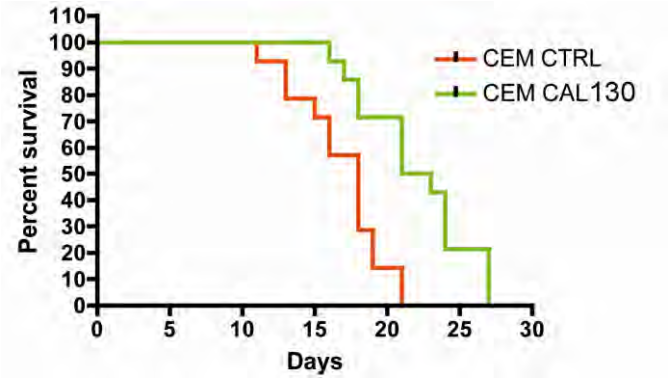

Figure 4: Survival analysis of CCRF-CEM cells treated with CAL130. The in vivo therapeutic effects of CAL130 in survival were tested in a intravenous xenograf experiment in which CCRF-CEM cells expressing the luciferase gene were injected intravenously. Animals with homogeneous tumor loads were treated with vehicle only or CAL130 and survival was analyzed in Kaplan-Meyer curves. Treatment with CAL130 extended the survival of T-ALL bearing mice in his experiment confirming the therapeutic activity of inhibiting PI3KG and PI3KD.

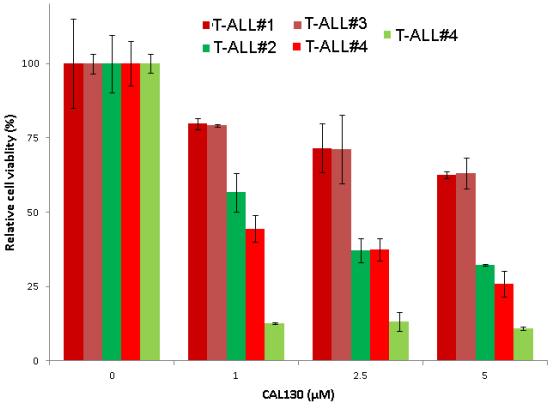

Figure 5: CAL130 effects in cell viability against primary human T-ALL samples in vitro. Primary human T-ALL lymphoblast cells were cultured in vitro. Active proliferation and sustained viability were supported by MS5 stroma cells expressing the DL1 NOTCH ligand and a cytokine cocktail including IL7, SCF, insulin and human serum. Viable cultures were treated with serial dilutions of CAL130 and cell viability was evaluated by flow cytometry based assay gating out stroma cells (GFP positive) and dead cells (stained with a live-cell impermeable die) and using counting beads for calibration. CAL130 showed a dose response antileukemic effect in this assay.

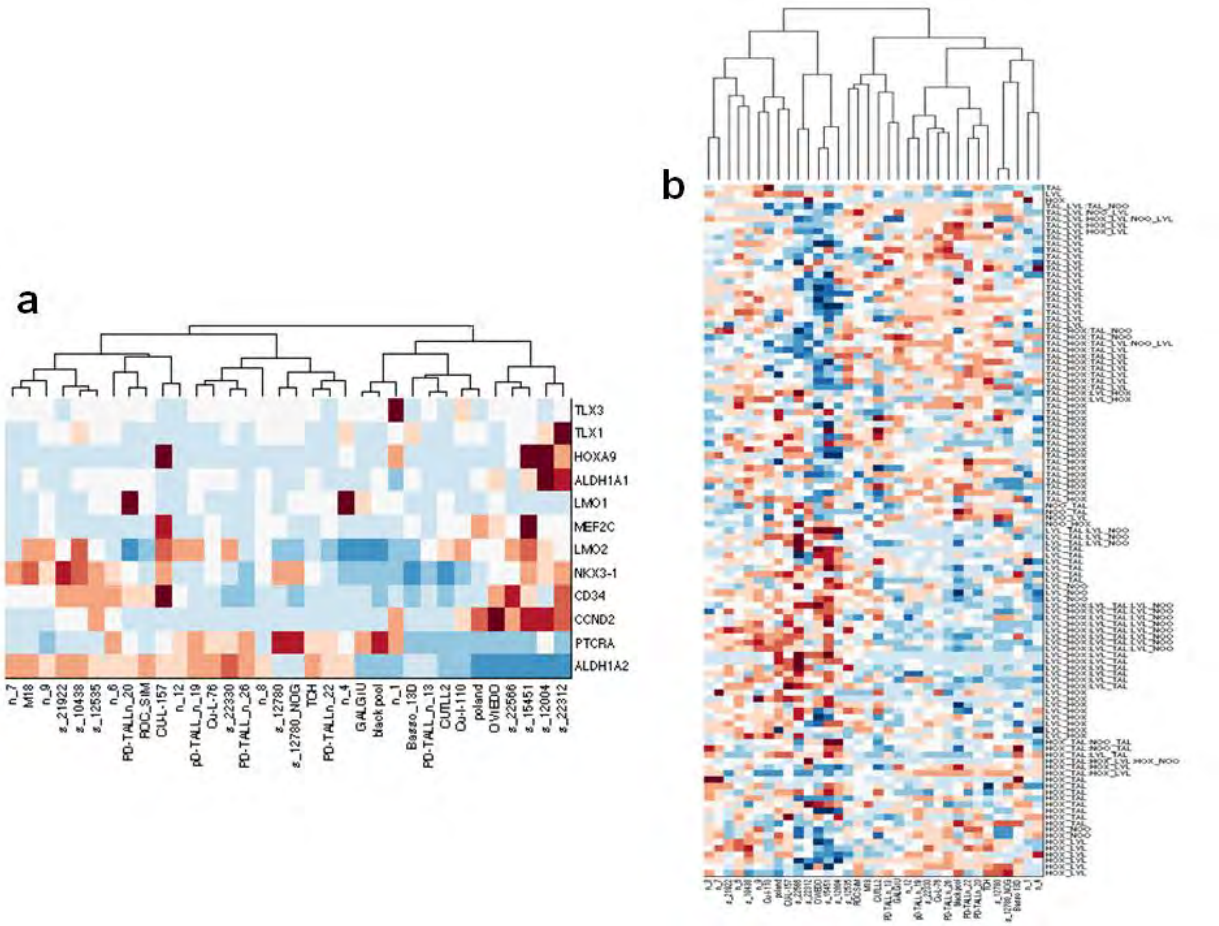

Figure 6. Microarray gene expression profiling of primary T-ALL xenografts. Unsupervised hierarchical clustering of human primary T-ALL xenografts. Relative expression values are color coded with red indicating higher levels of expression and blue indicating lower levels of expression. **a.** Differential expression of T-ALL oncogenes (TLX3, TLX1, LMO1, LMO2, MEF2C, HOXA9, CCND2, NKX3.1) and differentiation markers (CD34, ALDH1A1, ALDH1A2, PTCRA) delineating different genetic and molecular groups of T-ALL. **b.** Tumor xenograft classification based on unsupervised analysis of top differentially expressed genes.

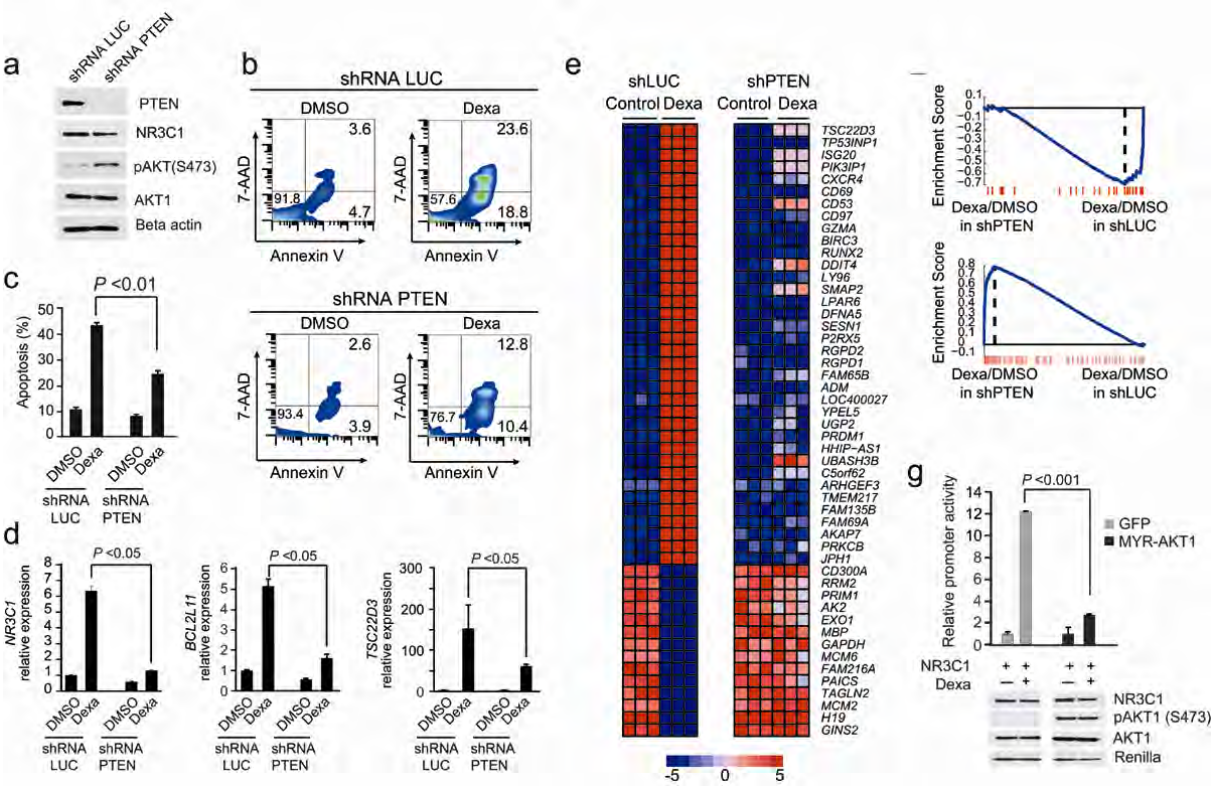

Figure 7. Activation of the PI3K-AKT signaling pathway via PTEN inactivation induces glucocorticoid resistance in T-ALL and blunts glucocorticoid-induced gene expression. **a**, Western blot analysis of PTEN expression and AKT1 activation in DND41 T-ALL cells expressing a shRNA targeting the PTEN tumor suppressor (shRNA PTEN) compared to control cells expressing a hairpin against luciferase (shRNA LUC). **b**, Representative plots and **c**, quantification of glucocorticoid-induced apoptosis in control and PTEN knockdown DND41 cells treated with dexamethasone (1μM) for 48 hours. Percentages of viable (lower left quadrant), apoptotic (lower right quadrant) and dead (upper right quadrant) are indicated. **d**, RT-PCR analysis of glucocorticoid response gene induction in control and PTEN knockdown DND41 cells treated with dexamethasone. **e**, Heat map representation of the top differentially expressed genes in DND41 shRNA LUC dexamethasone treated cells and corresponding transcript levels in DND41 shRNA PTEN vehicle only and dexamethasone treated samples. The scale bar shows color coded differential expression with red indicating higher levels and blue lower levels of expression. **f,** GSEA analysis of glucocorticoid regulated transcripts among differentially regulated genes in DND41 shRNA LUC dexamethasone treated cells compared with DND41 shRNA PTEN dexamethasone treated cells. Enrichment plots corresponding to glucocorticoid upregulated and glucocorticoid downregulated transcripts are shown. **g**, Luciferase reporter analysis of dexamethasone-induced glucocorticoid receptor transactivation in U2OS cells expressing MYR-AKT1 compared with GFP only expressing controls using a synthetic glucocorticoid response element reporter.

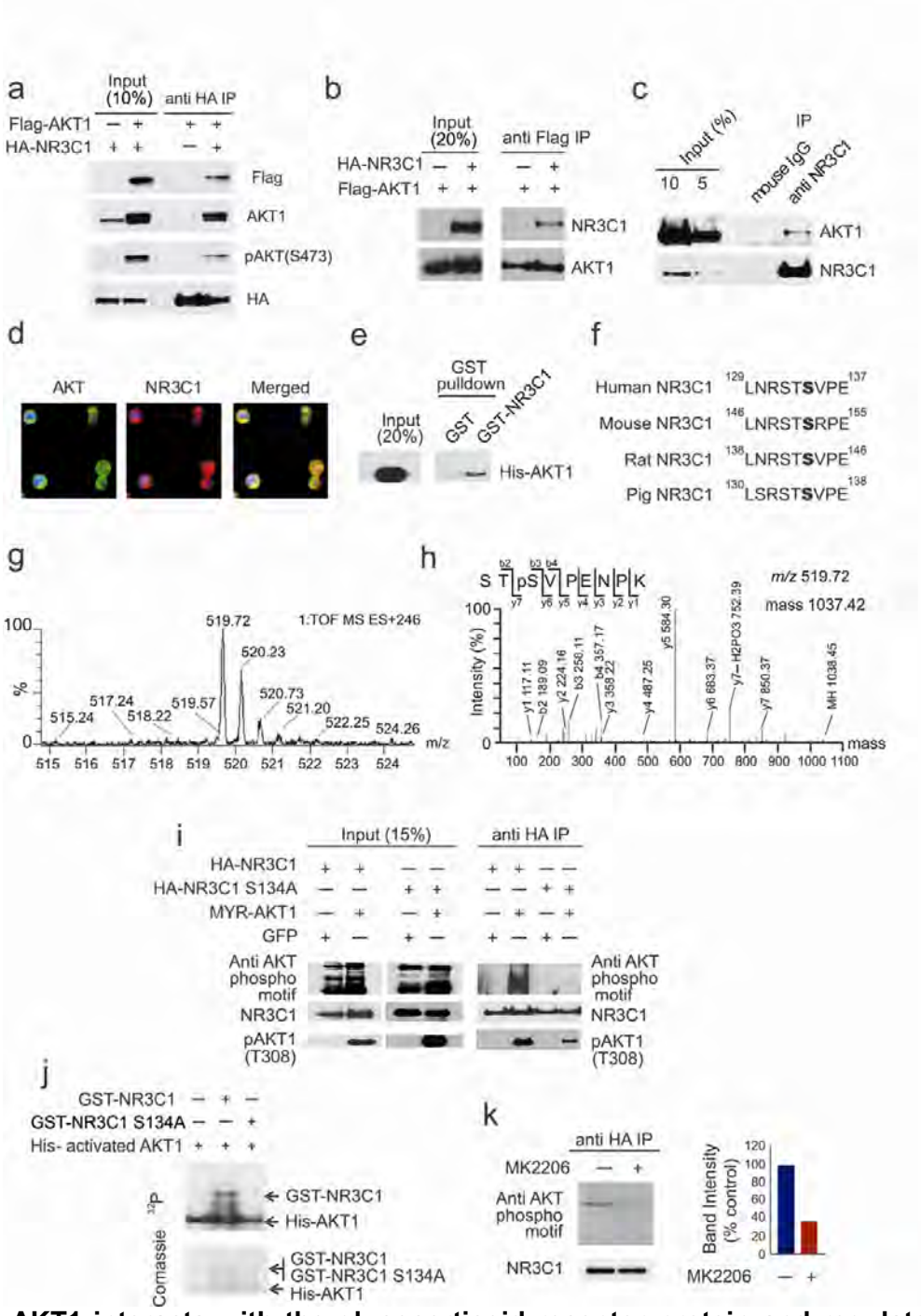

Figure 8. AKT1 interacts with the glucocorticoid receptor protein and regulates NR3C1 S134 phosphorylation. **a**, Western blot analysis of AKT1 and activated AKT1 after glucocorticoid receptor NR3C1 immunoprecipitation in 293T cells expressing Flag-tagged AKT1 and HA-tagged NR3C1. **b**, Western blot analysis of glucocorticoid receptor NR3C1 protein after AKT1 immunoprecipitation in 293T cells expressing Flag-tagged AKT1 and HA-tagged NR3C1. **c**, Western blot analysis of AKT1 after NR3C1 protein immunoprecipitation in DND-41 T-ALL cells. **d**, Immunofluorescence colocalization analysis of AKT (red) and NR3C1 (green) proteins in DND41 cells. Cell nuclei stained with TO-PRO3 are shown in blue. **e**, Analysis of AKT1-NR3C1 interaction via Western blot analysis of protein complexes recovered after NR3C1-GST pull down of recombinant His-tagged AKT1. **f**, Partial alignment of the glucocorticoid receptor

protein sequence flanking S134. **g**, ESI-MS/MS spectrum of monophosphorylated peptide STpS134VPENPK (S-132 to K-140) obtained after trypsin digestion of NR3C1 isolated from cells expressing constitutively active AKT1. **h**, Collision induced dissociation of the molecular ion, [M+2H]2+ at m/z 519.72 (M = 1037.42 Da) corresponding to S134. Characteristic b- and y-fragment ions including y7 which contains pSer and features the loss of 98 Da (elimination of phosphoric acid) are shown. **i**, Western blot analysis of NR3C1 phosphorylation using an antibody against the AKT phospho-motif in NR3C1 protein immunoprecipitates from U2OS cells expressing MYR-AKT1 together with HA-tagged wild type glucocorticoid receptor (HA-NR3C1) or an HA-tagged glucocorticoid receptor protein harboring a serine 134 to alanine substitution (HA-NR3C1 S134A). **j**, *In vitro* kinase analysis of AKT1 phosphorylation of recombinant wild type NR3C1 (GST-NR3C1) and NR3C1 S134A mutant (GST-NR3C1 S134A) protein. Top panel shows P^{32} autoradiography after SDS-PAGE. The corresponding protein loading for each reaction is shown at the bottom by Coomassie blue staining. **k**, Western blot analysis of NR3C1 phosphorylation using an anti AKT phospho-motif antibody in NR3C1 immunoprecipitates from CCRF-CEM cells expressing HA-NR3C1 treated with vehicle or the MK2206 AKT inhibitor.

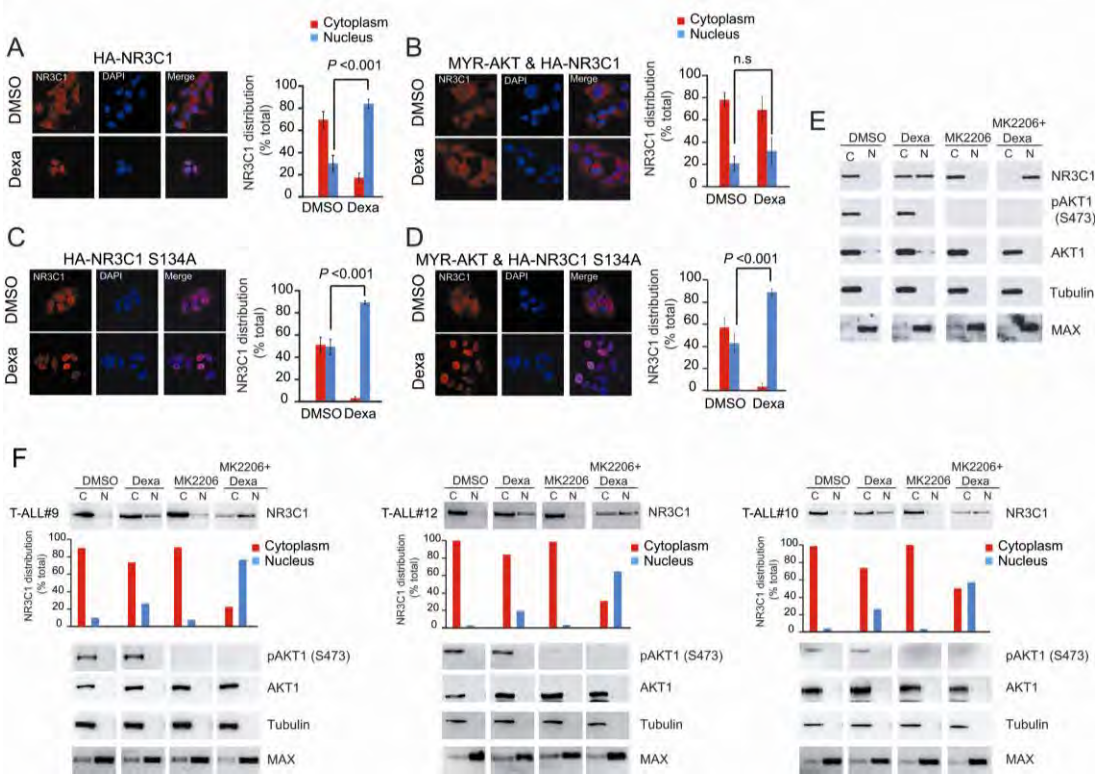

Figure 9. AKT1-mediated S134 phosphorylation of the NRC3C1 protein impairs dexamethasone-induced glucocorticoid receptor nuclear translocation. **a**, Confocal microscopy analysis and quantitation of the distribution of NR3C1 cellular localization in U2OS cells expressing HA-NRC31 in basal conditions (DMSO) and after dexamethasone (Dexa) stimulation. **b,** NR3C1 cellular localization in U2OS cells expressing HA-NRC31 and MYR-AKT1 in basal conditions and after dexamethasone stimulation. **c**, Cellular localization of NR3C1 in U2OS cells expressing the HA-NRC31 S134A mutant in basal conditions and after dexamethasone stimulation. **d**, Cellular localization of the HA-NRC31 S134A protein in U2OS cells expressing MYR-AKT1 in basal conditions and after dexamethasone stimulation. **e**, Cellular localization analysis of NR3C1 via nuclear and cytoplasmic cell fractionation and analysis of AKT1 signaling in cell lysates from CCRF-CEM T-ALL cells treated with vehicle only (DMSO), dexamethasone (Dexa), the MK2206 AKT inhibitor and MK2206 plus dexamethasone. **f**, Cellular localization analysis of NR3C1 via nuclear and cytoplasmic cell fractionation as in **e** in cell lysates from primary T-ALL lymphoblasts. Tubulin and MAX proteins are shown as

controls for cytosolic and nuclear fractions, respectively in **e** and **f**. C: cytoplasmic fraction; N: nuclear fraction.

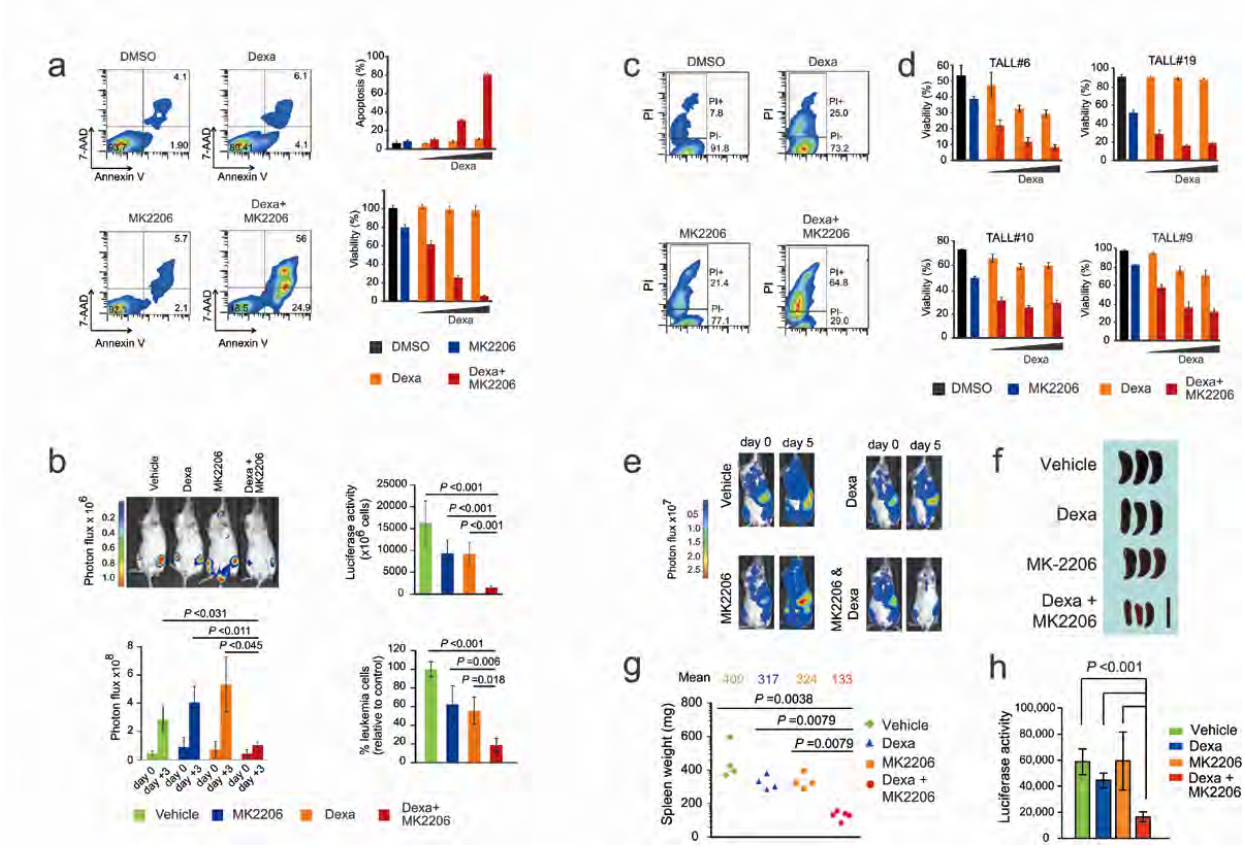

Figure 10. Pharmacologic inhibition of AKT with MK2206 reverses glucocorticoid resistance in human T-ALL. a, Representative plots and apoptosis and cell viability quantification in CCRF-CEM T-ALL cells treated with vehicle only, MK2206, dexamethasone (Dexa) or dexamethasone plus MK2206 (Dexa + MK2206) in combination *in vitro*. **b**, Tumor load quantification *in vivo* by bioluminescence imaging and analysis of luciferase activity and human CD45 expressing cells in the bone marrow of CCRF-CEM T-ALL xenografts treated with vehicle only, MK2206, dexamethasone or MK2206 plus dexamethasone. **c**, Representative plots and **d**, quantification cell viability in primary T-ALL samples treated with vehicle only, MK2206 dexamethasone alone and dexamethasone plus MK2206 in combination. Percentages of viable (PI −), and non-viable (PI +) cells are indicated. **e**, Representative examples of primary human T-ALL mouse xenografts showing changes in tumor load; **f**, spleen size; **g**, spleen weight and **h**, luciferase activity in bone marrow after treatment with vehicle only, MK2206, dexamethasone or MK2206 plus dexamethasone. Scale bar: 2 cm.

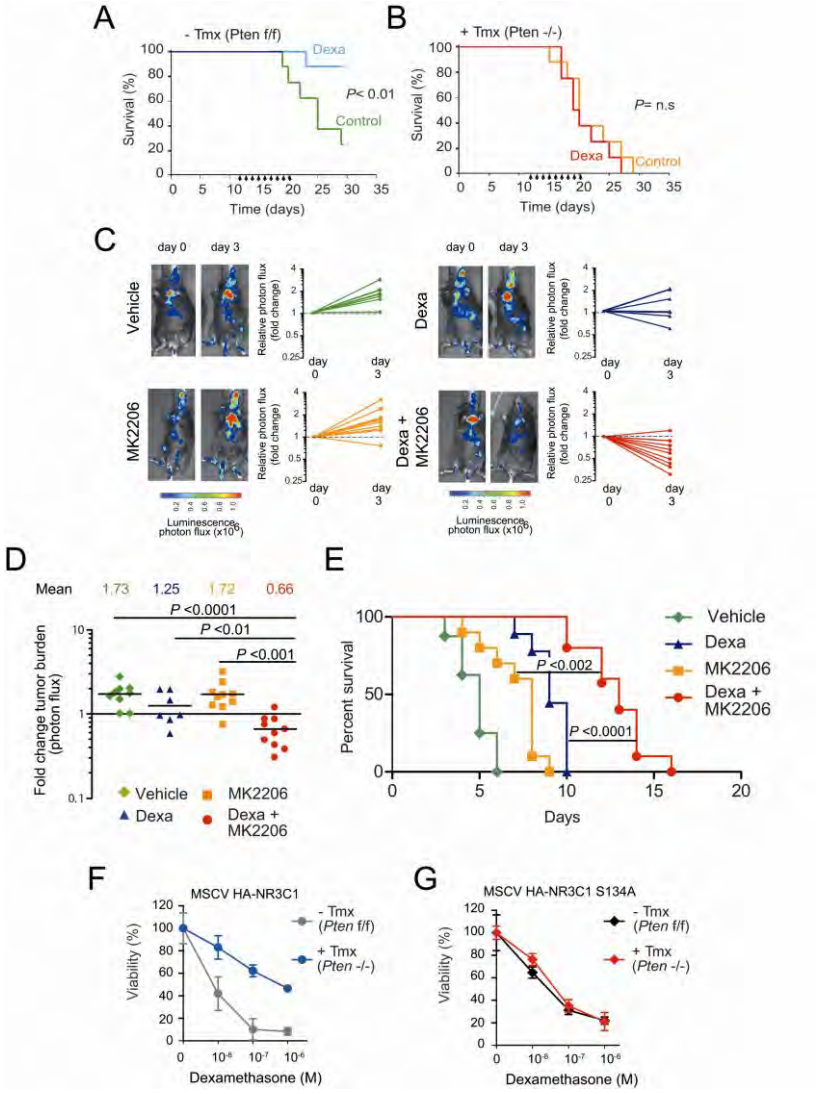

Figure 11. Pharmacologic inhibition of AKT reverses glucocorticoid resistance in a mouse model of glucorticoid resistant T-ALL

(**a, b**) Kaplan-Meier curve in mice treated with dexamethasone (Dexa) or vehicle (Control) after allograft transplantation of *Pten*-non-deleted [–Tmx (*Pten*$^{f/f}$)] or *Pten*-deleted [+Tmx (*Pten*$^{-/-}$)] *NOTCH1*-induced T-ALL tumor cells. Arrows indicate drug treatment. (**c, d**) Representative images, changes in bioluminescence by *in vivo* imaging and analysis of treatment response in mice allografted with *NOTCH1* induced *Pten* deleted mouse leukemia cells treated with vehicle only, MK2206 (10 mg kg^{-1} via oral gavage twice a day), dexamethasone (Dexa; 5 mg kg^{-1}) or MK2206 (10 mg kg^{-1} twice a day) plus dexamethasone (5 mg kg^{-1}) (Dexa + MK2206). (**e**) Kaplan-Meier overall survival curve in mice allografted with *NOTCH1* induced *Pten* deleted mouse leukemia cells and treated with vehicle only (control), MK2206 (10 mg kg^{-1} via oral gavage twice a day), dexamethasone (Dexa; 5 mg kg^{-1}) or MK2206 (10 mg kg^{-1} twice a day), plus dexamethasone (5 mg kg^{-1}) (Dexa + MK2206). (**f,g**) Quantification of glucocorticoid-induced loss of viability in *NOTCH1* induced *Pten* non deleted [–Tmx (*Pten* f/f)] or *Pten* deleted [+Tmx (*Pten* –/–)] mouse leukemia cells infected with retroviruses expressing the wild type glucocorticoid receptor NR3C1 (MSCV HA-NR3C1) or the S134A glucocorticoid receptor NR3C1 mutant protein (MSCV HA-NR3C1 S134A). Data in **f** and **g** are represented as mean ± s.d.